THERMAL BARRIER COATING MODELLING FOR STRESS ANALYSIS

By

Yajie Hu

Thesis submitted to the University of Ottawa
in partial fulfillment of the requirements for the Master of Applied Science,
Mechanical Engineering

Department of Mechanical Engineering
Faculty of Engineering
University of Ottawa

ABSTRACT

Thermal barrier coatings (TBCs) have been used widely in aerospace and land-based gas turbines. The TBC system consists of a top coat layer, a thermally grown oxide (TGO), a bond coat layer and a substrate. The growth kinetics of the TGO significantly affects the durability of TBCs. At a critical TGO thickness, the growth stresses exceed the ceramic-bond coat interface strength, resulting in TBC system failure. Regardless of the deposition method used, it is vitally important to accurately predict the TBC lifetime by investigating the determinants of the failure. The main objective of this study was to investigate the effect of oxidation stress induced by TGO layer in high temperature cycling environment through a series of reliable numerical simulations. Indeed, this oxidation stress is a known factor of interface degradation, and may result in failure of the ceramic-metal interface.

A 2-D finite element model of the TBC was built via ANSYS APDL software, to conduct parametric studies of increasing complexity. The model accounted for elasticity first, before creep was integrated. Then, the model included swelling induced by phase transformation associated with oxidation, incorporating the effect of volumetric expansion of the newly grown TGO. This coupled oxidation constitutive approach was implemented for a typical air plasma spray deposited TBC coating. The interfacial radial stresses induced by the gradual oxidation were investigated. Different morphologies of the TBC interface were also considered to analyze the roughness effect on interface stresses. A complete model including swelling, creep, aging effects on the TBC layers at a given roughness was finally investigated.

ACKNOWLEDGEMENTS

I would like to convey my gratitude my supervisor, Dr. Michel Labrosse and Dr. Kuiying Chen. Without Dr. Labrosse's support during all the meetings and discussions, I would never have accomplished so far. Every time when I thought it was tough to keep on going, it was Dr. Labrosse who provided me support along the way. His patience and kindness boosted my confidence and encouraged me to conquer whatever was in front of me. He is intelligent, knowledgeable and is the gentlest, modest, most humble professor I have ever encountered; it was a true honor to learn from him.

I would also like to thank my partner Christopher Rocco for his sacrifice during my study. Most importantly, I would like to dedicate this to my parents, who love, nurture and support me for every step and every decision in my life.

ABBREVIATIONS

APS	Air Plasma Spray
BC	Bond Coat
CTE	Coefficient of Thermal Expansion
DOF	Degree of Freedom
EB-PVD	Electron Beam Physical Vapor Deposition
FEM	Finite Element Method
PBR	Pilling Bedworth Ratio
SEM	Scanning Electron Microscopy
TBC	Thermal Barrier Coating
TGO	Thermally Grown Oxide
TC	Top Coat
YSZ	Yttrium Stabilised Zirconia

α	Thermal expansion coefficient, K^{-1}
E	Young's Modulus, $\mathrm{N.m}^{-2}$
h	Thickness, m
h_{ox}	TGO Thickness due to external oxidation, m
k	parabolic constant for oxidation
R	Universal gas constant
T	Temperature, K
t_{ox}	Oxidation time, s
v	Poisson ratio
m	Growth exponent (0.667)

TABLE OF CONTENTS

LIST OF TABLES

LIST OF FIGURES

1 INTRODUCTION

1.1 RATIONALE

There has been significant advancement of the thermal barrier coating materials used in the gas industry in the last century. As gas as a new power source further kicks in, the durability of turbine blades, which is considered the most crucial part to future technology for power generation, must be improved to be able to endure the demands of high gas service temperature. Gas turbine durability is governed by events like crack nucleation, which leads to buckling and spallation. Ceramic coating like thermal barrier coating (TBC) is established as an effective approach to lower the service temperature for the substrate metal layer of the turbine material [Busso et al., 2009].

To enhance the capability of the metallic substrate of the turbine components, TBC is applied to internally cooled metallic gas turbine blades to reduce the metal temperature when the part is subjected to burning gas, while protecting the Ni-based substrate of the turbine blade against other severe environmental and detrimental oxidation damage such as creep or fatigue. By applying the TBC coating, the subjected underlying material can reduce its temperature by $100 - 300°C$ compared to the substrate [Padture et al., 2002]. Thus, to prolong the life span of turbines, the extensive study of the effect of material characteristics of TBC is extremely important. In particular, the coating material chosen for gas turbine application should have superior thermal properties for high temperature application, to protect the turbine blades from hot gas.

As TBC is believed to improve gas turbine life span and efficiency, Fig.1.1 offers an overview of where TBC is applied to internal gas turbine. The turbine efficiency is governed by the operating temperature. In most of the cases for power system operation, the system is held at peak temperature isothermally with very few thermal cycles, whereas most of the propulsion systems experience multiple thermal cycles. Such differences in thermal loading history can result in different failure mechanisms, making the thermal loading profile a parameter of prime importance when studying the life span of TBC system.

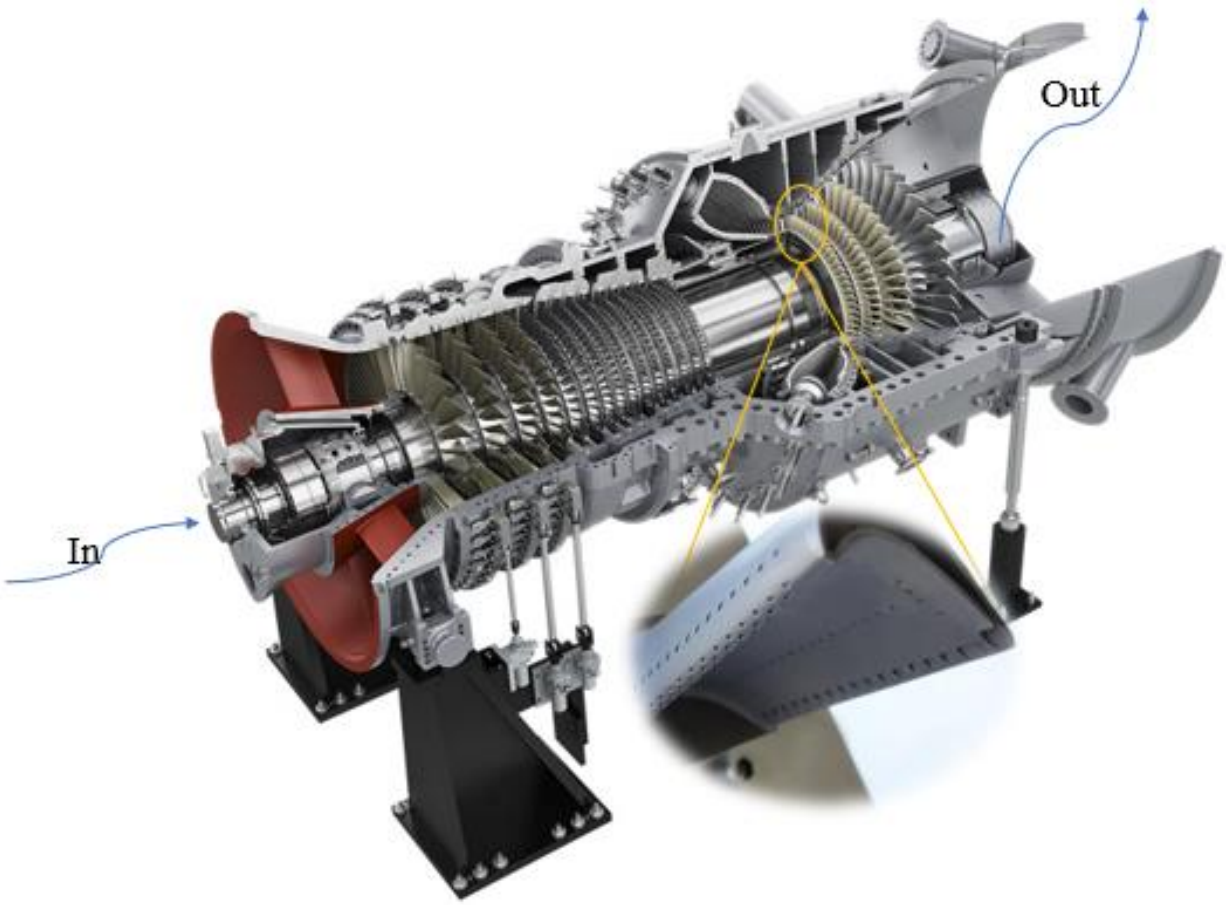

Figure 1.1. Cross section of a Land-Based turbine (SIEMENS [Taylor, M., Gray, S., and Evans, H.,2006. Contract Report. SIEMENS]), the section circled in yellow shows the high temperature turbine.

Building a reliable TBC system while mastering the high temperature environment has long been the objective of researchers. Toward this goal, investigating the system's function during service is important, and so is the construction of a numerical model where changes can be implemented to analyze different effects. A numerical model can indeed assist greatly, especially in combination with an experimental framework.

1.2 OBJECTIVES

For gas turbine application, reliable computation simulation could give access to the expected mechanical stresses and behaviour of materials during the desired temperature cycles before experiments are started, allowing researchers to whittle down unnecessary options for complex experimental work. Modeling and simulation are a more flexible approach that not only requires less experimental equipment, but that can also be a time-efficient solution as material data can be changed easily through coding.

In finite element (FE) simulation, as used herein, several areas need to be taken into consideration: geometry, material behaviour, loading conditions and boundary conditions. This work will be focused on mainly two different areas—geometry and material properties. The loading conditions were carefully selected to model a burning rig test for verification of baseline simulations against the results from Rösler et al. [2001]. These loading conditions will then be modified in various ways to model more realistically turbine working conditions. The boundary conditions were the same throughout the thesis, and will be explained in detail in Chapter 4.

Although there are several widely used TBC deposition methods, such as electron beam physical vapour deposition (EB-PVD), air plasma sprayed (APS) and chemical vapour deposition (CVD), this study will be focused on the modeling of APS TBC. Compared to EB-PVD, APS is believed to be a cheaper, yet effective coating method when it comes to ceramic coating deposition. However, the present work is only a first approach to more extended work. For instance, the model could consider EB-PVD by introducing simple changes in geometry and material characteristics of the top coat layer, from homogeneous to anisotropic material properties.

The objectives for this study were to produce a reliable TBC system FE model for investigating the time-evolution of the bond coat creep and plastic behaviour, as well as radial residual stresses due to oxide growth and thermal cycling close to the TGO layer.

1.3 CONTRIBUTIONS

The material properties considered were meant to allow for an increasingly deeper investigation of their separate effects on stress distribution. A preliminary verification of the results from this study was obtained by reproducing the FE model presented in [Rösler et al., 2001]. Afterwards, the initial model was built-upon to incorporate more realistic thermal cycling conditions and integrate more material behaviour effects which should be included for more credible simulations of long thermal cycles. The effects of aging and creep that occur in the TC layer, along with the plastic behaviour of the BC layer, were implemented. The material effects were implemented separately and incrementally to provide a better understanding of the effect on stress/creep of the TBC system from each individual material behaviour. Finally, the effects of different interface profiles on stresses during thermal cycles were analyzed. The future design of the material composition for the coating could benefit from the conclusions of the FE model presented herein.

1.4 THESIS ORGANIZATION

In the present work, the TBC residual stress distribution is studied as a preliminary test. TGO thickness modelling is then carried out. The evolution of the stress distribution is examined. The TGO interface roughness is considered.

This thesis is constructed as follows. In Chapter 2, a review of the work done by other researchers is presented, which also includes an introduction of the TBC system as background information. In Chapter 3, the material characteristics of each component of the TBC system are explained in detail, followed by the design concern of the model, which gives a general scope of what should be included and how the FE model should be constructed. The material model data are also calibrated from experimental data. In Chapter 4, details of the FE modeling are presented, including the modeling procedure, element selection for the FE model, the geometry with mesh, thermal loading profile, boundary conditions, and finally, the material behaviour calibration for

the FE model, which is an extension of Chapter 3. The reproduction of Rösler's [Rösler et al., 2001] model is then conducted in Chapter 4, where the results of the FE model are discussed and compared. The stress assessment was carried out in the following order:

1. Thermal loading without considering BC creep behaviour, to study the effect of thermal expansion mismatch upon cooling with purely elastic material behaviour in the absence of TGO growth.

2. Including the BC creep behaviour during thermal loading, but without TGO growth, running the analysis for very short holding time at elevated temperature to assume a burner rig test environment.

3. Introducing TGO growth in the model with no TGO creep. This is where the growth kinetics will be illustrated by the FE model.

4. Adding TGO creep to the FE model.

   All the result from these cases will be compared and discussed with respect to the reference model [Rösler et al., 2001]. Then in Chapter 5, an extension of the reference model will be made to include a variety of geometric variations to the interface, such as a flat surface, a sinusoidal model with different roughness amplitudes, and a more realistic model produced from SEM imaging. The results will be discussed thoroughly, in different case scenarios, conducted parametrically, such as:

5. Incorporating the plastic properties of BC and TGO layers.

6. Incorporating the effect of TC sintering by implementing a different Young's modulus as a function of dwelling/oxidation time.

7. Incorporating the effect of TC creep and the combined effect of creep and sintering.

   Finally, in Chapter 6, conclusions will be drawn.

2 LITERATURE REVIEW

TBC is a coating system that consists of several layers aimed at maintaining a large temperature difference between the coating surface and the load bearing alloy. With adequate backside cooling, the system can remain a high thermal gradient between constituents. The resting benefit is a significant increase in service temperature which, in turn, improves system efficiency.

Gas turbines rely on thermal barrier coating systems as high performance at elevated temperature is desired for superalloy turbines. Introduced in the early 1950's, TBC coating and the cooling system of turbine blades have been improved through composition and microstructure. In this chapter, the composition of TBC system will be reviewed, along with past research work relevant to the present study.

2.1 COMPOSITION OF TBC SYSTEM

As depicted in Fig.2.1, the TBC under consideration consists of four constituents: (i) a ceramic top coat (TC) layer which, as a consequence of its low thermal conductivity, is meant to insulate the substrate from the heat source; (ii) an underlying bond coat (BC) layer which, as its name implies, binds the ceramic TC to the substrate. BC provides protection of the substrate from oxidative attack and hot gas steam corrosion; (iii) the protective, thermally grown oxide (TGO) layer, which predominantly consists of α-alumina. It is a thin layer that develops during deposition between the ceramic TC and the metallic BC. TGO forms due to the reaction of oxygen coming in from the near oxide-permeable TC layer, reacting with the aluminum in BC; finally, (iv) the superalloy substrate layer that sustains the structural loading. All the layers interact with each other to control the performance of the coating.

a) b)

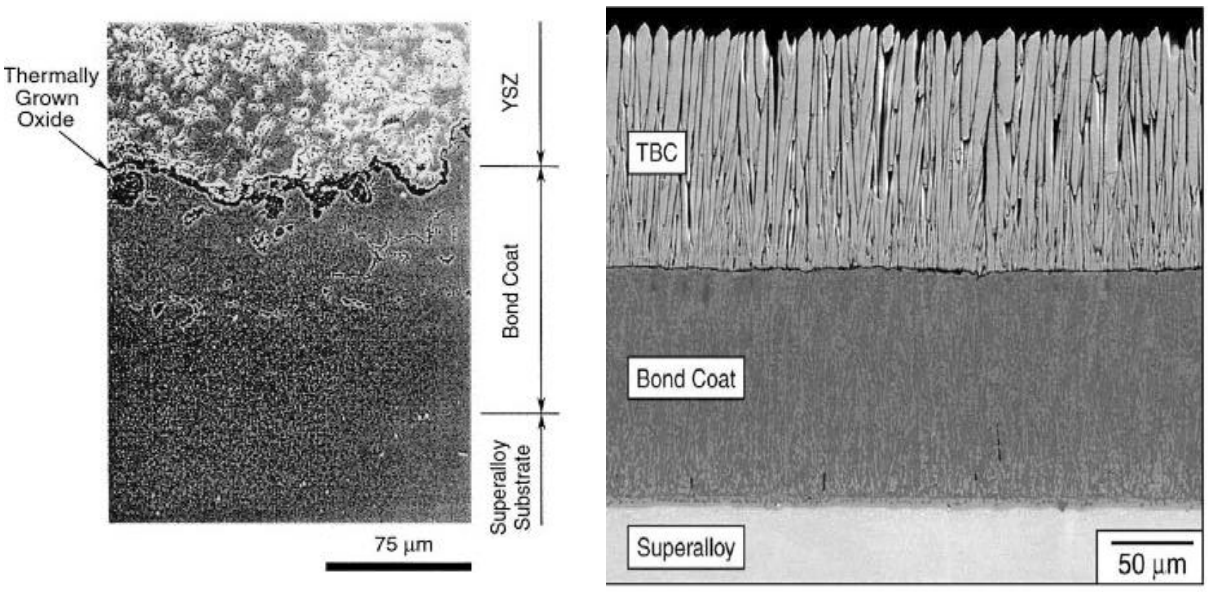

Figure 2.1. Scanning electron micrograph of the layered a) APS TBC system b) EB-PVD TBC system showing the TBC system in three layers, sitting on top of the metallic substrate [Busso et al., 2001].

2.1.1 **Top Coat ceramic layer**

Variations in temperature can lead to undesired geometry deformation in applications which undergo large temperature gradients during work cycle. The main goal in designing TBC being to insulate the underlying metal against high temperature gas attack in the gas turbine engine to suppress temperature induced failures, materials with a low coefficient of thermal expansion (CTE) over a wide range of temperatures are generally sought. Yttria stabilized zirconia (YSZ) has been favored because of its low thermal conductivity and high fracture toughness.

Indeed, the most used commercial ceramic TC layer at present consists of YSZ in a cubic/tetragonal form. Compared to other oxides, Yttria (Y_2O_3) has been empirically proven to be a suitable material to stabilize zirconia (ZrO_2) due to its ability to exist in polymorph structures.

The YSZ TC material has one of the lowest thermal conductivity amongst all ceramics. It is not sensitive to temperature and provides a good thermal insulation. Specifically, at $1{,}150\ ℃$ service temperature, its thermal conductivity is only around $1.22\ \mathrm{Wm^{-1}K^{-1}}$ for $8\ \mathrm{wt.\%YSZ}$. With a reduced thermal conductivity, the TBC system is able to create a greater temperature drop for the underlying component while parts in service undergo high temperature from gases.

On the other hand, the YSZ TC layer has relatively high CTE, at approximately $9.5 \times 10^{-6}\ ℃^{-1}$, which is close to that of the underlying substrate ($\sim 14 \times 10^{-6}\ ℃^{-1}$). The smaller the difference in CTE, the better the mitigation of thermal expansion mismatch under thermal cycles. As illustrated in Fig.2.5, a thermal expansion mismatch still exists, and introduces residual stresses which may be problematic as they can lead to crack propagation within constituents.

Finally, YSZ's high melting point (roughly $2{,}700℃$) is well suited to current technology's demand of elevated temperature during service for gas turbines.

2.1.2 **Bond Coat metallic layer**

BC being the intermediate layer between TC and the substrate, its existence ensures good chemical and mechanical adhesion between the ceramic and the superalloy. The metallic BC layer typically consists of NiCoCrAlY.

BC is rich in aluminum, which ensures that α-alumina forms before other oxides. It also promotes low oxygen diffusivity and outstanding adherence.

BC layer oxidation is arguably the most crucial influence for the degradation mechanism when determining the lifetime of the TBC system. Indeed, large residual compression stresses ($3 - 6\ \mathrm{GPa}$) [Evan et al., 2001] have been observed in the oxidized BC layer in experiments while cooling down the system to ambient temperature. These stresses were primarily induced by the thermal expansion mismatch of the new oxide layer with regard to the substrate.

Additionally, the BC's creep and plastic characteristics directly affect the system performance. The creep and yielding of the BC alleviate the system stress that generated from the thermal expansion misfit stress thereby slowdown the cyclic yielding locally around the undulation at the TBC constituent's interface.

2.1.3 **Thermally grown oxide layer**

During the TBC deposition process, a thin layer of TGO consisting of dense α-alumina is initially formed at the BC-TC interface, due to the high temperature diffusion of aluminum, together with the diffusion of oxygen to the BC-TC interface [Bednarz, P., 2007]. During operation at high temperature, this thin layer of oxide gradually thickens over time, protecting the system from further oxidation and providing great adhesion between TC and BC. However, during cooling, large compressive stresses are observed in TGO layers, mainly coming from the new TGO growth stress, reaching roughly 1 GPa (more details in Section 5.2.2.3). As changes in residual stress during thermal cycles are largely affected by TGO growth and the mismatch between TGO and other TBC constituents, the characteristics of the TGO layer are major determinants of the TBC system's durability.

2.2 EFFECT OF THE DEPOSITION METHOD ON RESIDUAL STRESS

While studying the TBC system, it is important to consider the different methods used for deposition because they bring unique characteristics to the coating, as their microstructures affect its material characteristics.

The common deposition methods for TBC are electron beam physical vapored deposition (EB-PVD) and air plasma sprayed (APS) deposition. APS is a cheaper and effective way of depositing ceramic coating. It is widely used in gas turbine and diesel engines and greatly favored for

commercial use. The disadvantage of APS coating is that due to the various splats boundaries and microcracks generated during deposition, there maybe early spallation limiting the service life of the coating. On the other hand, EB-PVD provides the TBC with a very fine columnar structure, and a much smoother interface compared to APS. The microstructure of the EB-PVD TBC exhibits a higher strain tolerance and can be used for higher service temperatures because of the greater thermal gradients it can sustain. Due to its porosity, the EB-PVD coating is also a protection against erosion. However, the EB-PVD TBC has a higher thermal conductivity resulting from its columnar structure, compared to that of APS TBC afforded by a lamellar structure with many ellipsoid pores.

2.3 MATERIAL CHARACTERIZATION AND DESIGN CONCERNS

The following section is intended to provide a better understanding of the microstructure and the mechanical behavior of each constituent in the TBC system, as this will be necessary for the forthcoming FE analysis. This analysis will include the elastic and plastic effect of the constituents. In this section, the relevant material properties of each layer will be listed and discussed. Since creep damage could lead to failure of the coating system during extreme temperature service, the creep behaviour will also be discussed, along with the plastic behaviour. Finally, the design concerns of each layer of the TBC will be introduced.

2.3.1 **Material properties of the YSZ ceramic layer**

A typical YSZ TC morphology produced by either EB-PVD or APS mainly contains yttria stabilised zirconia (YSZ), as illustrated in Fig 2.1 a) and b).

With TC's complex inhomogeneous microstructure, several properties need to be included while studying TC's mechanical behaviour. First is the porosity, and second is the aging effect. Because

of its complex microstructure, the YSZ TC will be treated as a transversely isotropic elastic material for simplicity, as discussed next.

2.3.1.1 Porosity of the transversely isotropic YSZ TC

According to the literature, due to sintering taking effect after long isothermal cycles (for example, 13,500 hrs at 870 °C [Frachon, 2013]), the evolution of the microstructure results in a significant decrease in porosity. Therefore, densification of the material should be accounted for when modeling the TBC system.

Inside the YSZ TC layer, the microstructure can be divided into two sections. Close to the top of the ceramic layer, the external porosity is quasi-constant and is dependent on the time-temperature thermal loading, whereas the ceramic at the location close to the oxide layer has a much lower porosity. On average, at the end of a 1,000-hour long exposure time at high temperature, the TC layer's two zones exhibit microstructures with porosities that are 8% different. The external porosity ranges from 5 to 14%, while the internal porosity (in the zone close to the TGO layer) is well below 5%.

In the present study, the internal porosity will be set at 5%. The external porosity will be decreasing almost linearly through high temperature exposure due to the consolidation from the sintering effect. The initial value of external porosity will be set at 15% and gradually decreased roughly to 10%.

The sintering phenomenon resulting in a decrease in porosity will be reflected by the material's Young's modulus. As the service time at high temperature increases, the material densifies, and the elastic stiffness of the TC material increases, which further increases residual stresses.

Tilman [Beck, T. et al., 2008] introduced a function to illustrate the change in Young's modulus with respect to heat time. In Chapter 3, this function will be calibrated to fit the current model. In the paper published by Zhu et al. in 2015, as shown in Fig. 2.2, the change in Young's modulus

due to sintering was also analysed using a graphical expression which also aligned with Tilman's function.

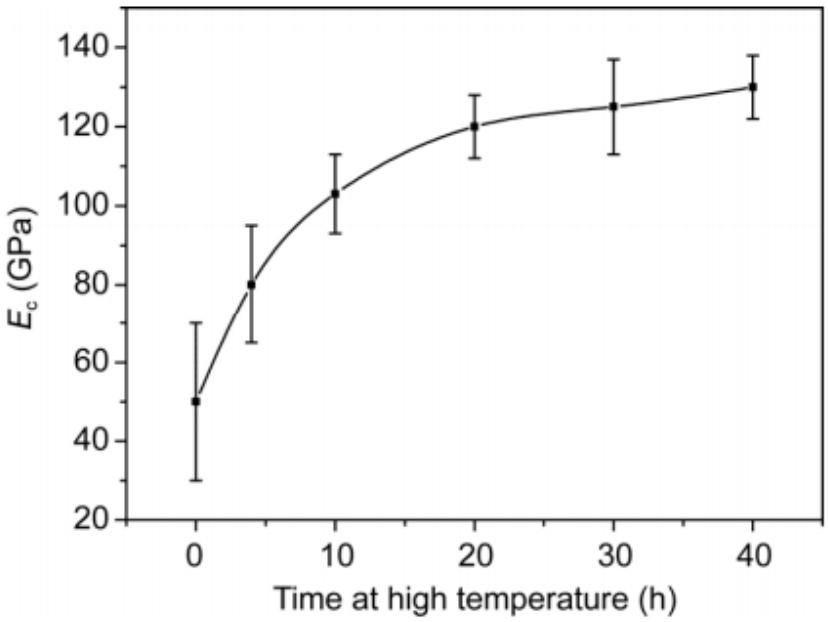

Figure 2.2. Evolution of elastic modulus of TC estimated by the indentation tests, with error bars for standard deviation [Zhu et al., 2015].

2.3.1.2 Creep behaviour of the TC ceramic layer

In [Freburg et al., 1998], creep properties of TC were shown to induce non-zero residual stresses across the coating upon cooling down even in the absence of the TGO growth during thermal cycling, whereas the TBC coating system's residual stresses return to zero after cooling down when the TC creep is absent. This was also observed in [Zhu et al., 2005], whose FE model results are reproduced in Fig. 2.3 for the TBC coating: when the creep behaviour is not included, the maximum tensile stress presents a different trend than with creep in the TC layer, irrespective of the inclusion of sintering effect in the TC layer. The result of the case with no creep contradicted the experimental observation. Therefore, we conclude that the creep behaviour is important to include in simulations.

In the present study, creep will be represented by the following power law:

$$\dot{\varepsilon}_{eq}^{cr} = C_1 \sigma_{eq}^{C_2} \, e^{-\frac{C3}{T}} \qquad (2.1)$$

where T is absolute temperature, an C_1, C_2 and C_3 are fitted parameters. These creep parameters are fitted from the average experimental data [Taylor et al., 2007 and Cheng et al., 1998].

The function above was calibrated from the Norton secondary creep function [Frachon. 2013]:

$$\dot{\varepsilon}_{eq}^{cr} = A\left(\frac{\sigma_{eq}}{\sigma_0}\right)^n e^{-\left(\frac{Q}{RT}\right)} \quad (2.2)$$

where A is the creep constant, set at 5.1×10^{16}; Q is the activation energy, set at 690 KJ/mol; R is the fundamental molar gas constant (8.314 J/mol), and σ_0 is a scaling parameter fixed and equal to 100 MPa. The creep exponent value n is 1.85. The material constants A, and Q were taken from the experimental data averaged from Y-doped alumina and pure alumina, and σ_{eq} is the Von Mises equivalent stress.

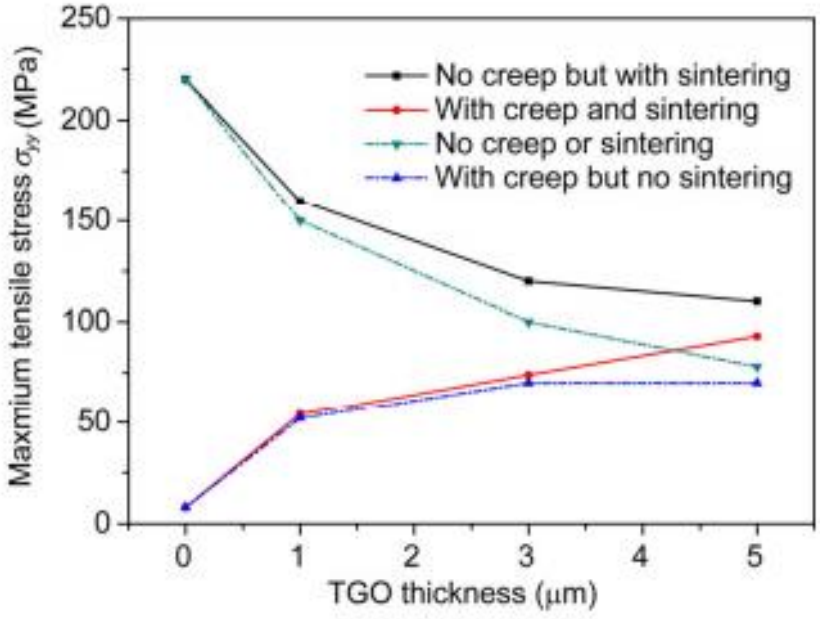

Figure 2.3. Effects of creep and sintering on the maximum tensile stress in TC [Zhu et al., 2015].

2.3.2 **Material properties of the TGO layer**

Even though the TGO layer is relatively thin compared to the other TBC constituents, it is very important when considering the lifetime of the TBC system. TGO brings extra CTE mismatch between constituents and induces large growth stresses from its locally large deformation (volumetric expansion) on the constrained interface. This thin layer that develops at the BC ceramic interface is where the damage usually develops, and is responsible for a decrease in interface toughness [Guo et al., 2007]. Moreover, the increase in the oxide thickness during service also increases the stored elastic strain energy per unit area, which in turn causes TBC spallation. Therefore, the TGO layer behaviour plays an important role in the TBC lifetime. The following section will focus on: (i) the elastic behaviour of the TGO layer; (ii) the evolution of the TGO thickness; and (iii) the creep behaviour of the TGO layer.

2.3.2.1 **Elastic behaviour for the TGO layer**

In the FE model introduced in this thesis, the TGO material will be regarded to have visco-elastic characteristic with no plastic strain occurring.

The elastic properties of the TGO will be isotropic and homogeneous as the main component is α-alumina. Its Young's modulus and Poisson's ratio will be taken from experiments [Cheng et al., 1998], and extrapolated as functions of the temperature:

$$E = 410 - 0.041T \qquad (2.3)$$

$$\nu = 0.23 - 210^{-5}T. \qquad (2.4)$$

where E is in GPa and temperature is described in Kelvin. Table 1 summarizes the TGO elastic properties at various temperatures along with BC and TC elastic properties. The data shown in Table. 1 are only limited to certain temperatures, but because of the temperature dependency of

the material properties, the interpolation of Young's modulus of the TGO layer was needed, due to its impact on stresses over the whole TBC system.

2.3.2.2 TGO growth kinetics

A key physical feature from the BC layer is its oxidation behaviour. The TGO formation allows the system to form a non-porous and adhesive layer. Because α-Al_2O_3 is responsible for the spallation failure of the TBC system in many ways, we need to investigate the oxidation growth kinetic to better understand the lifetime of the TBC system.

From a chemical point of view, the oxidation occurs not only at the outer interface where the outward diffusion of Al occurs, but also at the inner interface. Yet, the outward diffusion is more relevant to the formation of α-alumina. Therefore, for simplicity of the model, only outward diffusion of the Al cation is considered.

Busso et al. [2001] used a growth law function to describe the oxidation thickness with respect to time, which becomes very helpful for the development of the calibrated oxidation model that will be described in Chapter 3. Also, Beck [Beck et al., 2008] suggested an incremental calculation method for the calculation of TGO growth within each thermal cycle during thermal cycling as a companion to the parabolic law that other researchers like [Busso et al., 2001] proposed. The result obtained using the author's method was described in a graph which will be useful for a comparison with the current model results.

2.3.2.3 Creep behaviour of the oxide layer

The long-term creep properties of the TGO layer may affect the lifetime of the TBC system operating at elevated temperature. The creep behaviour of TGO can be described with a function which is dependent on temperature and stress, as done for TC creep:

$$\dot{\varepsilon}_{eq}^{cr} = A\left(\frac{\sigma_{eq}}{\sigma_0}\right)^n e^{-\left(\frac{Q}{RT}\right)} \qquad (2.5)$$

To better meet the needs of the simulation software used in this study, this function will be transformed as explained in the following chapter.

2.3.3 BC material characteristics

The BC layer has arguably a great influence on the ability of the TC layer to resist spallation, owing to its creep and the plastic characteristics. For a general model, the total strain is decomposed into plastic and elastic components:

$$\varepsilon = \varepsilon_{el} + \varepsilon_{pl} \qquad (2.6)$$

where the creep behaviour of BC allows for stress relaxation. BC's material elastic and plastic characteristics are discussed in the following section.

2.3.3.1 BC's elastic behaviour

The BC described in this work consists of NiCoCrAlY. It is an isotropic multiphase material whose microstructure evolves with oxidation time. Its Young's modulus also depends on temperature, while its Poisson's ratio of 0.3 is independent of temperature. To describe the temperature-dependent elastic material properties of the BC, data are listed in Table 1. It is worth noting that in this study, the orientation of the TC-BC interface roughness is not considered to affect the elastic properties. In other words, all the properties listed in the table will be used as global values.

Material	Bond Coat			Oxide			Ceramic (Topcoat)		
Temperature	*E*	*α*	*v*	*E*	*α*	*v*	*E*	α	*v*
(°C)	**(GPa)**	**(10^{-6}°C^{-1})**		**(GPa)**	**(10^{-6}°C^{-1})**		**(GPa)**	**(10^{-6}°C^{-1})**	
25	117	12.3	0.3	400	8	0.3	67	9.7	0.1
200	113	11.9	↓	390	8.3	↓	64	9.8	↓
600	104	15.2		370	8.7		60	9.9	
800	99	16.3		355	9		58	10	
1000	94	17.2		325	9.3		58	10.1	
1100	92	17.7		320	9.5		56	↓	

Table 1. Elastic material data for each of the TBC constituents [Cheng et al., 1998, Freborg et al., 1998 and Frost et al., 1982].

2.3.3.2 BC inelastic behaviour

The BC layer has weak creep material properties which allow the TBC system to relax the stress induced during oxidation and thermal expansion mismatch during cooling. Busso et al. [2001] proposed a homogenisation method for the creep properties of the multiphase material, taking experimental results as a basis. For the present study, it was also decided to adopt equation (2.2) for the BC layer, but simplify it as described in Chapter 3.

In addition to the rate-independent creep behaviour, the BC plastic behaviour also holds an important position in the study of residual stress. The plasticity of the layer has both rate-dependent and rate-independent components, and the yield stress depends on the temperature of the material. The yield stress is listed in Table 2, taken from Cheng et al.'s [1998] experimental data. The plastic stress term of the BC layer can be modeled as bilinear isotropic hardening as the model undergoes cyclic thermal loading (Fig. 3.8). The back stress tensor for the bilinear kinematic hardening evolves so that the effective stress versus effective strain curve is bilinear. The change in plastic strain is imposed by temperature: if the temperature remains unchanged, then is no change in plastic strain. The bilinear isotropic hardening concept will be further described in Chapter 3.

σ_y(MPa)		
$T(^0C)$	*BC*	*TGO*
20	*426*	*8000*
400	*396*	↓
600	*260*	
800	*199*	
1000	*120*	*300*

Table 2. Plastic properties of the bond coat and thermally grown oxide layer [Lapin, J., 1997].

2.4 STRESSES AND FAILURE MECHANISMS

It is critical to understand the role of stresses in the failure mechanism of TBC systems. Two main stress sources can lead to failure, as addressed in the following subsections.

2.4.1 The effect of thermal expansion mismatch upon residual stress and the introduction of relative CTE

Thermal expansion mismatch upon cooling exerts a great influence on TBC system failure. At low temperature, an in-plane stress is generated by the thermal expansion mismatch between the TBC constituents and the substrate layer, as seen in Fig. 2.5 (b).

Analytically, the in-plane stress in the TBC constituents can be formulated as follows:

$$\sigma_{11}^{th} = \frac{\Delta\varepsilon_{th}}{1-\nu} E_1 \qquad (2.7)$$

where σ_{11}^{th} is the in-plane stress that is generated by thermal expansion mismatch between the TBC layers and the substrate, and $\Delta\varepsilon_{th}$ is the relative thermal expansion strain between the TBC constituents and the bottom substrate layer. $\Delta\varepsilon_{th}$ can be expressed as:

$$\Delta\varepsilon_{th}^{i}=\varepsilon_{th}^{i}-\varepsilon_{th}^{sub}=\Delta\alpha^{i}(T)\Delta T \qquad (2.8)$$

where subscript i refers to one of the YSZ, TGO or the BC layers. $\Delta\alpha^{i}(T)$ denotes the relative thermal expansion coefficient between the TBC layers and substrate, as illustrated in Fig.2.5 (b).

In the present study, the thermal expansion mismatch during deposition will be omitted, only considering instead the thermal expansion mismatch during the time during service at the peak temperature T_{peak}. Therefore, σ_{11}^{th} can be expressed as:

$$\sigma_{11}^{th}=\frac{\Delta\alpha^{TGO}(T)(T-T_{peak})}{1-\nu^{TGO}}E_{1}^{TGO} \qquad (2.9)$$

When the temperature cools down to ambient temperature, a large compressive stress is induced, and is explained by the difference in thermal expansion coefficient between the TGO and the substrate.

At high temperature, the in-plane stress is generated by the BC oxidation growth strain, which can be expressed analytically as:

$$\sigma_{11}^{ox}=\frac{\varepsilon_{ox}}{1-\nu}E_{TGO} \qquad (2.10)$$

where ε_{ox} denotes the BC-TGO transition zone oxide growth strain generated at high temperature during BC oxidation and E_{TGO} denotes the Young's modulus of the newly grown TGO.

The thermal properties of each constituent are listed in Table 1. The analytical results regarding thermal expansion mismatch will be compared to FE results in the following chapter.

2.4.2 **Oxidation induced growth stress**

Upon oxidation, the metallic BC is gradually transformed into new oxide, and the volumetric expansion is induced at the TGO-BC interface. The growth of TGO affects the stress distribution

in two ways: on the one hand, the low CTE of the TGO changes the pattern of thermal expansion mismatch, as discussed in Section 2.4.1; on the other hand, transverse growth strain is induced by the alumina that forms inside TGO grain boundaries. Such growth strain associated with the BC oxidation reaction is responsible for inducing high compressive stresses at high temperature. Unlike the stress induced by thermal expansion mismatch, the oxidation growth strain occurs predominantly on one of the interfaces close to the TC-TGO where the new oxidation occurs, rather than uniformly throughout the TGO layer.

The anisotropic growth strain represents the overall volume increase upon oxidation. This mechanism is one of the main sources of stresses in TBC systems. According to a study [Frachon, J., 2013], the ratio between normal and transverse strain components is

$$\varepsilon_N = 87\varepsilon_T \qquad (2.11)$$

The stress associated with such growth strain is arguably one of the major driving forces to create damage close to the TGO-BC interface at high temperature, giving rise to further spallation (at the TC-TGO interface).

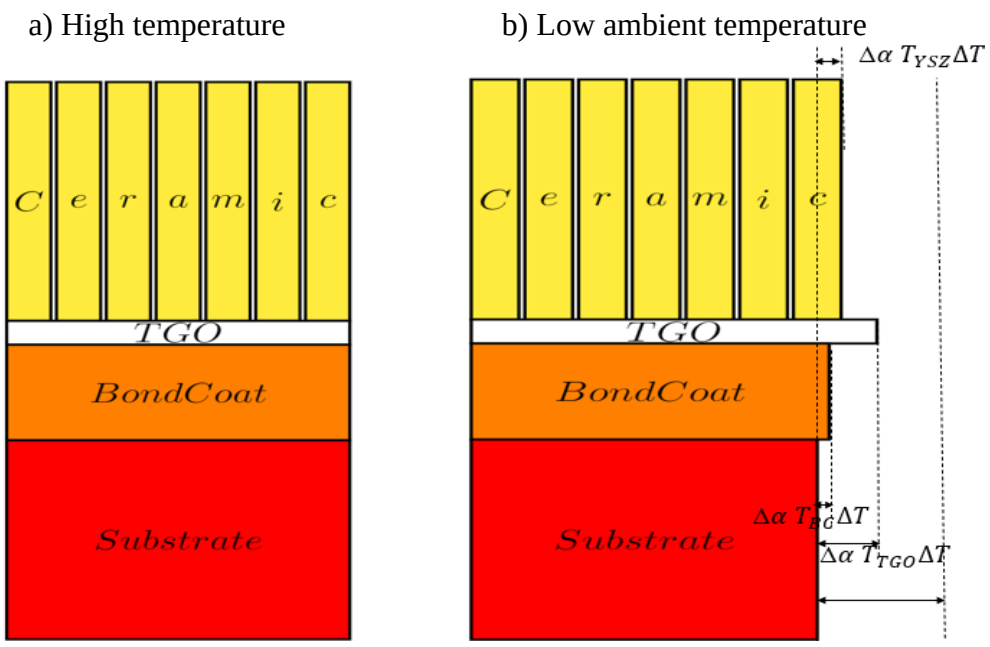

Figure 2.4. Illustration of the thermal expansion mismatch between TBC layers and substrate. Note that this is only an illustration for showing the concept of a difference in thermal expansion coefficient properties, as the system itself does now actually expand into different widths as each of the TBC constituents are assumed to be perfectly bonded.

2.5 KNOWLEDGE GAP AND PROPOSED IMPROVEMENTS

Many researchers have carried out numerical simulations of TBC. For instance, Freborg [1998] studied the oxidation induced stress in TBC and made a thorough review of each individual effect of the materials' mechanical behaviours. Yet, the model had limitations regarding the failure mechanisms. Factors such as sintering phase changes in the oxide, BC and ceramic layers were not studied. Compositional changes during thermal cycles were not investigated.

Evans et al. studied TBC residual stress. In particular, [Evan et al., 2001] discussed in detail the mechanisms that govern the durability of the TBC system. The authors provided in depth information about each layer of the TBC systems regarding composition, properties and stresses related to the specific phenomena within the constituents. They also discussed the failure mechanisms associated with each of the layers' mechanisms. In the description of the failure mechanisms, the author used a systemic approach for discussing the influence of composition on different TGO design and performance.

Wei [2006]'s work was a valuable resource of experimental data. They discussed in detail the effect of temperature on rumpling, compared the TGO growth law with experimental findings. They represented the roughness variation throughout hundreds of cycles using a Fourier series decomposition. They analyzed the microstructural evolution near the spallation, as well as the average lifetime at different temperatures. Lastly, they discussed the average stress induced by TGO growth, which was also a valuable reference for comparison with the model developed herein. Furthermore, according to their analysis, spallation decreases by a factor of 5 when the cycling hot temperature increases by 100 ℃. This significant impact of temperature on lifetime motivated us to use a high temperature of heating (1,150 ℃) for a shorter modeling duration, to try and reach results similar to those obtained at lower holding temperature.

In Lapin [1997], the effect of aging in the high temperature ranges from $1{,}023 - 1{,}373$ K was investigated along with the mechanical and the micro structure of a directly solidified Ni_3Al based alloy. Through the experimental testing, the author presented the lamellae structure of the alloy, via SEM and TEM graph, and established the relationship between aging temperature and volume

fraction of the lamellas. Eventually, through a series of stress, strain and strength analyses of the aged alloy, the stability criterion, strain-hardening rate's correlation with aging was described. In addition to this, other references were beneficial for the understanding and modeling of the sintering effect and the viscosity that accompanied with the annealing process. In particular works by Frachon, Zhu, Baker, Busso, and Ahrens.

Amongst many other papers, Rösler et al. [2001] did in-depth simulation work on the APS TBC, and carried out a series of parametric studies of the stress state in TBCs, including the effects of creep and cooling stresses. Compared to Freborg's [1998] work, the model was enhanced; the microstructure, such as the porosity effect on material properties was considered; the effect of the material characteristics through the evolution of the composition of the layers was also included, and the FE mesh was more refined as well. Rösler also devised a simple mechanical model for understanding the radial stresses in a simpler manner. However, the model is still too simple to understand the effect fully. We would like to enhance Rösler's work on the model geometry, and give detailed illustration of the swelling effect's influence on the residual stress distribution, as it is potentially quite influential, and could be elaborated further for a better understanding of the material behavioural.

[Aktaa et al., 2005] assessed TBC system failure mechanisms using a fracture mechanics approach. They first constructed a TBC system model using finite element (FE) analysis. They considered all layers to be isotropic and linear-elastic, except for the BC layer's stationary creep assumption. They compared residual stresses. i.e. the stresses after heating and cooling, with or without the inclusion of the TGO growth. They investigated the influence of the roughness on the residual stress by comparing different interface amplitudes. Based on the residual stress distributions, the authors concluded that since the quantitative increment in the residual stress and the qualitative distribution of the stress remained unchanged, cracks may only be formed in the peak region of the roughness, very close to the interface. The authors then investigated the mechanisms of crack propagation after initiation. This article was a very helpful reference for validating residual stress results in the current thesis. It was also an inspiration to study the influence of roughness on residual stress, and to consider a half period of the coupon in the model due to the periodicity of the sine wave of the roughness, which saves computing time. Prompted by the linearly elastic assumption, we would like to extend the model into a more complex one to investigate plastic

phenomena that would have impact on longer thermal cycles, to enhance the analysis for sources of crack initiation.

[Ranjbar-Far et al., 2010] also use a parametric FE analysis to investigate the influence of material behaviour and interfacial roughness on the TBC system's residual stress. They used a flow chart to illustrate the numerical simulation steps. They imposed swelling as a strain rate into the model, used a local coordinate system, and quadratic six nodes triangular elements. This work inspired us to do a parallel study of the dynamic swelling with the static strain rate for representing swelling to validate further on Rösler (2010)'s work.

In the present study, it was decided to use FE analysis to conduct a systematic and parametric investigation of the influence, by modifying the TBC constituents' material behaviour progressively, of material behaviour on residual stress to gain insights on crack initiation location, and possible material composition refinements to optimize the coating. FE analysis was chosen because computational simulation is invaluable when dealing with complex interactions between nonlinear material behaviour. Because many previous FE analyses described in the literature yielded quite different results, it was important to build our own experience and revisit many previous investigations for progressive and systematic validation. The TBC system will be modeled as a 2-D structure, and feature mesh characteristics that are completely controllable by the user: each of the element width and length will be user-defined, making mesh refinement straightforward. The geometry will be analysed not only with the traditional sinusoidal profile introduced in the literature, but also based on SEM imaging. By investigating a wide range of material data, the model is expected to reach increasingly accurate information about residual stress distribution in TBC, allowing one to answer questions about individual material behaviour effects. The present work may eventually constitute a foundation for future assessments of TBC lifetime.

3 MODELING PROCEDURE

The description of the 2-D model will start with the criteria used for the software and element selection, followed by the model geometry, along with the boundary conditions description. Then, the parameters that describe the oxidation model will be introduced, along with the implementation of creep, swelling strain and plasticity into the model.

3.1 THE SOFTWARE AND ELEMENT SELECTION

Given the complexity of the phenomena to be modeled, the availability and the excellent capabilities of commercial code ANSYS version 19.2 (ANSYS, Canonsburg, Pennsylvania, USA), this is the FE package that was used in this thesis. ANSYS comes with the APDL package which allows for macro coding. Compared to the traditional GUI, scripting gives the user more direct control over the model, reducing chances of errors in a model as complex as the present one.

TBC simulation using FE analysis requires thermomechanical effects to be included, and this means that thermal and structural analyses need to be coupled, possibly in an iterative, sequential manner. There were a priori to possible avenues to do so:

1. Direct coupled field analysis, where thermal and mechanical solutions can be obtained simultaneously. This requires the use of thermal-mechanical coupled elements that are similar to structural elements but provide an extra degree of freedom for temperature.
2. Indirect coupled field analysis, where temperature distribution and history of temperature must be calculated and stored at first, then imported into each consecutive stress analysis load steps as thermal boundary conditions/temperature profiles. This requires the use of thermal elements first to analyze the thermal problem. Later in the process, thermal elements are replaced with compatible structural elements (the thermal and structural elements need to share common nodes) to continue with the structural analyses.

The first option, with PLANE233, a 2-D 8-node coupled-field solid element (Fig.3.1 a), provided the convenience of not having to switch elements in between coupled analyses, owing to its ability to support a structural-thermal combined physics. However, such element did not allow us to include swelling strain induced by the TGO growth. For this reason, the direct coupled filed analysis was not retained. Instead, indirect coupled field analysis was carried out using 2-D 4-node elements instead of an 8-node element (Fig.3.1 b). This saved computing time (944.42 s to compute a 2,400 s thermal loading shown in Fig.3.4 for purely elastic TBC constituents material behaviour for PLANE223 vs. 872.86 s for PLANE 55 and PLANE182 modeling using the same thermal profile and material behaviour) without sacrificing accuracy and stability, as long as a proper mesh sensitivity analysis would be performed. Moreover, the structural solid element could have the single DOF temperature element analyzed structurally. It also could be used as an axisymmetric element to determine the stress in the third direction. Therefore, PLANE55 thermal elements were selected for the thermal models, and PLANE182 structural element were used thereafter.

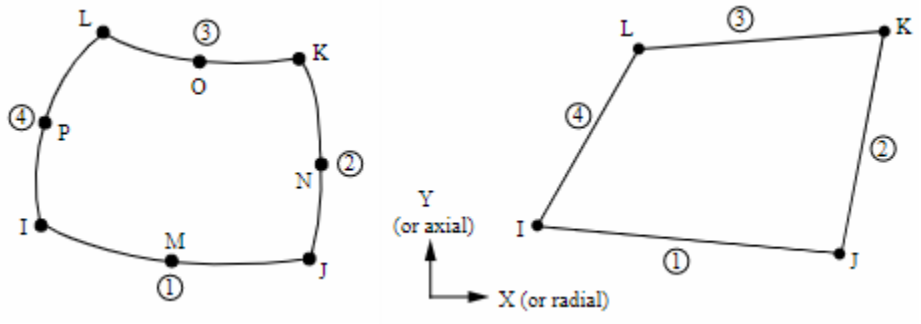

Figure 3.1. a) PLANE223 element geometry b) PLANE55/182 element geometry

The FE analyses for stress prediction in this thesis were carried out in three general steps. As shown in Fig.3.2, first, a thermal solution was generated with only the necessary thermal material properties incorporated. After solving for the temperature as a thermal loading history, the structural material properties were included, along with the structural displacement constraints, and different time-varying temperature load steps were imposed to the elements in the model for

transient structural analyses. All layers were assumed to be transversely isotropic and the as-received coupon analyzed was assumed to be initially stress free at room temperature.

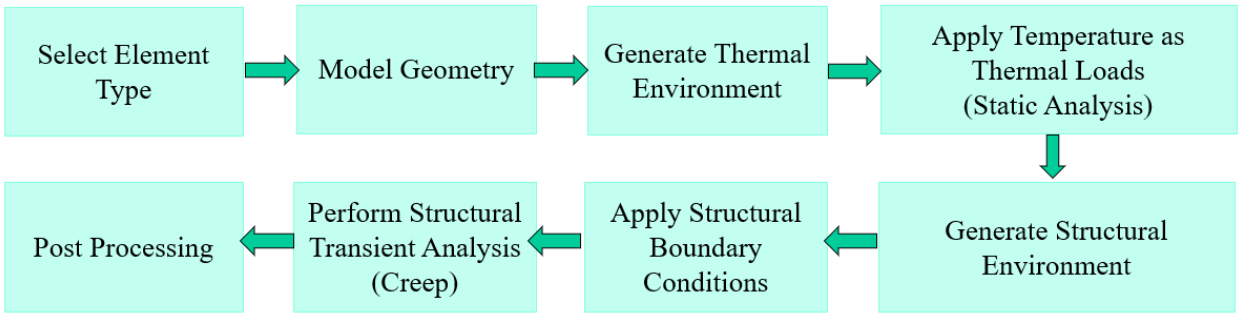

Figure 3.2. Flow chart of the FE modeling procedure used in the thesis

.

3.2 GEOMETRY

A three-layered axially symmetric two-dimensional sample was constructed as shown in Fig.3.3. As stated previously, the model geometry consisted of a substrate, a bond coat layer, and a top coat. During the initiation stage of the thermal cycle, a very thin layer of thermally grown oxide was formed in between of the BC-TC interface, and this layer will grow during the high temperature phases of the thermal cycling. The model represented a solid cylinder with infinite length in its axial direction on the substrate side.

Because the substrate can practically be considered as an elastic material and will hardly reach its yield stress, it was not the main focus while examining the lifetime of TBC system. Therefore, in the simplified 2-D model, the substrate was not modeled. Instead, a relative thermal coefficient was used for it, as explained in detail in Section 2.5.1. Conversely, the TGO layer is widely believed to be the determining factor of the thermal barrier coating system's failure due to spallation, and deserved attention.

The BC layer had a thickness of 130 μm. It consisted of $NiCoCrAl$. There was no initial TGO at the beginning of the simulation. The TC layer had an average thickness of 250 μm. These values were selected for easier comparison with the results from Rösler et al. [2001] in Chapter 4.

In Cheng et al. [1998]'s FE model, it was again validated that bending and rotation play little roles in the TBC system due to its thin nature. This prompted us to treat the 2-D model as flat. The geometric modeling of the complex TC-BC interface called for simplifications to make the approach tractable. Therefore, the TC-BC interface was first introduced as an idealized sinusoidal profile with an amplitude of 10 μm and a wavelength of 24 μm to match the study from Rösler et al. [2001].

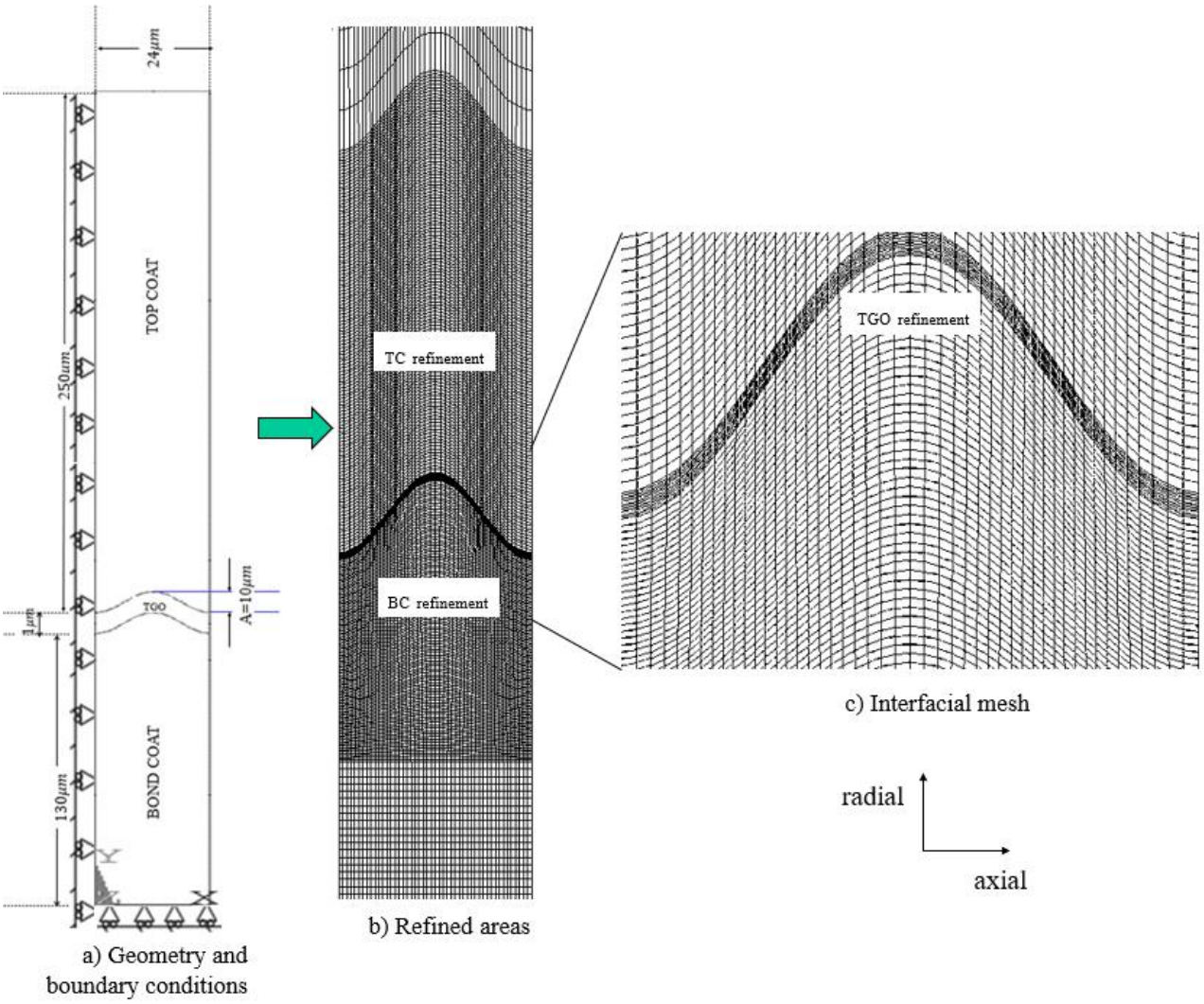

Figure 3.3. Cross sectional geometry of the axially symmetric model with a detailed mesh shown refined in certain TC, TGO and BC regions.

3.3 MESH CHARACTERISTICS

Because of the precision needed for modeling a small thickness growth for the TGO layer, the finite element model of the TBC system required a large number of elements, and an increasingly finer mesh near the TC-BC interface to allow for a good resolution of the residual stresses in the region. After a mesh sensitivity analysis[1], the FE model consisted of 30,001 nodes and 23,808

[1] More information about the mesh sensitivity analysis shown in Appendix-I.

axisymmetric elements as shown in Fig.3.3 b) and c). The average element size was 0.083 μm. The entire refined elements area had a thickness of 1 μm, consisting of a total of 12 layers (for the verification model in Chapter 4). These layers will be converted from BC to TGO during the simulation, as described in the following section.

Using a refined mesh only in some areas of the model saved significant time (days of computation) during thermal cycling. In addition, the ANSYS version was academic usage, the number of elements and nodes in the model was limited. Therefore, it was important to only refine the mesh in the regions that were affected by the loading in a complex fashion. For instance, in the region of TC closer to the TGO interface, the mesh density was increased by 2 compared to the other TC regions as reflected in Fig.3.3 b), to correctly represent the stress distribution.

3.4 BOUNDARY CONDITIONS

The thermal boundary condition was basically just the temperature loading defined in the thermal load steps and applied later in the structural analysis on the model. As the objective was to simulate a burner rig test during FE analysis, the other thermal properties were omitted.

As illustrated in Fig.3.3 a), the model was constrained on one side in the radial direction to simulate a full cylinder with no inner hole. All the nodes on the right-hand side of the model were able to move freely in the axial direction but were constrained to have the same radial displacement. The nodes at the bottom of the model (i.e. at the bottom of the BC layer) were constrained in the axial direction, as the substrate layer was relatively rigid and restrained any expansion of the coating material. This boundary condition was periodic along the axial direction to represent an infinitely long sample constrained in the axial direction.

3.5 TEMPERATURE PROFILE (THERMAL LOADING)

In the proposed FE model, one thermal cycle was described in three load steps. For simulating TBC's mechanical behaviour under various conditions, cyclic thermal loading was considered. During a thermal cycle, the temperature of the entire model was imposed as a homogeneous temperature distribution. Therefore, thermal properties such as conduction were deemed unnecessary.

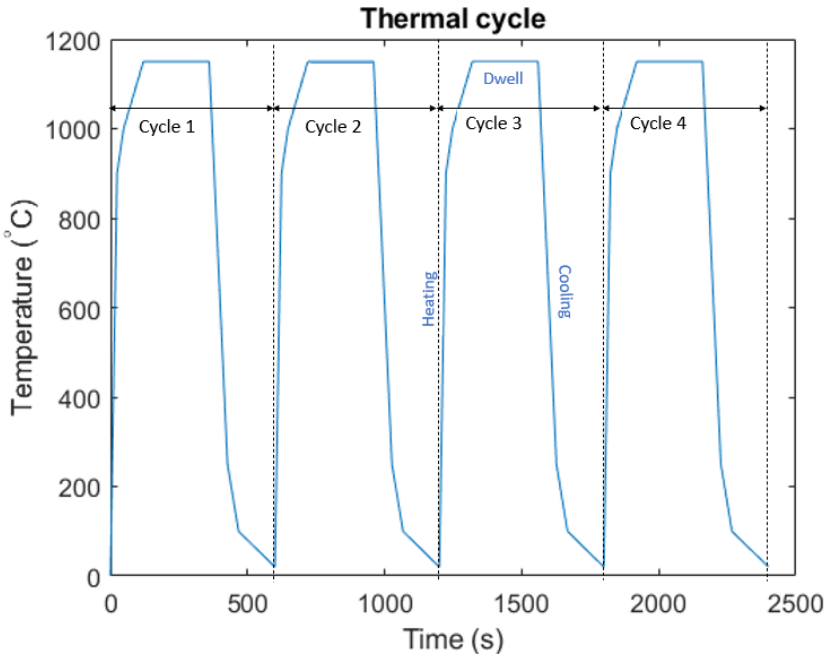

Figure 3.4. Temperature profile used in FE simulation for Chapter 4. Each thermal cycle was 600 s, with temperature ramping up from room temperature to peak temperature in 120 s, dwelling for 120 s and cooling down to ambient temperature in 240 s.

In the initial state, the room temperature was 20 °C and the TBC system was assumed to be stress free. This assumption was aligned with the literature for APS-TBC deposition [Rösler et al., 2001]. Then, the temperature ramped up to 1,150 °C in 120 seconds.

Throughout the steady state dwelling phase, the temperature was maintained at 1,150 °C for 240 s, during which time the oxide layer growth was examined. Because the case modeled did not feature internal cooling, there was no temperature gradient during this phase.

The temperature was finally ramped down to room temperature from the peak temperature, with an uneven cooling rate, for a period of 240 seconds.

To achieve uneven heating and cooling rates, several linearly interpolated sub-steps during the heating and cooling phases were included for modeling a more accurate thermal cycle. The approach followed in adding sub-steps was to not only imitate the true heating cycle, but also keep the load step static for the thermal analysis. Four cycles were analyzed, as shown in Fig. 3.4.

3.6 COUPLED FIELD ANALYSIS IMPLEMENTATION

As discussed in Section 3.1, using two separate, but compatible, elements for thermal and structural analyses, swelling strain could be included into the structural model. This method required coupling between fields by using load-transfer coupling. The load-transfer was accomplished by applying the thermal loading results to the structural model as boundary conditions in the form of set nodal temperatures. A Newton-Raphson technique was required to predict the results at each of the iteration for convergence of the solution.

In the structural analysis, there were both static and transient solutions depending on the nature of the load step. At low temperature, the creep and plastic behaviours were not dominant; therefore, the load steps were set as static. On the other hand, when the system was under heat, the analyses were set as transient to take creep, and plastic behaviour into account along with the active thermally grown oxidation.

3.7 IMPLEMENTATION OF MATERIAL BEHAVIOURS

In this section, the method of implementation for the important material parameters are introduced. As seen in Table 1, the material properties of the constituents were not constant. For instance, the TGO growth was modeled by changing BC material properties into those of new TGO as a function

of time; BC/TC/TGO creep was calibrated from published experimental data and fitted into the form of function that ANSYS could recognize. The swelling strain was modeled by adopting two methods for comparison. The relative thermal expansion was introduced, as discussed in Chapter 2. Plasticity and sintering were also calibrated for use in the extended model Chapter. Sintering of the TC layer was implemented via a new constant value of Young's modulus for each timestep of one layer of TGO's formation, based on the assumption that the rate of change in TC's Young's modulus was small during one time step of TGO formation.

3.7.1 **TGO growth kinetics and modeling**

For a realistic model where a long dwelling cycle could be used, the oxidation model was calibrated from reference [Busso et al, 2001]. When only inward oxidation was considered, the TGO thickening mechanisms during the holding temperature at $1{,}150\ ℃$ is in accordance with the following oxidation kinetics:

$$\mathrm{h_{ox}} = \mathrm{h_0} + kt_{ox}^{m} \qquad (3.1)$$

where h_{ox} is the TGO thickness locate at the metallic layer/ceramic layer interface, $\mathrm{h_0}$ is the specimen's oxide thickness at the end of the initiation thermal cycle (in Chapter 5, $\mathrm{h_0} = 0.0825\ \mu m$ will be the thickness generated during the initiation thermal cycle), $\boldsymbol{t_{ox}}$ is the oxidation time, which is the time the TBC is held at high temperature during the thermal cycles. The oxidation constant, $\boldsymbol{k}$ is equal to $4.91 \times 10^{-2}\ \mu m^{m} h^{-1}$ at 1,150℃. Noted that the oxide growth exponent m was set at $\frac{2}{3}$, which is a typical value obtained from a simple theory of oxidation diffusion process. The growth of a new TGO is considered parabolic up until the point where spallation takes place.

The equation (3.1) above predicts a total alumina TGO thickness of $3.85\ \mu m$ after a 500-hour period of exposure at $1{,}150\ ℃$. Fig.3.5 shows the oxidation growth with respect to oxidation time based on the function in equation (3.1).

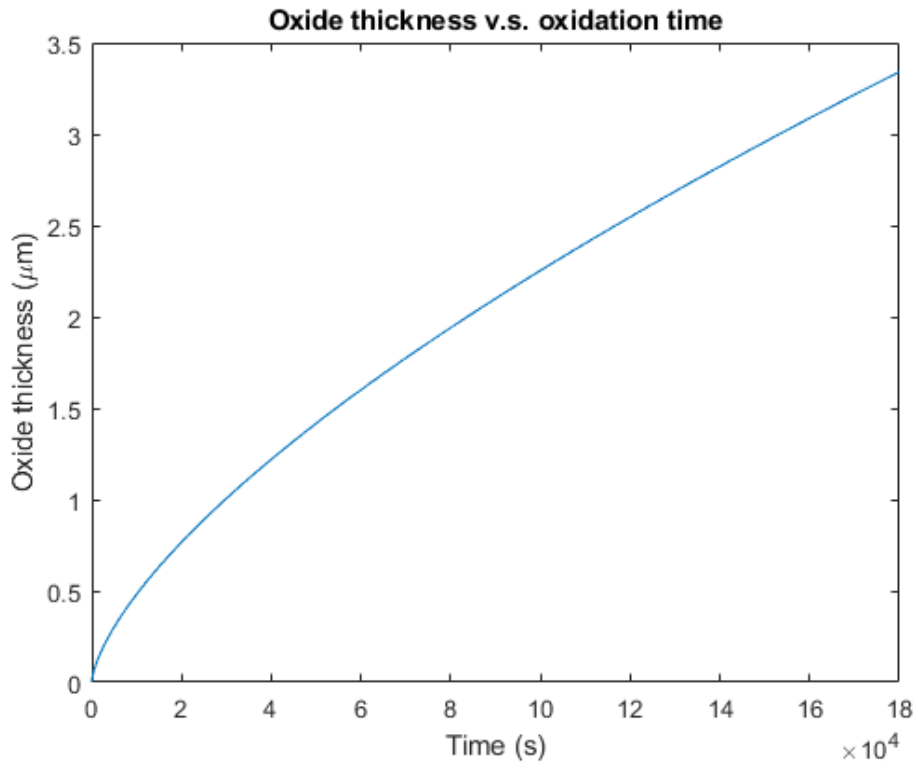

Figure 3.5. TGO growth calibration for a period of 50 hours at 1,150 °C.

For convenience, the growth rate was set to be constant as

$$\dot{h}_{gr} = \frac{r}{2*h_0} \qquad (3.2)$$

where $\dot{h}_{gr}$ was the growth rate, h_0 the initial TGO thickness and r is a fitting parameter. All values on the right-hand side of the equation (3.2) were constant; therefore, the growth rate was constant.

After determining the oxidation kinetics, the next step was to drive the spatial oxidation growth within finite element mesh. The model was layered in a way that the TGO elements could be controlled as functions of time. The TBC system is prone to oxidation only when the system is maintained at high temperature. When t_{ox} reached the time corresponding to a full layer of elements, the elements in this layer were transformed from BC material properties into TGO. The

thickness of each layer was manually adjustable by changing the thickness variable in the model to suit the simulation needs.

3.7.2 **Creep modeling**

Stress relaxation is important in understanding the stress evolution of the TBC system. It can be defined as developing strain under constant applied stress. The high temperature stress was implemented using time-independent creep simulation for simplicity. In the numerical simulation, the creep strain rate of the constituents obeyed the Norton secondary creep criterion, with an alteration that was compatible with ANSYS scripting:

$$\dot{\varepsilon}_{eq}^{cr} = B\sigma_{eq}^{n} \qquad (3.3)$$

where $\dot{\boldsymbol{\varepsilon}}_{\boldsymbol{eq}}^{\boldsymbol{cr}}$ was the strain rate(s^{-1}), $\boldsymbol{\sigma_{eq}}$ the equivalent stress (MPa), $\boldsymbol{B}$ a constant ($s^{-1}MPa^{-n}$) and n the power law creep exponent. It was implemented for TC, TGO and BC layers, with the parameter values listed in Table 3. These creep parameters were taken as average values from experimental data [Taylor et al., 2007].

Material	**T (°C)**	$\mathbf{B}[\frac{\mathbf{1}}{\mathbf{sPa^n}}]$	**n**
Bond Coat	≥ 1,000	$1.39x10^{-25}$	3
	≥ 1,150	$2.35x10^{-24}$	3
Oxide	≥ 1,000	$7.3x10^{-10}$	1
	≥ 1,150	$4.2x10^{-8}$	1
Ceramic	≥ 1,150	$2.57x10^{-26}$	3

Table 3. Creep properties of the TBC constituents [Taylor et al., 2007].

3.7.3 **Swelling strain Modeling**

In addition to the growth in the thickness direction that was modeled by changing the material properties from BC to TGO, the expansion of the crystallographic volume in the TGO during oxidation process could also be implemented as a form of material swelling. The swelling strain is also called growth strain. It is the strain that is induced by oxidation of the BC layer. During oxidation, the BC material is transformed into alumina. This transformation induces a 28% volumetric expansion (Pilling Bedward ratio; it was assumed that the growth stress was determined by the R_{PB} value. $R_{PB} = \frac{\boldsymbol{\rho} oxide \cdot \boldsymbol{M} oxide}{\boldsymbol{n} \cdot \boldsymbol{\rho} metal \cdot \boldsymbol{M} meta,}$ where $\boldsymbol{M}$ presents the atomic or molecular weight, $\boldsymbol{\rho}$ is the desity, and *n* denotes the number of metal atoms in unit oxide molecules [Pilling and Bedworth, 1923]). Two methods were used in this thesis to calibrate the volumetric expansion induced by oxidation, as the way of implementation for swelling strain may have great influence on the stress state. The first one consisted in using an initial state swelling strain; the second one consisted in using a dynamic swelling rate.

The initial state swell strain was implemented layer-by-layer. An initial radial swell strain value of 0.043 (the constant value seen in Fig. 3.6 at 600 s [Zhi and Hong, 2020]) was assigned to the elements that would change to TGO from BC at the first load step when the structural analysis starts. The value was near the constant value in Fig.3.6 after the thermal hot time reaches 600 s.This was a valid assumption since the material was not expected to exhibit oxidation until 720s into the second thermal cycle shown in Fig.3.4. Only when the corresponding layer converted from BC to TGO was the initial swell strain applied. This application method was simple and effective to some degree. It ensured the swelling was applied not only in the new TGO layer, but also in the previously converted TGO layers. However, it lacked accuracy, because it forced the swelling strain to be a constant, and only controlled by TGO growth. In addition, the swelling occurred instantaneously and simultaneously with the conversion of TGO.

The dynamic swelling rate, on the other hand, is controlled by an exponential function. From equation (3.2), one can also represent the strain rate that is induced by swelling with the following:

$$\dot{\varepsilon}_{sw} = \frac{\dot{h}_{gr}}{h_0} \quad (3.4)$$

where $\dot{\boldsymbol{\varepsilon}}_{\boldsymbol{sw}}$ is the constant swelling strain rate, $\boldsymbol{h_0}$ the initial TGO thickness, assumed to be 0.05 in current model, and $\dot{\boldsymbol{h}}_{\boldsymbol{gr}}$ is the growth rate of the TGO layer.

With all the information obtained previously, the swelling strain rate was around 10%. Each of the TBC layer was given different fitting parameters for representing a greater influence near the TC- BC interface, and smaller effect from the newly grown TGO layer. The total swell strain rate was governed by equation (3.4).

Ideally, the swelling strain fitted into exponential equation for simulation was expressed as [Busso, E.P., 1999],

$$\varepsilon_{sw} = a + bt_{tot} + c\,[exp\,(-dt_{tot})\text{-}1] \quad (3.5)$$

It was further simplified by assigning $d = 0$, leaving $\varepsilon_{sw} = a + bt_{tot}$, where t_{tot} is a time parameter representing the total time of the thermal cycling, as shown in Fig. 3.4. The removal of the fitting parameters c and d did not affect the accuracy of the swelling strain implementation.

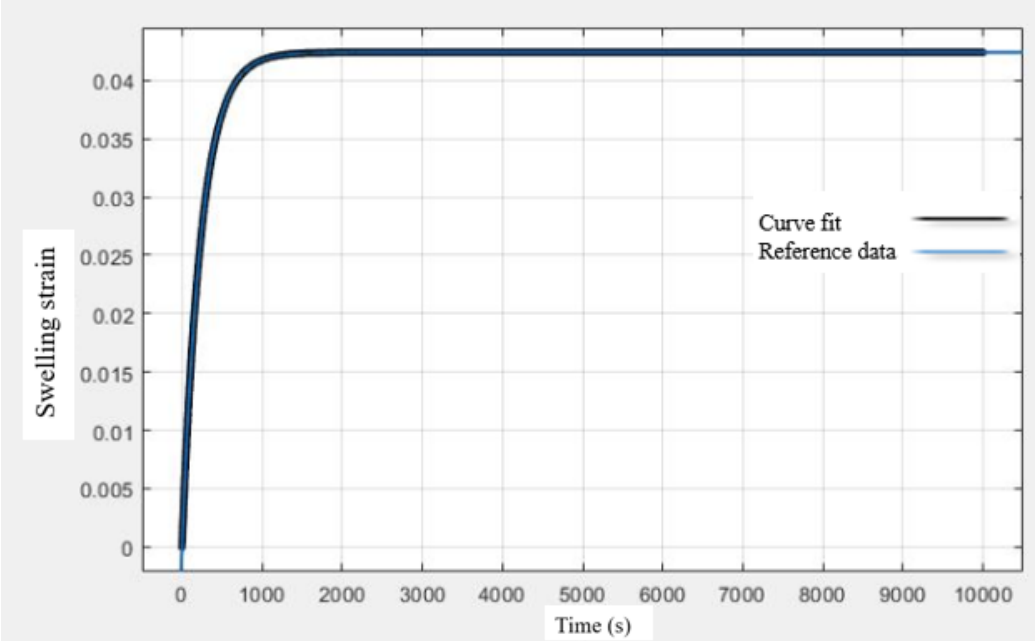

Figure 3.6. Fitting swelling strain function using ORIGIN version 10.5.70 (OriginLab corporation, Northampton, Massachusetts, USA).

3.7.4 **Relative thermal expansion coefficient calibration**

Because of the limited number of elements usable in ANSYS academic version, and also to speed up computation, the TBC FE model did not include the substrate layer. Although the mechanical behaviour of the substrate was not the focus of the current study, but it was important that the effect of the CTE mismatch between the substrate and other TBC layers are included. The approach for doing so in the FE model was to use a relative CTE between the substrate layer and the constituents ($\Delta\alpha^i = \alpha^{substrate} - \alpha^i$), as explained in Section 2.4.1. The substrate CTE and the relative CTE values are listed in Table 4, using the substrate's CTE as a baseline.

Relative thermal expansion coefficient				
Temperature (°C)	Substrate (10^{-6}°C^{-1})	Relative α_BC (10^{-6}°C^{-1})	Relative α_TGO (10^{-6}°C^{-1})	Relative α_TC (10^{-6}°C^{-1})
25	14.8	2.5	6.8	5.1
200	15.2	3.3	6.9	5.4
600	16.2	1	7.5	6.3
800	1.69	-14.61	-7.31	-8.31
1000	17.2	-15.45	-7.55	-8.35
1150	17.7	-15.9	-7.7	1.8

Table 4. Relative thermal expansion coefficient calculated using equation 2.2, based on each layer's experimental data obtained from Rösler et al., 2001 and Cheng et al., 1998.

3.7.5 **Plasticity implementation**

Rate-independent plasticity is an important cause of stress. In the proposed model, plasticity followed the bilinear isotropic hardening rule. It was used in BC, interpolated throughout the temperature profile, and in TGO at high temperature only. The yielding criterion was expressed as a sum of all the stress terms. The sum can be interpreted as equivalent stress σ_e. When the equivalent stress reaches the material yield stress parameter σ_y, the material starts to develop plastic strains. If σ_e value is less than the yielding stress, the material is elastic and deforms following the elastic stress-strain rule, as shown in Fig. 3.7, where E_t represents the tangent modulus, whose value was initially 80 MPa and 24 MPa at the 50th hour of simulation [Ranjbar-Far et al., 2010]. It was not possible for σ_e to exceed σ_y since plastic strains would develop instantaneously, thereby reducing the stress to the material yield. The yield stress value was selected from Table 2.

The hardening rule describes the change of the yield surface with progressive yielding, to establish the stress state for subsequent yielding. In the present model, isotropic hardening rule was adopted as the yield surface remained centered with respect to its initial center line and expanded in size with the development of the plastic strain.

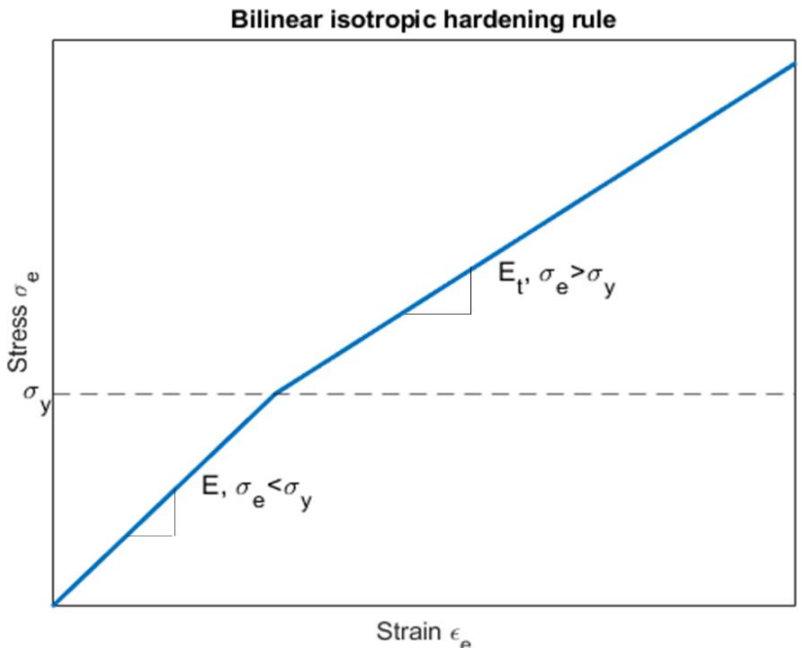

Figure 3.7. Graphical representation of the bilinear isotropic hardening rule.

The elastic strain was calculated as the difference between the total strain and the plastic strain.

3.7.6 **Sintering implementation**

TBC system stresses are strain-controlled; therefore, the sintering effect may increase the stresses in the TBC constituents. The sintering effect in the TC layer was reflected as a time-dependent increase in the Young's modulus. The Young's modulus's increase was then calibrated with the same trend as depicted in Fig.3.8, as inspired from [Beck et al., 2008]:

$$E_{TC} = E_{TC,ini}\,[2 - \exp\,(-t_{ox}/\tau_{sinter})] \qquad (3.6)$$

where $\boldsymbol{E_{TC}}$ and $\boldsymbol{E_{TC,ini}}$ are the Young's modulus of the TC layer after and before the sintering induced from thermal cycling. $\boldsymbol{t_{ox}}$ is the total oxidation time during dwelling, and $\boldsymbol{\tau_{sinter}}$ is a

constant originating from the function $\tau_{sinter} = H * T_{max}^{i}$ [Beck et al., 2008]. $\boldsymbol{H, I}$ are fitting constants (where, $H = 3.24 * 10^{75}$ s $and\ I = -22.993$) and the maximum temperature $\boldsymbol{T_{max}}$ is also a constant, in our case, $\boldsymbol{T_{max}} = 1{,}150$ °C. This function was implemented by calculating the sintered Young's modulus at each starting point of the new oxide layer formation at high temperature holding period, changing the material properties to the new Youngs' modulus at that time point. This was applicable because the mesh of the oxide prone layer was refined. From the previously stated relationship of the monotonic evolution of the Young's modulus, a graphical representation is shown in Fig. 3.6 at the end of the 50th hour of the oxidation time at 1,150 °C, the Young's modulus is about 1.7 times of its initial value, this is aligning with the literature [Caliez et al., 2003] and Fig.2.2.

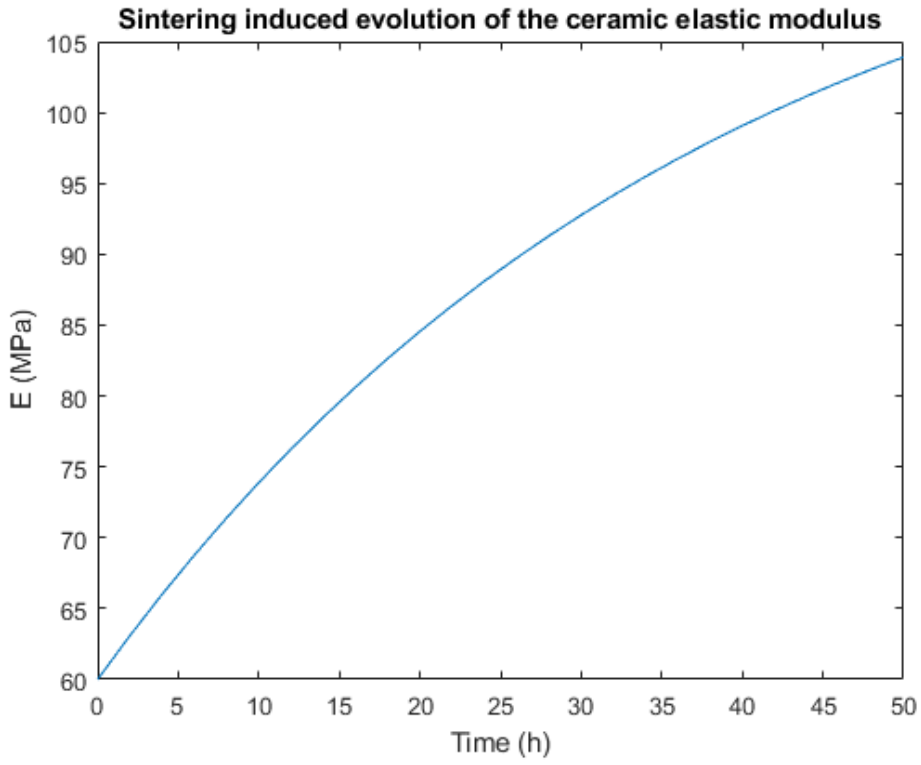

Figure 3.8. Sintering induced evolution of the ceramic elastic modulus with treatment time calibrated from Eq.3.6, at high temperature.

4 PARAMETRIC STUDIES OF STRESS DISTRIBUTIONS IN TBC

In this section, we present our findings from FE simulations of the impact of different material characteristics on radial stresses, because stresses in the lateral or axial direction are not of significant interest. To isolate the effect induced by each of TBC constituents' material parameters on stress distributions, a parametric study was carried out. Before applying the model to study more complex behaviour in longer thermal cycles, several verification runs were performed. The purpose of the verification runs was to test the element formulation and implementation and compare with the published results. In particular, three limiting and preliminary cases presenting the influence of material properties through thermal loading on radial residual stresses close to the TC-BC interface were compared with the literature. In later stages of model applications presented in Chapter 5, other mechanical behaviours of TBC constituents such as nonlinear behaviour of BC, sintering and creep behaviour of TC were then studied. Lastly, a longer thermal cycle was implemented for a more general representation of gas turbine's work cycle, along with some different morphologies, in Chapter 6.

Due to unavailable information on plasticity, creep behaviour, and oxidation induced swelling of the TBC system analyzed in [Rösler et al., 2001] which was used as a reference, the following assumptions were made:

- Swelling and creep behaviour only became apparent during high temperature dwelling period when oxidation time reached 20 seconds;
- Elastic and perfectly plastic behavior with isotropic hardening of BC and TGO were applied.

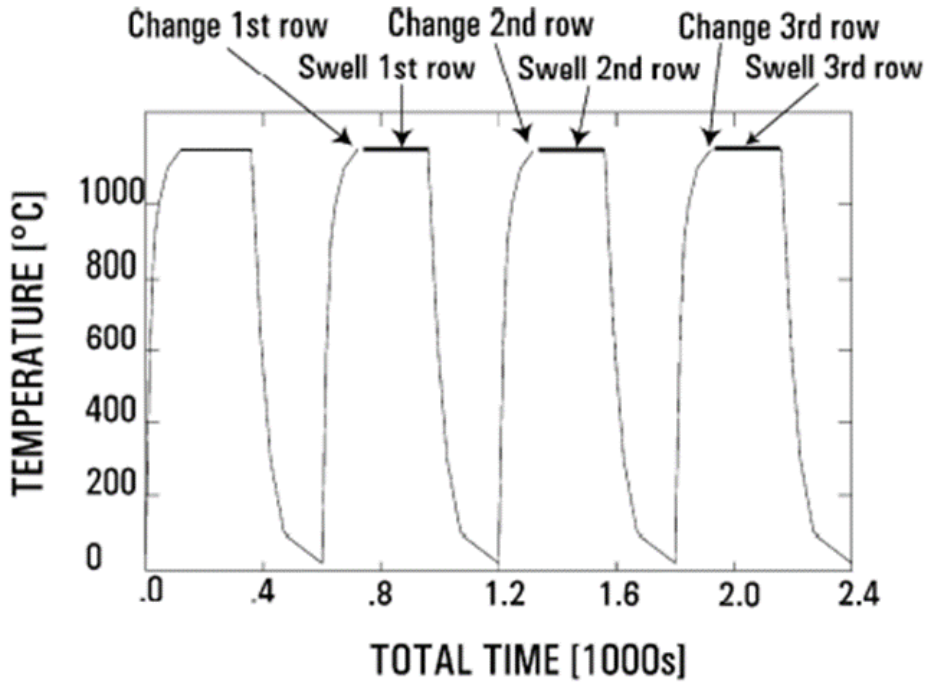

Figure 4.1. Thermal cycle used in the simulation from reference [Rösler et al., 2001]. The periods of material change of swelling used with a TGO layer are also shown.

The thermal cycle profile used in the following four case studies, as previously explained and shown in Chapter 3, was that in [Rösler et al., 2001], to try to replicate and verify the results.

Furthermore, to facilitate the comparison between the FE residual stress results obtained in the current analysis and those from the benchmark model in [Rösler et al., 2001], three similar locations were investigated at the top, peak and valley regions shown on Fig 4.2.

a) FE Model point of interest

b) Points of interest chosen by Rösler's model

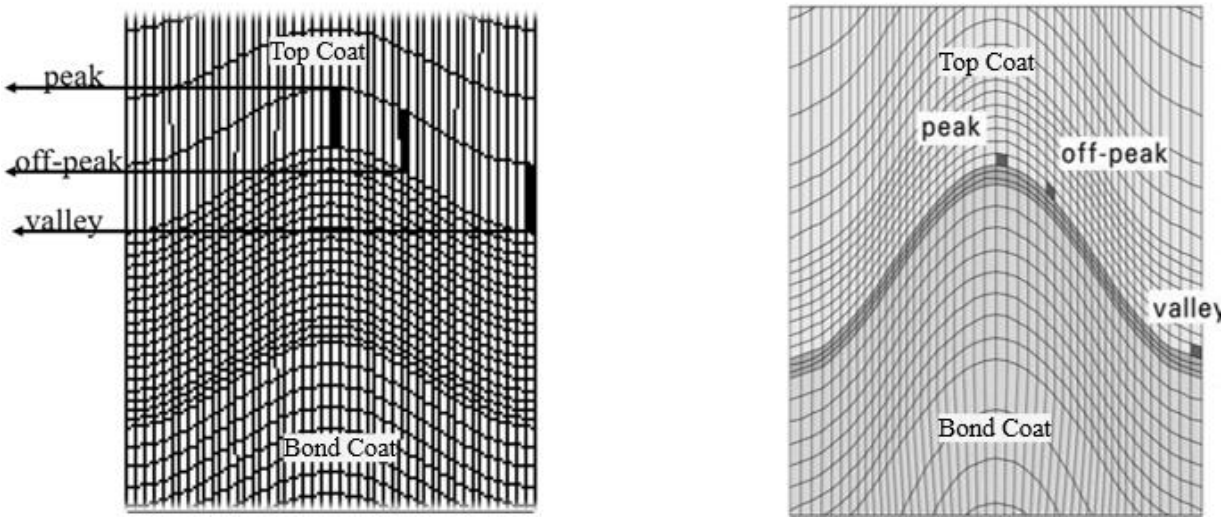

Figure 4.2. Three elements of interest comparison between present model and the reference model with a) from current FE model and b) from reference [Rösler et al., 2001].

4.1 PRELIMINARY RESULTS WITH THE ELASTIC MODEL IMPLEMENTATION

The first step in the study was to validate whether our FE model could provide credible results in an elastic simulation. In this scenario, all three TBC constituents were assumed to be elastic, without oxidation or swelling.

CASE	BC	TGO	YSZ(TC)
°*N 1*	Elastic	N/A	Iso-transverse elastic

4.1.1 **Results**

As shown in Fig.4.3, the stress distribution was the same across all four cycles. At peak region on the ceramic top coat, a compressive stress reached to a maximum of roughly 120 MPa at the end of the heating stage, with no significant change seen during dwelling, and the radial compressive stress gradually reached back to zero at the end of each thermal cycle. Meanwhile, at the valley location of TC, the same-magnitude of stress as in the peak region was seen (with an opposite sign). Lastly, in the off-peak region of TC, a maximum compressive stress of around 40 MPa was observed, which also went back to near zero at the end of each thermal cycle. For all the components of the TBC, the residual radial stress was well below 2 MPa by the end of each of the thermal cycle.

4.1.2 **Discussion**

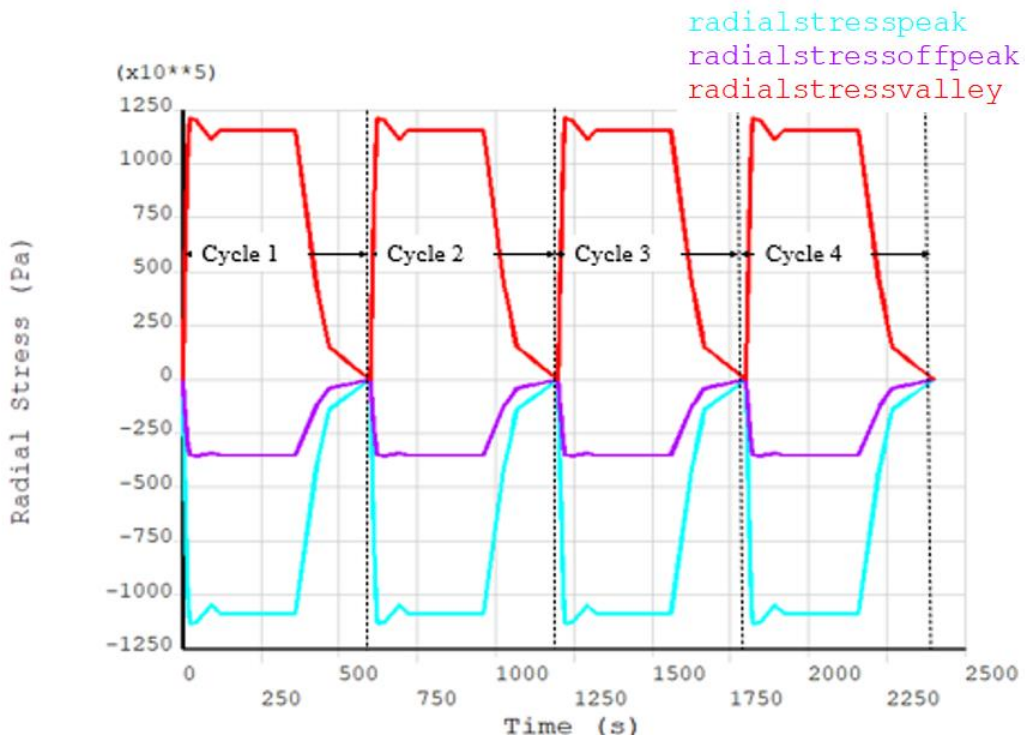

Figure 4.3. Time dependence of the radial TBC stress at "peak," "off-peak," "valley" according to linearly elastic material behaviour, with no TGO growth.

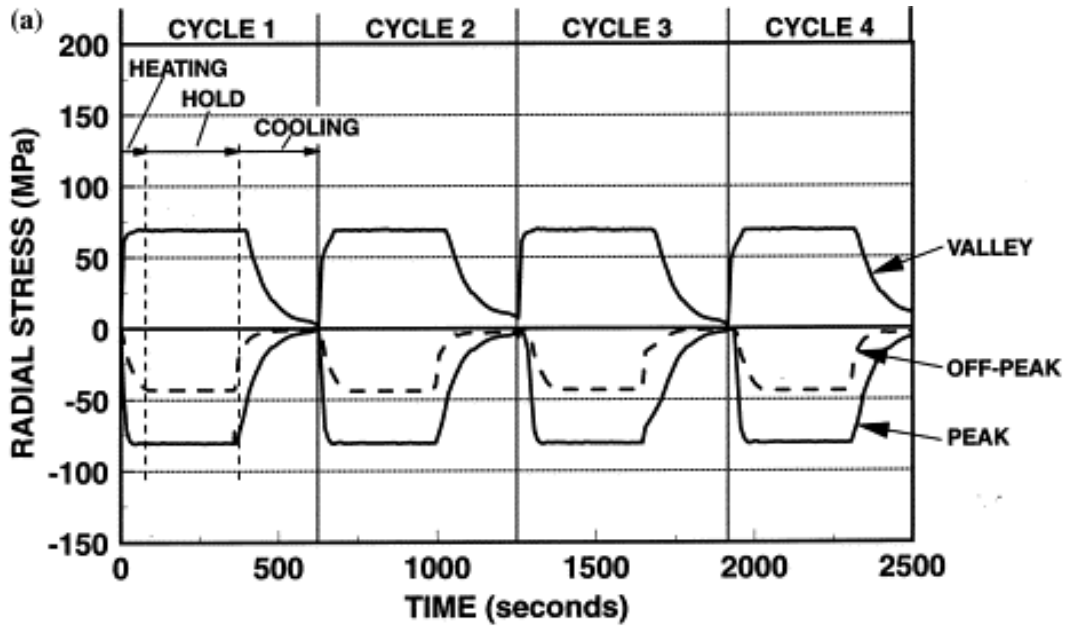

Figure 4.4. Stress history for the fully elastic TBC system in three regions along the ceramic/oxide interface for cycles without oxidation [Freborg et al., 1998].

In both Fig.4.3 and Fig. 4.4, one can see that the radial stress profile in the peak and valley locations have opposite signs and the same magnitude. In the off-peak location, the radial stress profile was similar to that in the peak location (although with a smaller magnitude), because the element of interest was selected closer to the peak location than the valley location.

During each thermal cycle, the radial stress increased as the heating took place. The compressive radial stress accumulated because of the thermal expansion mismatch between each TBC layers and the superalloy substrate. As explained in Section 3.7.4, this behaviour was captured by the relative thermal expansion coefficient. Because of the elasticity of the constituents, the radial stress remained constant during holding. After the cooling period at the end of each thermal cycle, radial stresses at all locations went down to near zero. This was expected since the main driving force for stress was the thermal expansion mismatch between the constituents, and the only interaction between the constituents are their Young's moduli and CTE changing with respect to time.

Due to the unknown material properties in [Freborg et al., 1998], and the slight difference in thermal profiles, a difference in magnitude can be seen in the radial stress in the comparison

between our model and that in [Freborg et al., 1998] for the elastic model. However, our goal was to examine how radial stress in an elastic model was only affected by the thermal expansion coefficients, and this goal was successfully reached.

4.2 MODELING WITH BC CREEP IN THE ELASTIC MODEL

It is informative to examine the stress distribution in the TBC system in absence of oxidation to get an insight into the effect BC creep alone, such that a stress evolution baseline could be established for further comparison. Following [Rösler et al., 2001], a thermal cycling analysis without TGO formation was carried out.

The objective of this case study was to analyse the influence of the BC creep behaviour on the residual radial stresses at low and dwelling temperature, and compare the stress distributions in three locations along the TC-BC interface.

CASE	BC	TGO	YSZ(TC)
°*N 2*	Elasto-viscous	N/A	Iso-transverse elastic

4.2.1 **Results**

From the result plotted in Fig.4.5 where stresses are presented as a function of time in three locations, it is apparent that the stress distribution remains the same over the last three thermal cycles comparing to that on the first cycle. The sign of the residual stress from the first thermal cycle was reversed in the following cycles, the tensile stress state resulted at the valley location becomes largely compressive, on the other hand, the peak and the off-peak location also presented opposite state of stress. The maximum residual stress value in the first cycle observed both at peak and valley region of the TC layer has the same stress state and magnitude observed in Fig. 4.3, which was the result for the case where all layers behave elastically in the TBC system. Upon

heating, the large tensile stress started to diminish and eventually during dwelling period, the stress of all TBC constituents ramped to zero. Whereas upon cooling, the peak location residual stress ramped up to a tensile stress maximum of up to 220 MPa by the end of each thermal cycle. In the peak and valley region of the TC layer, the residual stress shows opposite sign but matching magnitude.

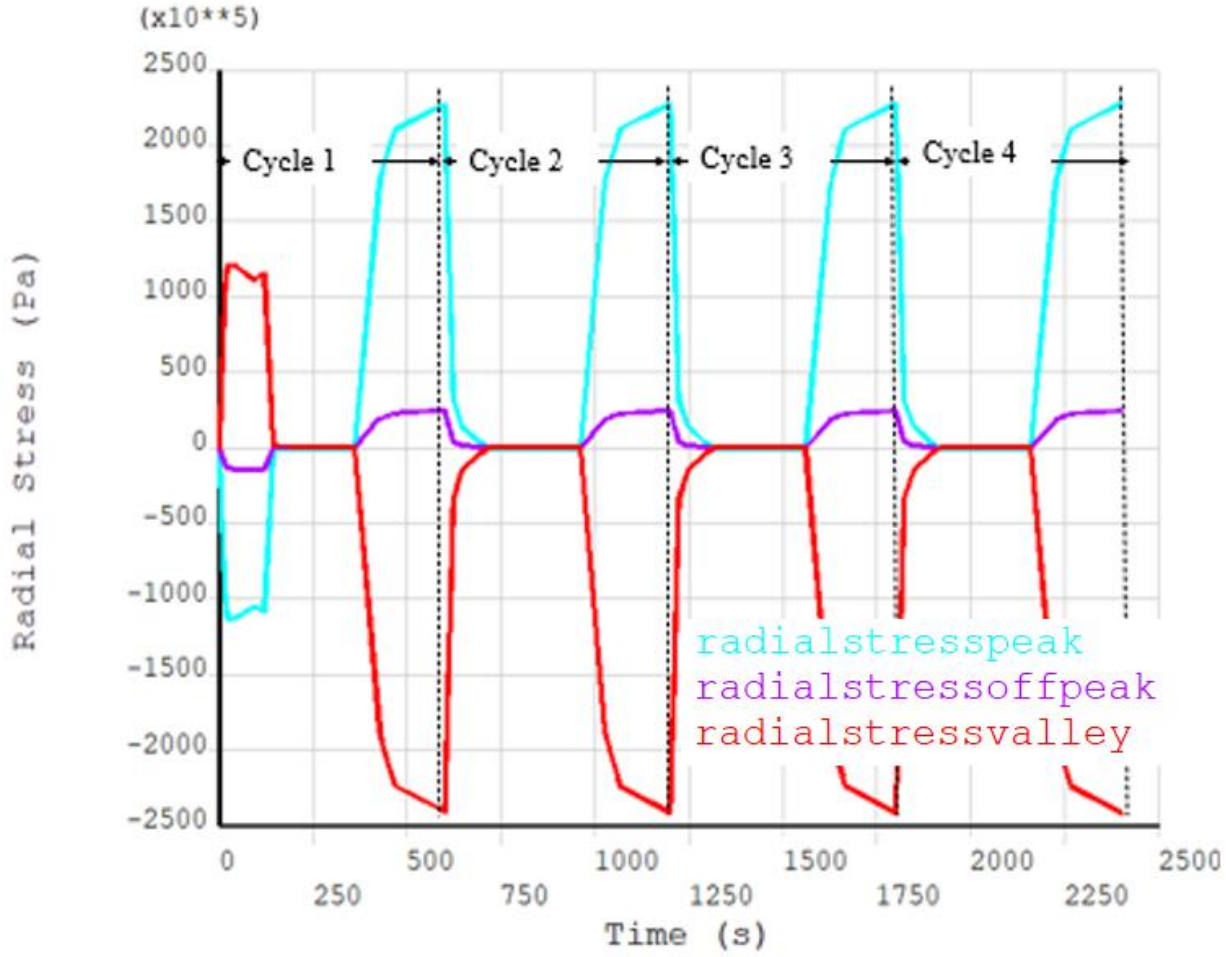

Figure 4.5. Time dependence of the radial stress in "peak," "off-peak," "valley", as affected by BC's creep behaviour, with no TGO growth.

4.2.2 **Discussion**

The stresses in Cycles 2-4 were reversed compared to the purely elastic situation in Section 4.1. This was mainly because thermal expansion mismatch was no longer the dominant stress source. The BC creep induced during cycling was so large that, at dwelling temperature, stresses that were induced by CTE mismatch relaxed to zero. When the system reached the cooling stage, thermal expansion again became predominant in the system, giving rise to maximum radial stresses of 220 MPa at the TC-BC interface.

The stress distribution was different in the first cycle because stress redistribution occurred at the beginning of heating, then completely relaxed to zero because of the strong effect of BC creep. When the first thermal cycling started and the temperature begun to rise, the CTE and Young's modulus difference in the constituents first caused a large stress increase in the constituents. A strong effect from the BC creep was triggered as soon as the temperature reached 750 °C (as BC only had significant creep behaviour in high temperature environment). This allowed stress to relax to zero for the first time. During the following cooling period, the stress increased largely due to thermal expansion mismatch. Throughout the rest of the thermal cycles, the effects of CTE mismatch and creep alternated.

Comparing the radial stresses in three locations in Fig.4.5 with the results published in Fig.4.6 [Rösler et al., 2001], one can observe that the stress magnitudes are similar. The maximum tensile stress at the peak location was slightly smaller than that of the maximum compressive stress at the valley location in both cases, however the difference in our results was not as substantial as was indicated in the reference [Rösler et al., 2001]. Nonetheless, in both cases, the tensile stresses in the peak location largely exceeded the yield strength of plasma sprayed TBC [Rejda et al., 1997].

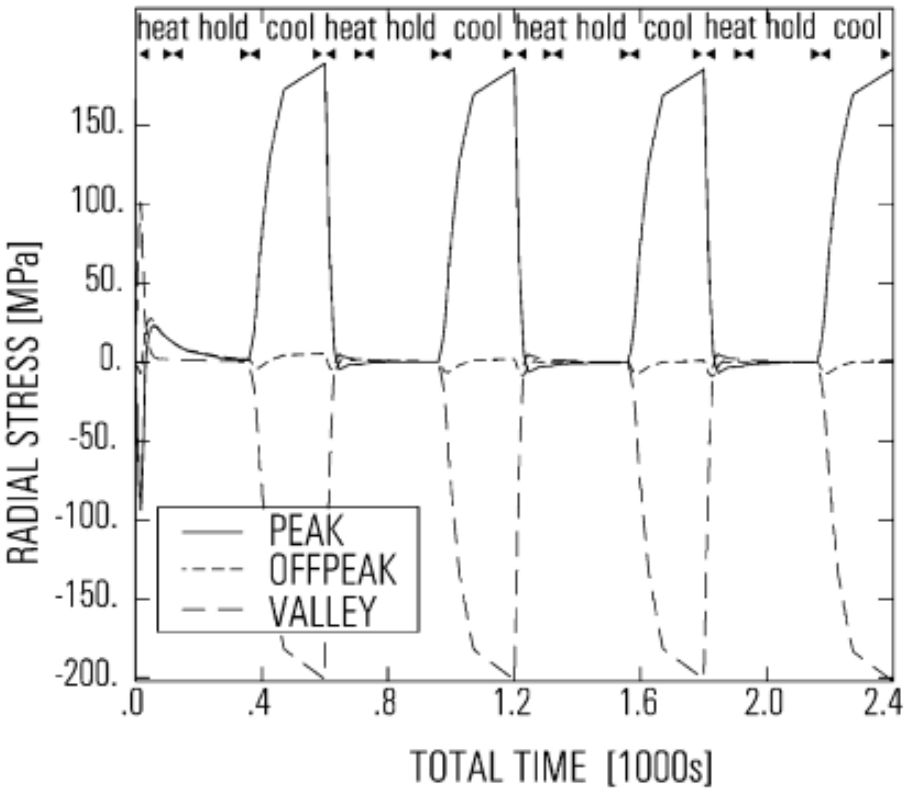

Figure 4.6. Time dependence of the radial TBC stress in "peak"," off-peak"," valley" according to linearly elastic material behaviour. No TGO formation included [Rösler et al., 2001].

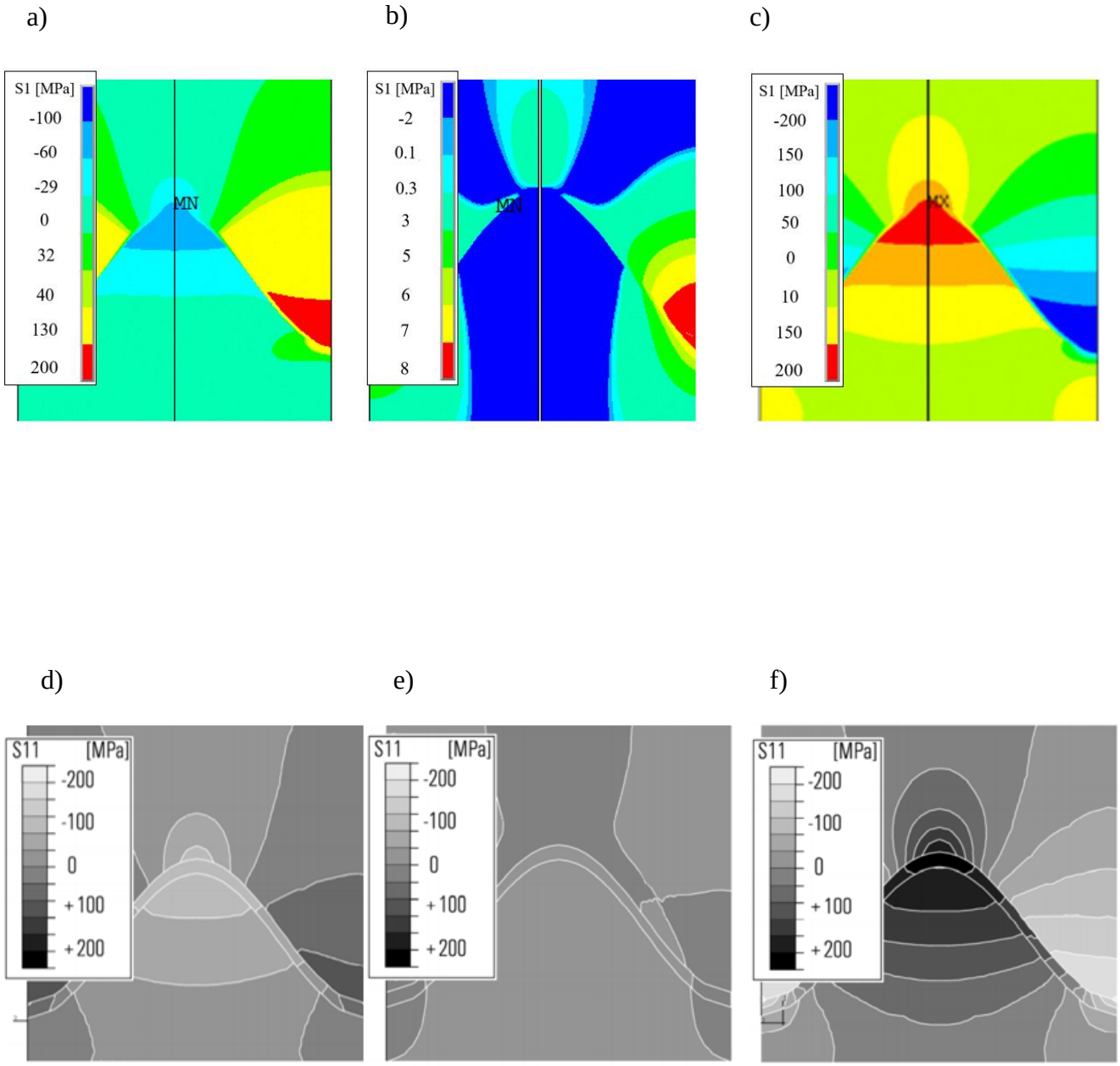

Figure 4.7. Contour plot comparison between model and the reference model at a) 20 s b) 360 s (end of the holding period) c) 600 s (end of first thermal cycle) versus d) 20 s (start up at 700 °C) e) 360 s (end of holding time, 1,150 °C) f) 600 s (end of first cycle, 20 °C).

4.3 MODELING TGO GROWTH WITH AN ELASTIC TGO MODEL

To determine the oxidation induced strain in isolation, the following case study was carried while neglecting the effects of creep and plasticity. In the following section, a model with linearly elastic TGO growth is introduced. The BC had the same elasto-viscous behavior as stated in the previous case. The TGO grew as a function of time, as introduced in Section 3.7.1, and behaved elastically. Therefore, no creep was considered, and the only growth stress was generated by the swelling strain induced by volumetric expansion. The goal of this study was to investigate the effect of newly grown oxide on the residual stress in TC: swelling effect induced by volumetric expansion from the BC oxidation and the thermal expansion coefficient mismatch between layers.

This case study consisted of two different attempts. The approach aimed to verify that the swelling rate had a significant impact on the residual stress.

Fig.4.9 a) shows the results obtained from a constant swelling strain of 0.043 in the radial direction, while it was $1/10$ of that in the lateral direction as done in various published works [Bendarz, 2007; Bialas, 2008; Zhi and Hong, 2020]. In the direction perpendicular to the plane, the oxidation swelling strain is always assumed to be zero.

Fig.4.9 b) shows the results obtained from a homogeneously distributed, exponential swelling strain function as explained in Chapter 4.

CASE	BC	TGO	YSZ(TC)
°N 3	Elasto-viscous	Elastic	Iso-transverse elastic

Fig.4.8 a)- d) shows the predicted evolution of thermally grown thickness along the interface of TC and BC layers after 1,2,3 and 4 cycles to match the conditions studied in [Rösler et al.,2001]. In the four thermal cycles modeled, the first cycle assumed no TGO growth occurred, while each of the following cycle induced a 0.33 μm growth with a total TGO thickness of 1 μm at the end

of the fourth cycle during high temperature dwelling. It was assumed that the oxide growth only took place at the holding temperature during the thermal loading.

a) Cycle 2, no oxidation

b) Cycle 2, 1st TGO layer oxidated

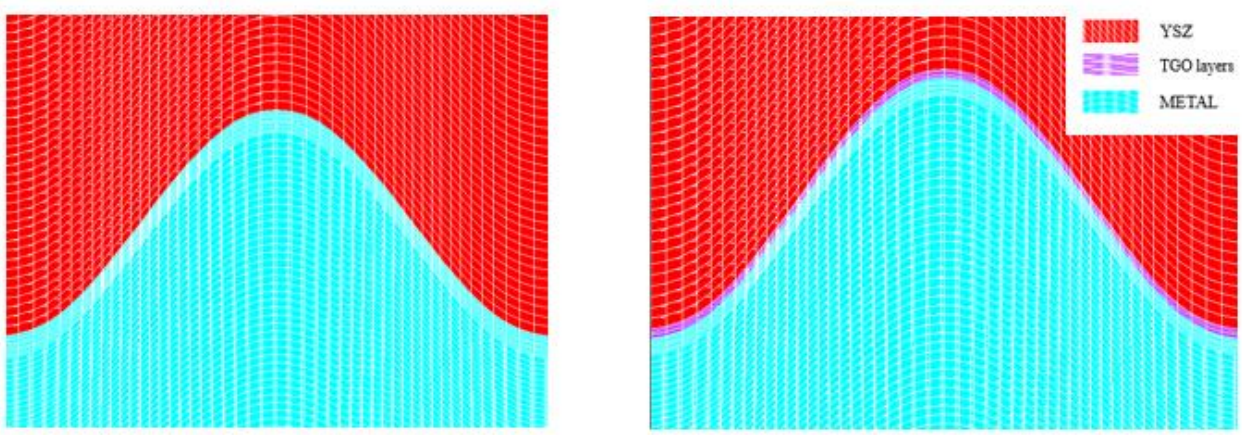

c) Cycle 3, 2nd TGO layer oxidated

d) Cycle 4, Fully oxidated TGO layers

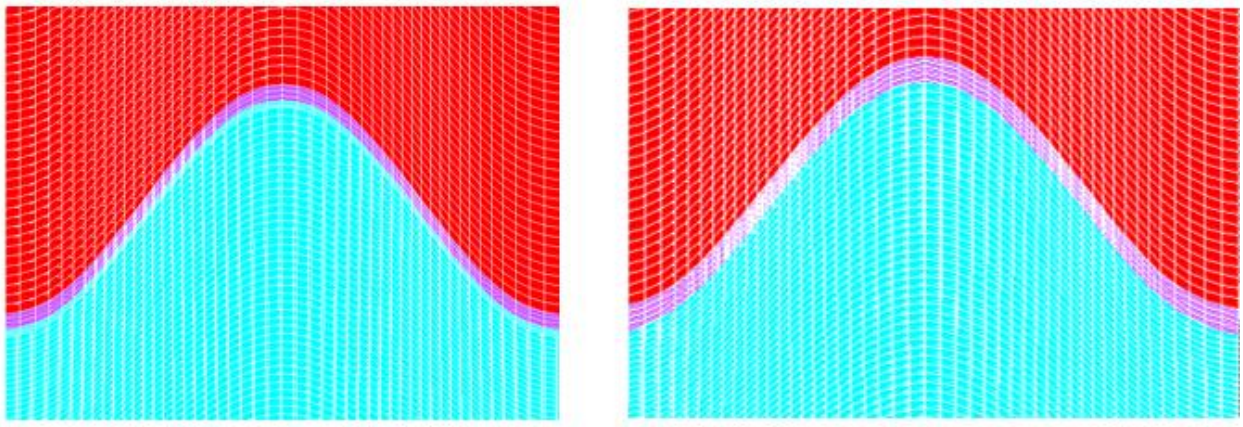

Figure 4.8. TGO growth induced in the model. At a) initiation of the thermal cycles, no oxidation was formed, b) first layer of TGO was formed at the TC-BC interface, c) a second layer of TGO was formed at high temperature d) the third layer of BC was transformed into TGO at last thermal cycle.

4.3.1 **Results**

For the case with an anisotropic constant swelling strain, as shown in Fig.4.9 a), at the first cycle, the maximum tensile stress was around 230 MPa in the peak location of the TC. The stress state reversed into a large compressive stress with a maximum of 1.75 GPa, then through the thermal cycling, the compressive stress gradually reduced to 1.5 GPa. In the peak location of the TC, the stress was at around 250 MPa by the end of cooling in the first cycle. At the beginning of the dwelling stage, the radial stress had reversed into a tensile state. It stayed tensile until the end of the fourth cycle and slowly reduced to 500 MPa. The maximum tensile stress in the peak location was seen at the end of cooling in the second thermal cycle, with a value of around 620 MPa. The off-peak location shared similar stress magnitudes and stress states with the peak location.

For the case where an exponential swell strain was considered in the radial direction, the results in Fig.4.9 b) show that in the peak and valley locations, the stress state was also reversed at the beginning of high temperature holding in the second thermal cycle. The maximum tensile stress in the valley location was 1.25 GPa. Whereas the maximum compressive radial stress was 1.53 GPa, they were both seen at the end of cooling during the second thermal cycle, and they all diminished in the following thermal cycles. The radial stress in the off-peak location always maintained a near zero value from the beginning of the second cycle and only grew slightly, at a slow pace.

a)

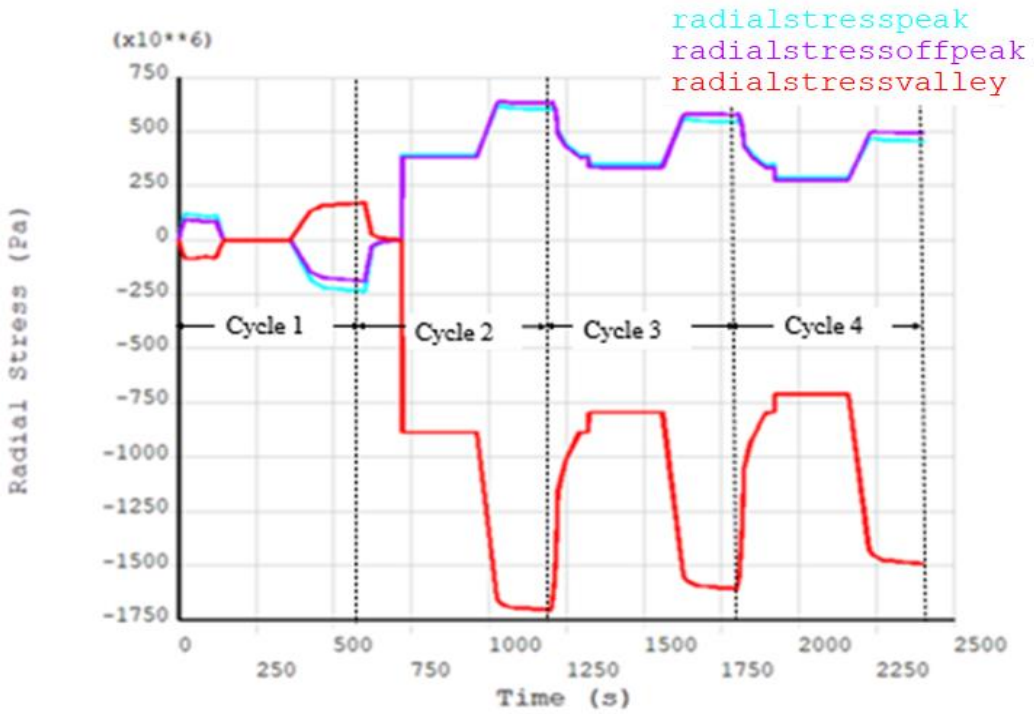

b)

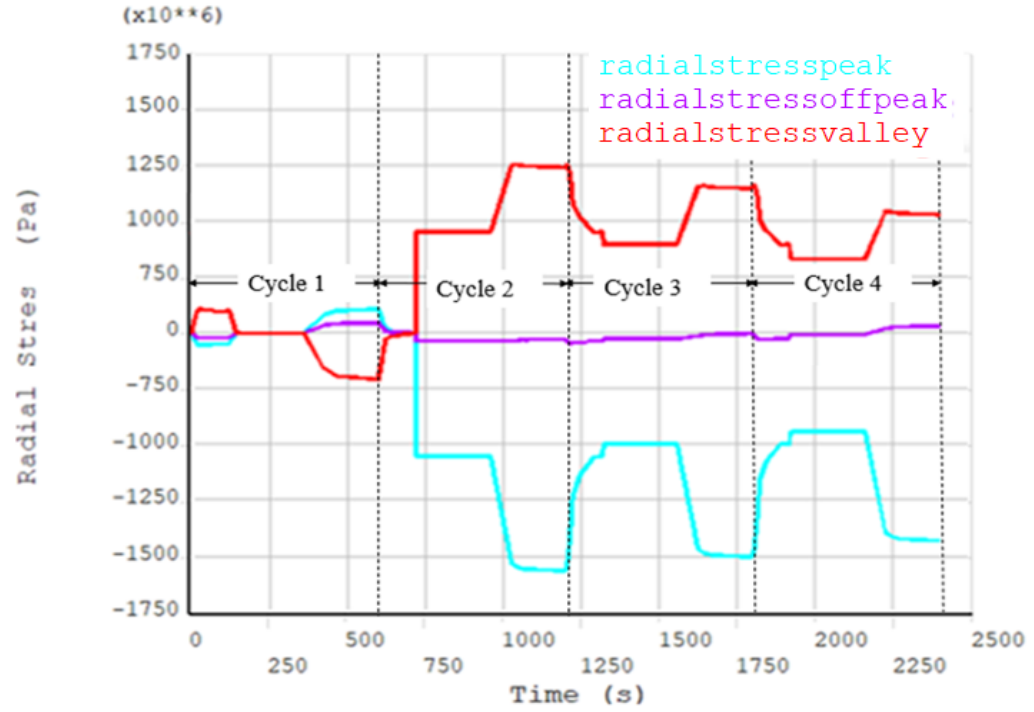

Figure 4.9. Time dependence of the radial TBC stress in "peak"," off-peak"," valley" locations according to linearly elastic material behaviour, with linear elastic TGO growth, an oxide growth rate of 0.33 *μm per cycle assumed, where a) a constant swelling rate was used, b) a time-variant swelling rate was used, the rate was initially large. As the TGO grew thicker, swelling strain grew smaller.*

4.3.2 **Discussion**

When there was no TGO growth in the first thermal cycle, the radial stresses remained identical to the elastic model studied previously. The stresses only started to deviate at high temperature, when the TGO began to grow. The compressive stress reached 1.5 GPa, which is much higher than the yield stress of TC [Rejda et al., 1997]. Overall, one can observe that swelling greatly amplified radial stresses.

Compared to the results in [Rösler et al., 2001], the results in Fig.4.9 b) seem to be different at the end of the last thermal cycle. This could be ascribed to the differences in modeling the swelling rate, as we had incomplete information about the swelling function implemented in the reference.

From the two swelling models used in the simulations shown in Fig4.9 a) and b), one can conclude that the swelling in [Rösler et al., 2001] (Fig.4.10) most likely featured a dynamic swelling rate. All cases share a near zero value radial stress in the off-peak location, a compressive stress in the peak location, and a tensile stress in the valley location. The maximum stresses are seen at the end of the second thermal cycle in Fig.4.9 b) and Fig.4.10.

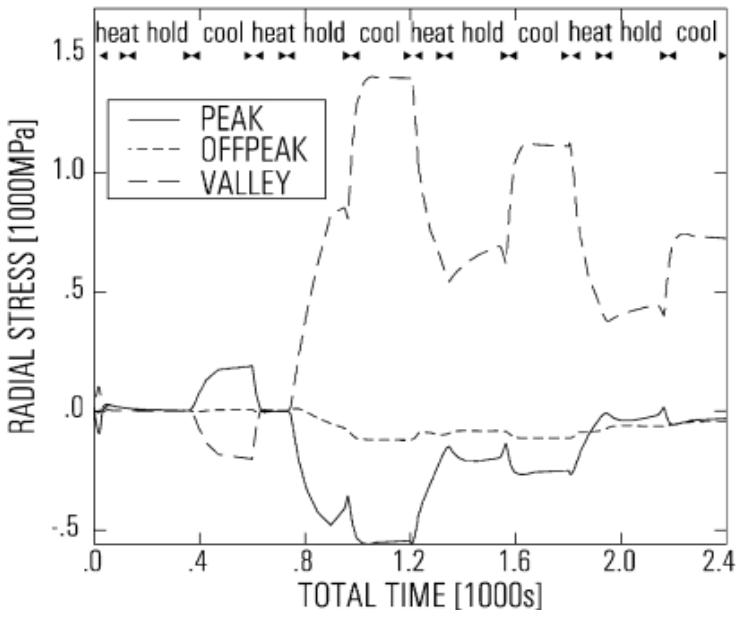

Figure 4.10. Time dependence of the radial TBC stress in "peak"," off-peak"," valley" locations. Linear elastic behaviour of the TGO and an oxide growth rate of 0.33 *μm per cycle were assumed [Rösler et al., 2001].*

However, the intensity of change in stress was much greater in the reference, as shown in Fig.4.10. The peak location first went through a reversal of stress to maximum compressive stress of 0.5 GPa at the end of second cycle, then gradually went back to a tensile stress, and finally reached a small compressive stress. In the valley location, on the other hand, the maximum value was close to what we obtained, but it diminished faster, dropped to a value of 0.5 GPa at the end of 4^{th} cycle compared to 1.03 GPa seen in Fig.4.9 b). These variations may all be due to differences in how swelling was modelled. In addition, in our model, the swell and creep were both introduced from the 20^{th} second of the dwelling period, whereas in the reference, BC creep started from the beginning of the dwelling stage, and swelling started at 20 s.

Nonetheless, it is apparent the swelling reversed the stress state in all cases. At the end of each thermal cycle when the system reached ambient temperature, large tensile stresses appeared in at the valley location. The effects of swelling were substantial, and their magnitude strongly depended on the ratio of swelling and creep relaxation rates. Overall, TGO growth induced volume change reversed the stress state at the TC- BC interface.

4.4 MODELING TGO CREEP IN THE TGO GROWTH MODEL

At low temperature, the TGO behaviour can be considered elastic; however, while the TBC system is exposed to high temperatures such that TGO growth is initiated, the creep behaviour of TGO should also be considered. Thus, the following model took into account the creep effect of TGO, with the other material layers bearing the same material properties as in the previous case.

CASE	BC	TGO	YSZ(TC)
°*N 4*	Elasto-viscous	Elasto-viscous	Iso-transverse elastic

4.4.1 **Results**

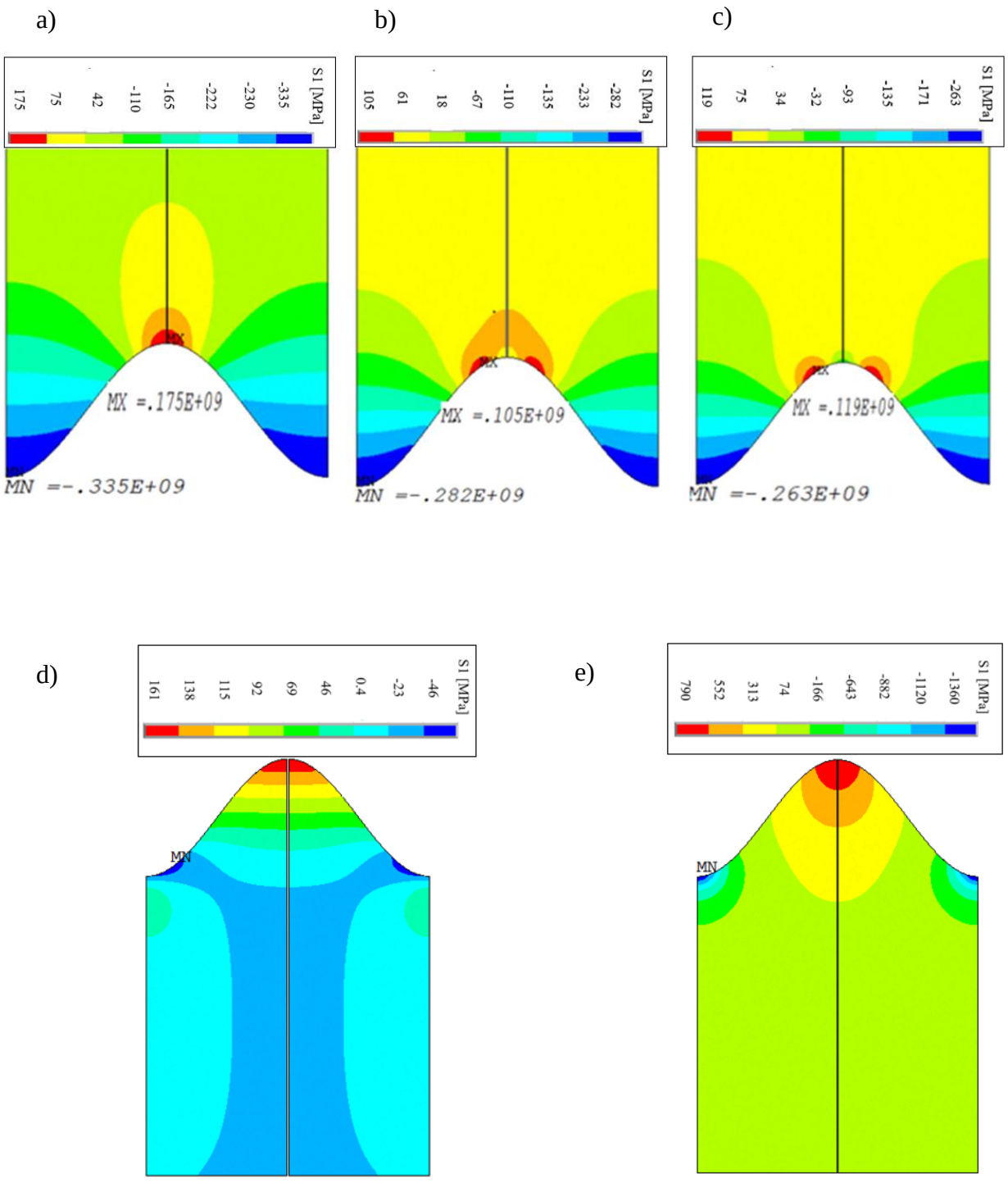

Figure 4.11. Stress contour plots for a) TC at the end of first cycle when t=600 s; b) TC at the end of third cycle when t=1,800 s; c) TC at the end of last cycle when t=2,400 s; d) BC at the end of third cycle when t=1,800 s; e) BC at the end of third cycle when t=2,400 s.

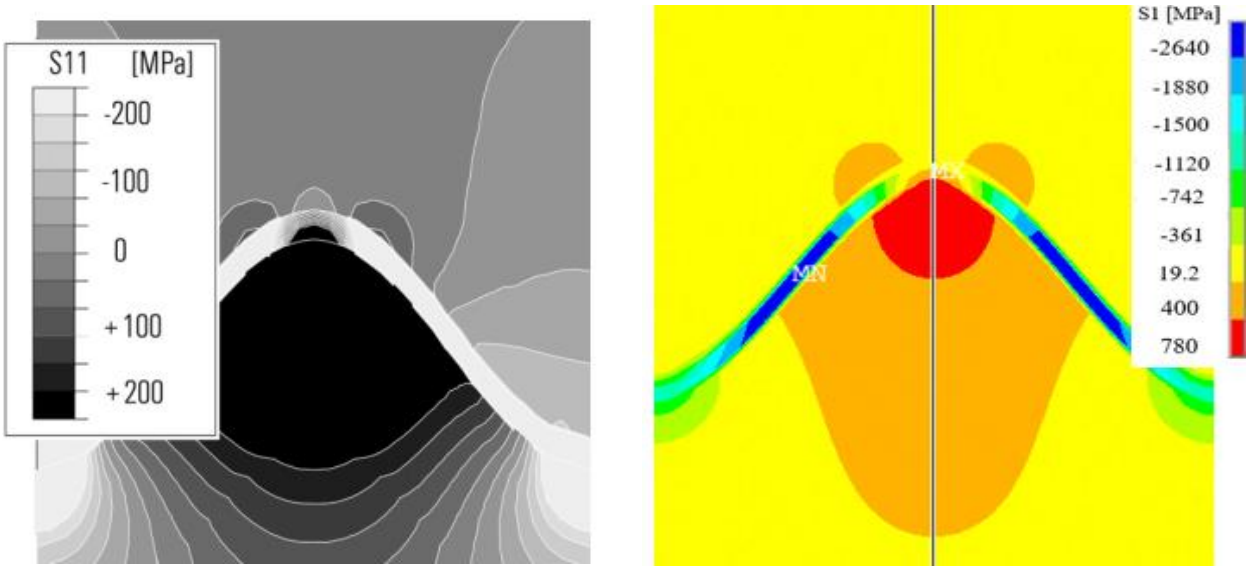

a) TBC Radial Stress Distribution at t=600 s

b) TBC Radial Stress Distribution at t=600 s

Figure 4.12. Side-by-side comparison of radial stress during 4th cycle after cooling to 20 °C *with a) extracted from the reference [Rösler et al., 2001; Fig.9]; b) TBC model cooled after 600 s, at the end of 1st thermal cycle.*

The results of radial stress evolution are summarized in Fig.4.11 and Fig.4.12. It can be noticed that the magnitude of the TC stress diminished with respect to cycle time. The tensile stress region for TC was shifted away from the vicinity of the peak to the off-peak location.

A maximum tensile stress of 175 MPa was seen in the peak location in Fig.4.11 a), in addition to a maximum compressive stress of 335 MPa in the valley location at the end of the first thermal cycle. At the end of the third thermal cycle, the maximum tensile stress moved to side of the peak location, with a maximum stress of 105 MPa. At the end of the 4th cycle, the peak location's stress state reversed to a slight compression.

In the valley location, the radial stress remained in the compressive state at all four times, when the temperature cooled down to 20 °C. It was initially larger at 335 MPa and at the end of the 4th cycle, reduced to 263 MPa.

The BC radial stresses are shown in Fig. 4.11 d) and e). They grew larger from the end of the first cycle to the end of the 4th cycle, with a tensile stress value of 161 MPa and 790 MPa, respectively. The compressive stresses grew significantly from 46 MPa to 1.36 GPa.

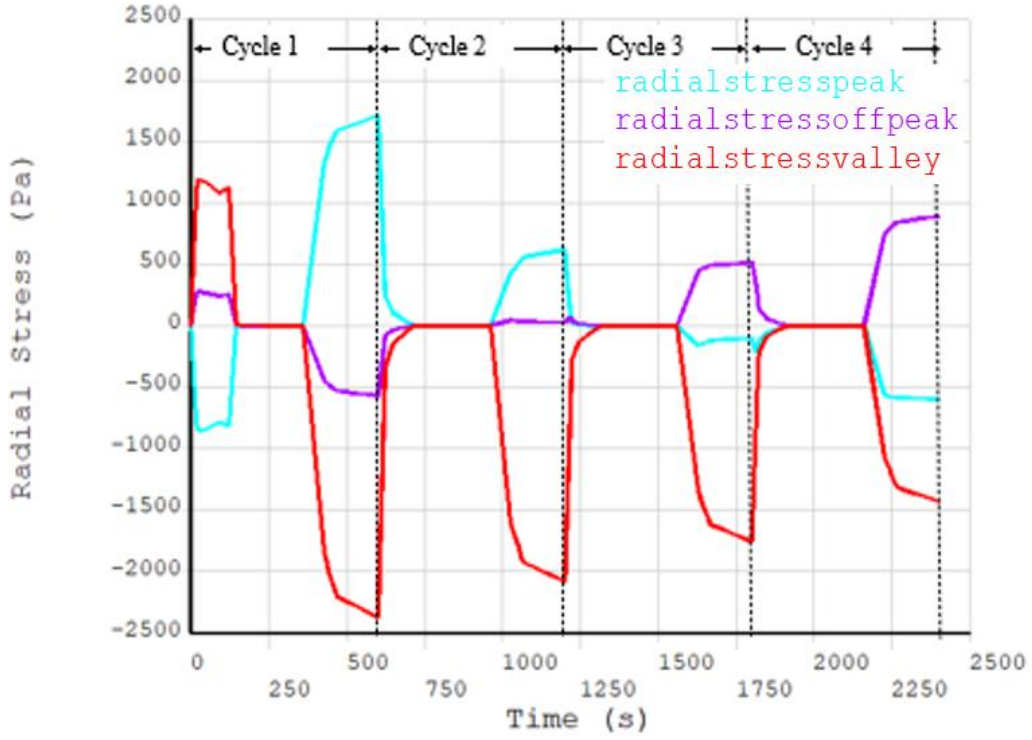

Figure 4.13. Time dependence of the radial TBC stress in "peak"," off-peak"," valley" locations. Elastic-viscous-plastic behaviour of the TGO and an oxide growth rate of 0.33 μm per cycle were assumed.

4.4.2 **Discussion**

By examining Fig. 4.13, one can see that all the stresses were essentially zero during the dwelling period, whereas they were amplified when swelling was the dominant effect in Section 4.3. It can be concluded that swelling and TGO creep are two opposite mechanisms: swelling amplifies the radial stress whereas creep diminishes them. Under the right conditions, the swelling stresses induced by the TGO growth may be relaxed by the TGO creep properties.

The first cycle stress distribution was the same as seen in the previous case study, as shown in Fig.4.13. In the second cycle, the off-peak location radial stress stayed at a near zero value, then became tensile at the third and amplified at the 4th cycle's cool down period. The stresses in valley location always stayed compressive. When the temperature in the TBC system was ramped down to room temperature at the end of each cycle, the largest stresses were seen for all TBC components (Fig.4.13).

The magnitude of TC compressive stresses in the valley location were greater than the tensile stresses in the other regions. This could be a consequence of the in-plane stress state which is tensile in the TBC, thus leading to reduced effective stresses and creep rates in the "valley" region [Rösler et al., 2001].

On the other hand, the effect of alumina growth cannot be overlooked. The TC cooling stress at each cycle diminished as TGO continued to grow. The maximum tensile stresses at the peak location also diminished from 171 MPa at the end of 1st thermal cycle to 78.9 MPa after the completion of the 4th cycle where 1 μm of alumina was formed. This TC stress evolution was controlled by TGO's large Young's modulus. The deformation occurring in BC was absorbed by alumina, so the thermal expansion mismatch induced by BC was not completely transferred to the TC layer. It is known that the TGO layer acts like a barrier between the TC and BC layers, which could be the reason behind why the stresses in TC at the end of the high temperature holding period and the cooling period looked very similar to those of the elastic case shown in Section 4.2. In the meantime, the maximum tensile stresses in BC were much greater (five-fold) than when TGO was not considered. Recalling that the stress induced by thermal expansion mismatch between TGO and the substrate can be described as $\sigma_{11}^{th} = \frac{\Delta\alpha^i(T)(T-T_{peak})}{1-\nu^i} E_1^i$, where $\boldsymbol{\Delta\alpha^{TGO}(T)}$ is the relative CTE. Since TGO has the lowest thermal expansion coefficient, the large strains induced by BC deformation were partially shielded by TGO in contact with TC layer. Therefore, the stress in TC was only affected by the thermal expansion mismatch and swelling of the TGO. Lastly, creep in TGO relaxed the stresses induced by thermal expansion mismatch from the TC layer during hot time. Therefore, the residual stresses diminished as TGO continued to grow.

In the TGO layer, the maximum compressive stress was observed in the off-peak vicinity during cooling, as seen in Fig.4.11. The stress distribution is different from that in the case when the TGO creep was not considered (Section 4.2).

The extremely large compression in the TGO layer, at 2.64 GPa, agrees with the literature (2.5 GPa in [Wei et al., 2006]). However, this result was not utterly realistic as the thermal cycle time in the model was very short compared to a real case.

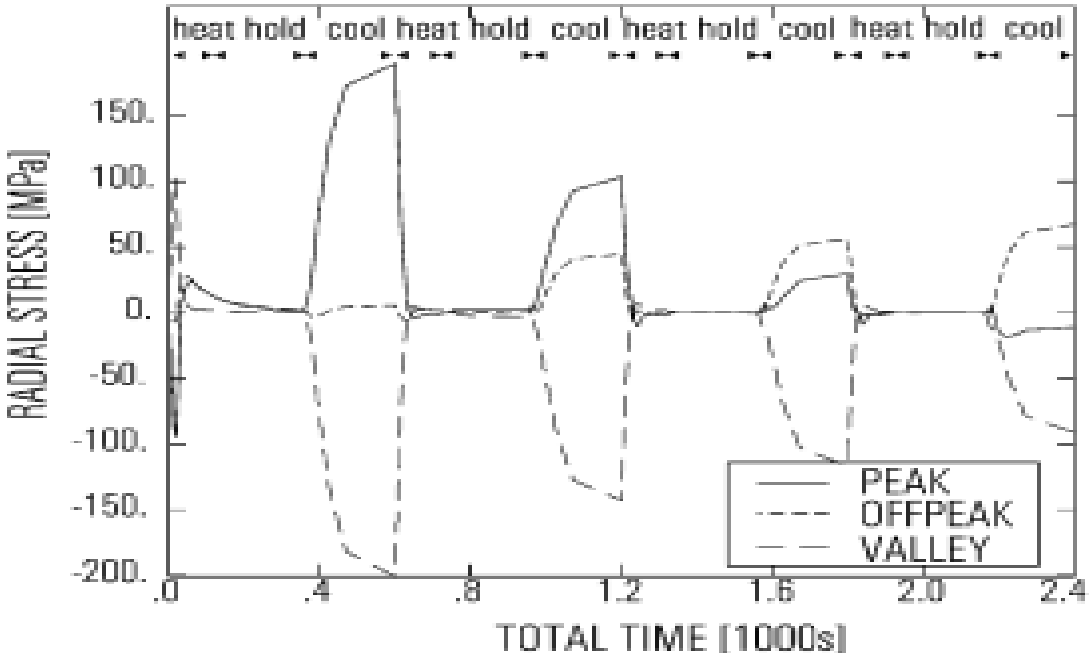

Figure 4.14. Time dependence of the radial TBC stress in "peak"," off-peak"," valley" locations. Elastic-visco-plastic behaviour of the TGO and an oxide growth rate of 0.33 *μm per cycle were assumed [Rösler et al., 2001].*

4.5 GENERAL DISCUSSION

In this chapter, a parametric FE study including different parameters influencing the mechanical behaviour of the TBC was carried out, based on published experimental and numerical works. Some key parameters, such as oxidation of TGO, and stress relaxation at the BC-TGO interface, were incorporated. The radial stress results provided a basic understanding of the TBC system's mechanical behaviour through separate material behaviours of each TBC constituents. Based on the cases considered, some conclusions can be for the sinusoidal TBC interface profile. The main findings can be summarized as follows:

It is apparent that the TGO swelling rate had a great influence on the stress state of the whole TBC system, as the magnitude of the stress induced by swelling varied significantly with different swelling rates. When the swelling rate was fast compared to the creep strain rate in TGO, then the swelling effect dominated, as those two had opposite effects. When the swelling rate was insignificant compared to the creep strain rate, the dominant effect in the system was the thermal expansion mismatch.

There were large compressive stresses in the TGO off-peak region. In the TC peak and nearby off-peak regions, large tensile stresses were observed. Theses are all possible regions for crack initiation. In future analyses, the BC creep should be taken into account as it also has an opposite effect to swelling, such that there could be greater relaxation of the swelling induced strain. A thicker TGO should also be modeled, because 1 μm as modelled so far is not sufficient to study the failure mechanisms of the TBC system. This is where we'd like to extend the analysis in the following chapter. There should also be a study of the sintering effect of the TC layer when the TBC system endures a longer cycling period.

5 EXTENDED PARAMETRIC STUDY OF THE FE MODEL

The variable associated with the TBC model can be classified into four categories, the geometry, the material properties, the boundary conditions and the loading (here, thermal loading). The goal of the following parametric analysis was to investigate the effect of certain parameters on the results given by the FE model.

From the experimental work, it is known that locally, a small variation in the geometry could result in a significant difference in the stress field close to the oxide, which is usually the location of damage nucleation and growth [Aktaa et al., 2005]. To investigate such finding, a series of FE models were analyzed for the effect of interface roughness on the stress state.

In addition, TBC systems are expected to undergo high temperatures for long periods of time. Thus, studying stress distributions between TBC constituents during long thermal cycles is needed to further investigate the aspects affecting the coating lifetime. To do so, longer thermal cycles were adopted in the following section, also accounted for the possible densification of the ceramic, the plastic behaviour of the constituents and creep in TC.

5.1 GEOMETRY DEFINITION

In the following section, the TGO morphology of the model is the main interest, as it is expected that the TGO layer has a critical influence on the local stress field which may affect the interface toughness. First, a walkthrough of how a realistic morphology profile was constructed using Fourier analysis is conducted. Then different roughness profiles will be put together to explore the differences in radial stress induced by geometry.

5.1.1 **A realistic TBC model mesh**

In [Frachon, 2013], the oxide mean profile obtained from SEM was described by Fourier series. The profile was ultimately decomposed into 6 spatial frequencies:

$$P(x) \approx F(x) = a_0 + \sum_k^6 a_k \cos\left(k \frac{2\pi x}{\omega}\right) + b_k \sin\left(k \frac{2\pi x}{\omega}\right) \qquad (5.1)$$

where $\boldsymbol{\omega}$ is the mean wavelength. The value of the parameter $\boldsymbol{a_k}$, $\boldsymbol{b_k}$ representing the TGO mean profile with the six frequencies related to function (5.1) listed below.

f_k	$\frac{1}{\omega}$	$\frac{2}{\omega}$	$\frac{3}{\omega}$	$\frac{4}{\omega}$	$\frac{5}{\omega}$	$\frac{6}{\omega}$
a_k	-0.25	-0.016	0.04	0.2	0.01	-0.03
b_k	-0.03	-0.25	-0.17	-0.12	-0.09	0.05

Table 5. The six spatial frequencies and associated Fourier's coefficients (a_k, b_k) of the TGO mean profile [Frachon, 2013].

The Fourier series was interpolated in ANSYS using cubic splines. The mesh was generated in the same fashion as described in Chapter 3. The length and width of the elements were controlled at the beginning of the geometry data input. The meshed TBC system is shown in Fig.5.1 c).

Because we did not have access to our own SEM images, we used data from [Frachon, 2013]. However, the method illustrated here (Fourier series decomposition, selection of an appropriate number of harmonics, and interpolation using splines) is expected to be fairly general.

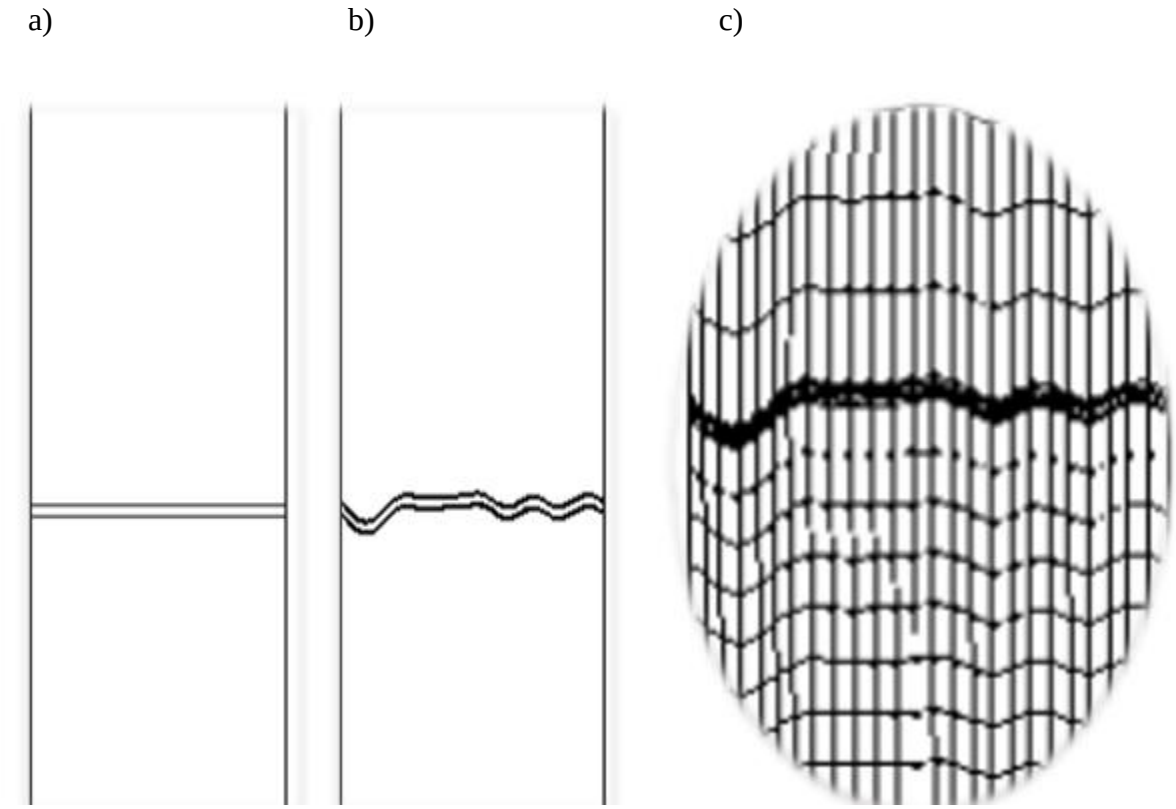

Figure 5.1. TBC realistic profile evolution, from a) a flat TBC to b) the TBC interface generated with the Fourier transfer function c) the mesh generated with the realistic profile.

5.1.2 **TBC residual stresses in different interfacial roughness profiles**

Due to the rough TC-BC interface from the deposition, highly localized compressive and tensile stress appear after heating in the valley and peak locations, respectively.

The results illustrated in Fig.5.2 pertain to four roughness profiles that underwent a 600 second thermal cycle between ambient and a temperature $1{,}150\,°C$. The amplitude of the mean wavelength varied from $5-20\,\mu m$, as commonly used in the literature [Busso, Freborg, Rösler, Sfar et al.]. The selected range of amplitudes was also compared with the realistic amplitude determined by Fourier series. As stated in Chapter 4, with no oxidation assumed, the main stress source is only the thermal expansion mismatch. The TBC roughness causes the thermal expansion

mismatch stress to redistribute, with the stress minimum in the valley location and large tensile stress in the peak location. As can be seen in Figure 5.2, the amplitude of the interface wavelength was the determinant of the stress distribution and intensity. When the amplitude was larger, the radial stress was higher. From $A = 5$ μm to $A = 20$ μm, the maximum tensile stress

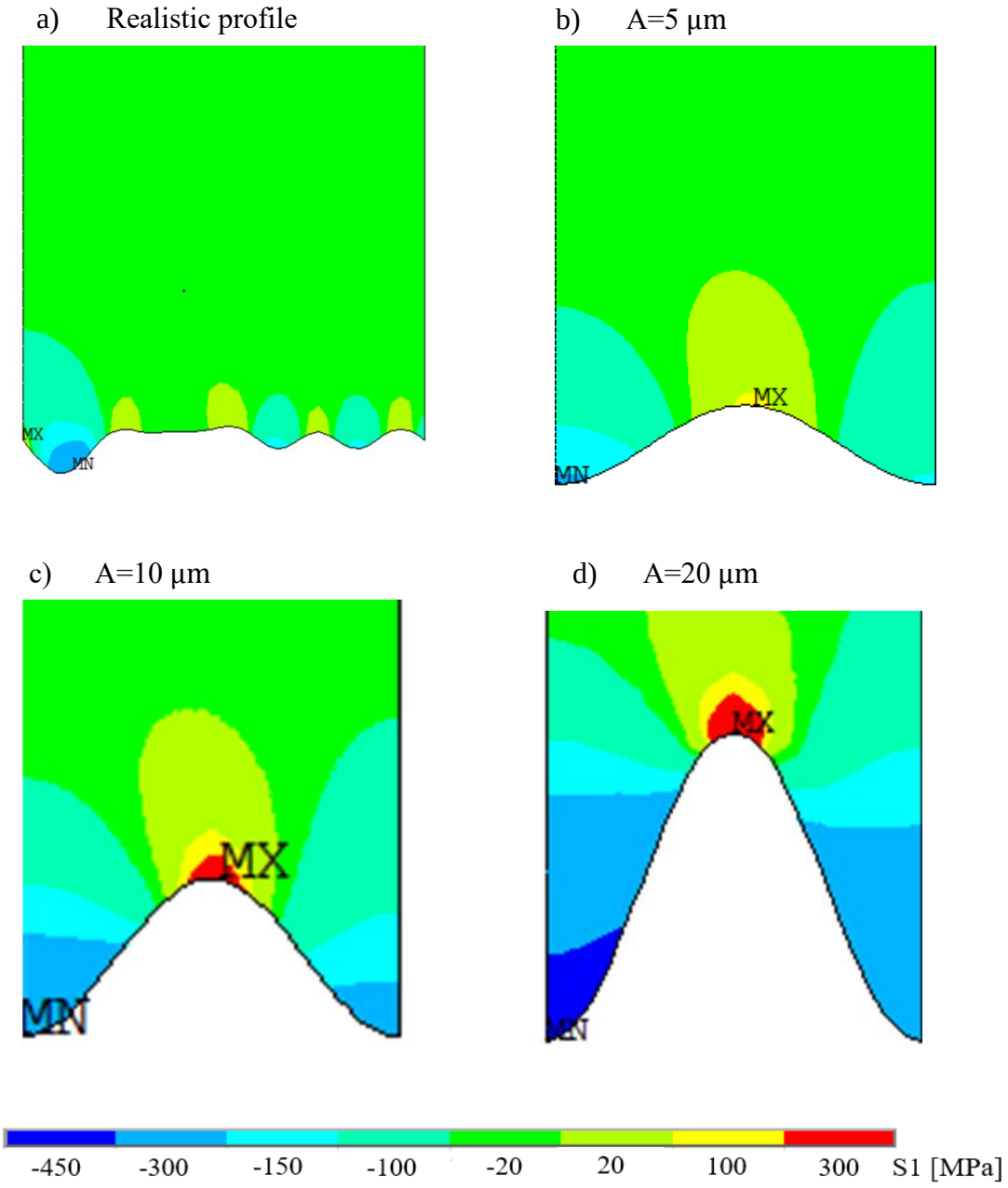

Figure 5.2. Contour plot of different roughness profiles' radial residual stress after 600 s long cycle with no TGO growth.

increased substantially from 73 to 300 MPa. Larger tensile residual stress could lead to crack initiation, which may propagate and lead to material failure at the interfacial asperities. Nonetheless, within the TBC roughness range studied, all the tensile stress maxima presented in the peak location of the interface. Therefore, we could select a relatively simple yet convincing roughness for the brevity of the next section of analysis. In the following approach, the sinusoidal interface was of a wavelength of 48 μm and amplitude of 10 μm. These values are commonly obtained through observations of coating micrographs and have been used in the literature before [Busso, Freborg, Rösler, Sfar et al.].

Even though the roughness and the result in Fig.5.2 a) obtained was very convincing, we were still faced with the limitation of a maximum of 32,000 elements or nodes in the academic version of ANSYS. This did not allow for a complete mesh sensitivity analysis. Also, doing the same kind of computation would require a lot more time investment on the realistic profile comparing to that of the simplified profile, moreover, the experimental data from the literature are not complete, there is no significant cause to simulate some existing SEM image that would not suite our purpose. Therefore, we will just keep the realistic TBC modeling as a method in mind for future use for more precise calculation when we need to conduct the analysis for studying the failure mechanisms/ lifetime prediction. In the following section, the sinusoidal profile is used again.

5.2 LONGER THERMAL CYCLES WITH PARAMETRIC STUDY OF MATERIAL PROPERTIES

In the real world of TBC system operation, the cycle time is much longer than that stated in Chapters 3 and 4, which was for material isothermal testing purposes. Especially for the land-based turbine, the operation time is much longer, while the cool down and heat up periods are relatively short. As shown in Fig. 5.3, the model proposed next consisted of four thermal cycles. The first 600 second cycle was relatively short, aiming to reproduce the turbine's initiation period, that is, before the turbine started the working cycles. Then, the thermal cycles were much longer,

namely one day for the high temperature dwelling, 20 minutes to heat up and 40 minutes to cool down, in accordance with the literature [Frachon, J., 2009].

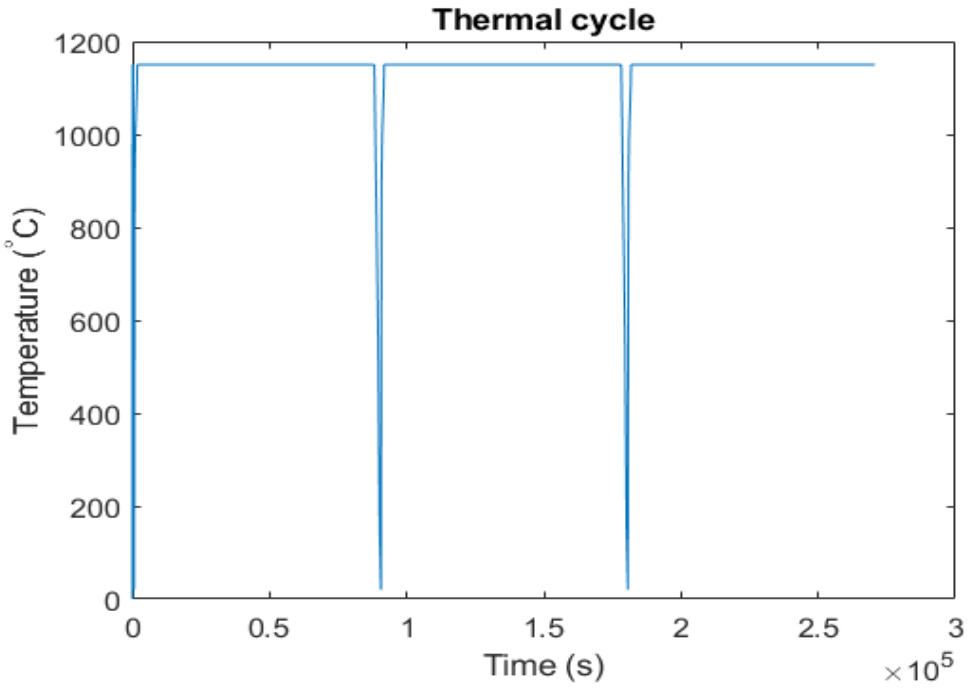

Figure 5.3. Long thermal cycles used in FE analysis, starting with a short 600 s initiation period where the initial thickness of TGO was generated, followed by three long thermal cycles including a heating period of 1,200 s, dwelling for a day and a cool down period of 2,400 s for each cycle. The total cycling time was 50 hours and there were 2.2 long cycles modeled.

Along with longer thermal cycles, the TBC materials underwent even more complex changes in their material characteristics. While in the short thermal cycle, there was no phase transformation in TC, through the longer service time, TC layer would undergo and creep. While BC layer's rate-dependent creep behaviour was considered, there was also rate independent plastic behaviour that could exist in the material. The following section will compare each behaviour separately, to examine the effect of each on the whole system's residual stress field. The swelling model was the exponential swelling. The stress distribution with BC creep for the long thermal cycle was set as the nominal case, where the stresses were maximal at the end of each thermal cycle, when the

system ramped down to ambient temperature. The peak location of the TC layer had the maximum tensile stress whereas the valley location presented the maximum compressive stress.

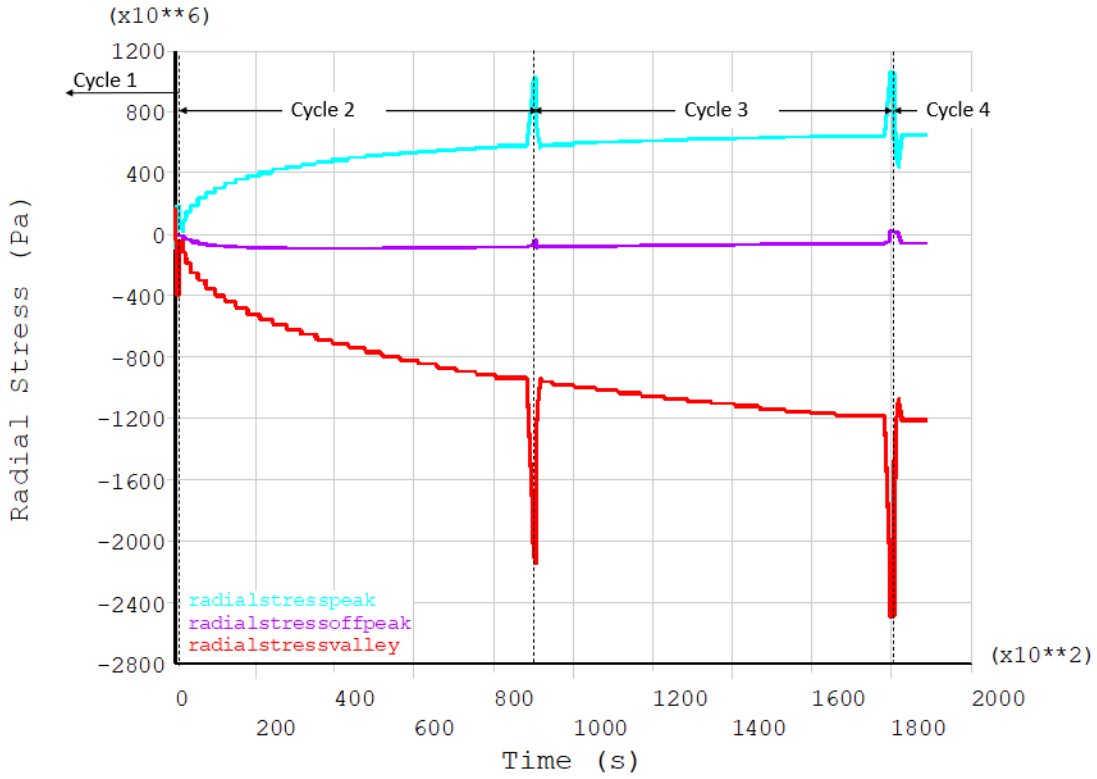

Figure 5.4. Residual stress distribution of the TC layer at peak, valley and off-peak location for Benchmark case, where BC, TGO are both elasto-plastic, TC behaves elastically.

5.2.1 **The effect of the BC plastic behaviour**

From Figure 5.4 one can find that when BC creep was in effect, the residual stress during hot time was not fully relaxed by creep, the system still has considerably high stress after cooling. As a result, the plastic deformation should be accounted for in the BC layer.

CASE	BC	TGO	YSZ(TC)
°N 4	Elasto-viscous	Elasto-viscous	Iso-transverse elastic
°N 5	Elasto-visco-plastic	Elasto-visco-plastic	Iso-transverse elastic

The BC plastic behaviour captured the nonlinearity of the BC material. It was simulated by imparting the plastic characteristics illustrated in Section 3.7.5, following the bilinear isotropic hardening rule. Furthermore, during the cooling and reheating stages of the thermal cycle, the BC layer behaved elastically, because of the rapid increase in the yield stress at lower temperatures [He, Hutchinson and Evan, 2003].

5.2.1.1 Results

In the result shown in Fig.5.5 for the case where BC plasticity is in effect, the system presented a residual stress growth after each cycle, and the maximum stress in all locations were obtained at the end of cooling. In the first cycle, radial stress cycled from around 140 to -200 MPa in the valley location.

After a long dwelling period, at the end of the second thermal cycle, the valley location no longer had the maximum stress of all locations in TC; the off-peak location started to present a higher tensile stress at 160 MPa, and the peak location residual stress became compressive, with a maximum compressive stress of 220 MPa. At the end of the third thermal cycle, the stress state stayed the same as it was in the previous thermal cycle. However, the maximum tensile stress rose to 310 MPa, the valley location's tensile stress also became a bit more pronounced compared to format the end of cycle 2. The compressive stress became approximately 1.8 times larger.

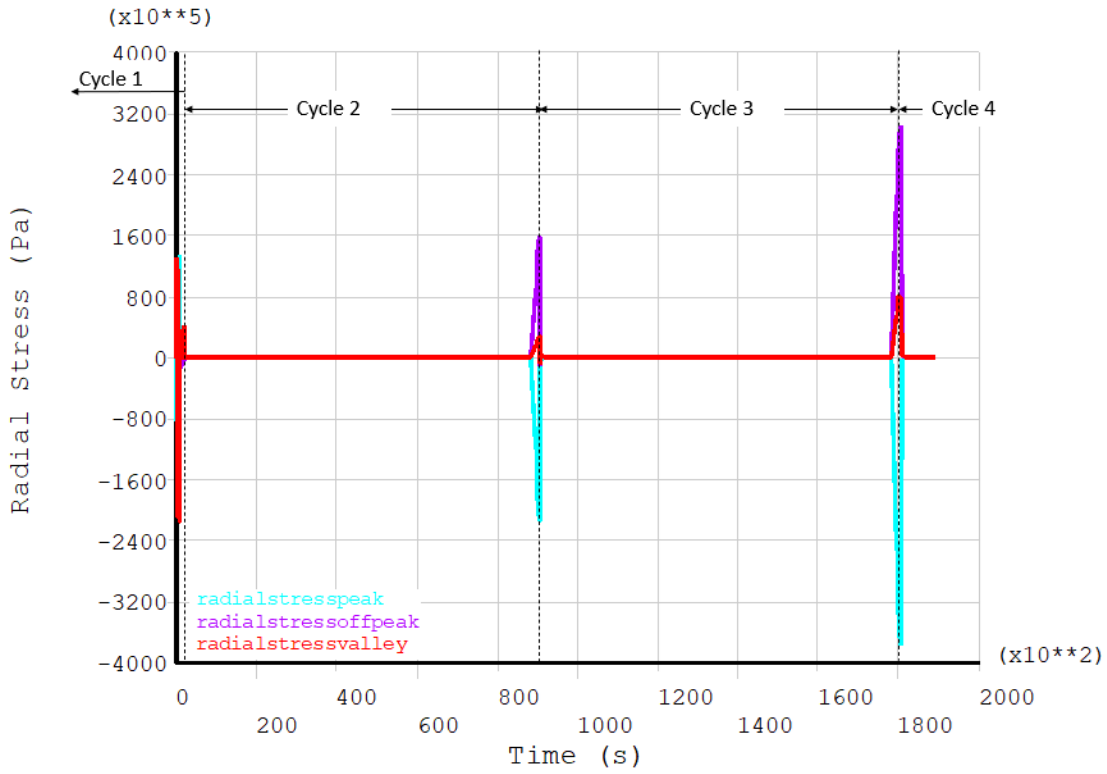

Figure 5.5. Radial residual stress plot for Case where BC, TGO are elasto-visco-plastic, and the TC layer still behaves elastically.

5.2.1.2 Discussion

From Fig. 5.5, we can see that the BC plastic behaviour influenced the TC stress distribution greatly compared to Fig.5.4. The stress state was reversed by taking the BC plasticity into consideration. Without BC plastic deformation, the maximum tensile stress showed inn the valley location; whereas with BC plasticity, the maximum radial residual stress presented at the off-peak location. From Fig. 5.4 and Fig. 5.5, it is noticeable that the stress gradient of the maximum compressive stress decreased with BC plasticity included. This may be explained by the fact that the stress from the off-peak location was more dominant in this case. The tensile zone at the TC layer was extended. The combined effect of the valley and the off-peak location residual stresses was largely tensile, resulting in a smaller stress difference compared to the peak location. In

a) Whole TBC system stress contour plot at 90,600 s

b) Whole TBC system stress contour plot at 180,600 s

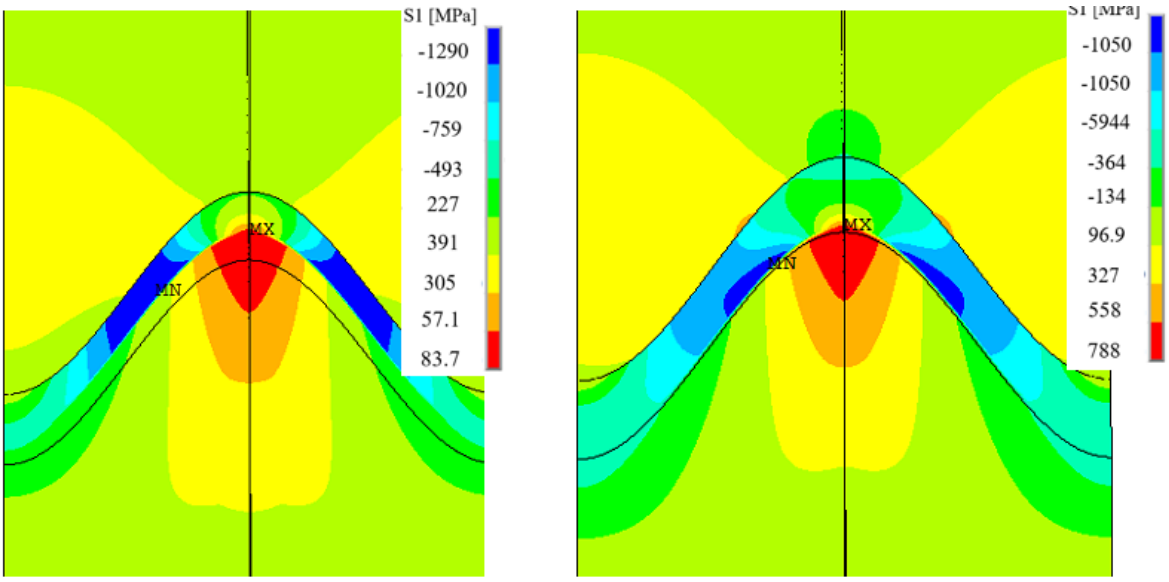

c) TC layer residual stress contour plot at 90,600 s

d) TC layer residual stress contour plot at 180,600 s

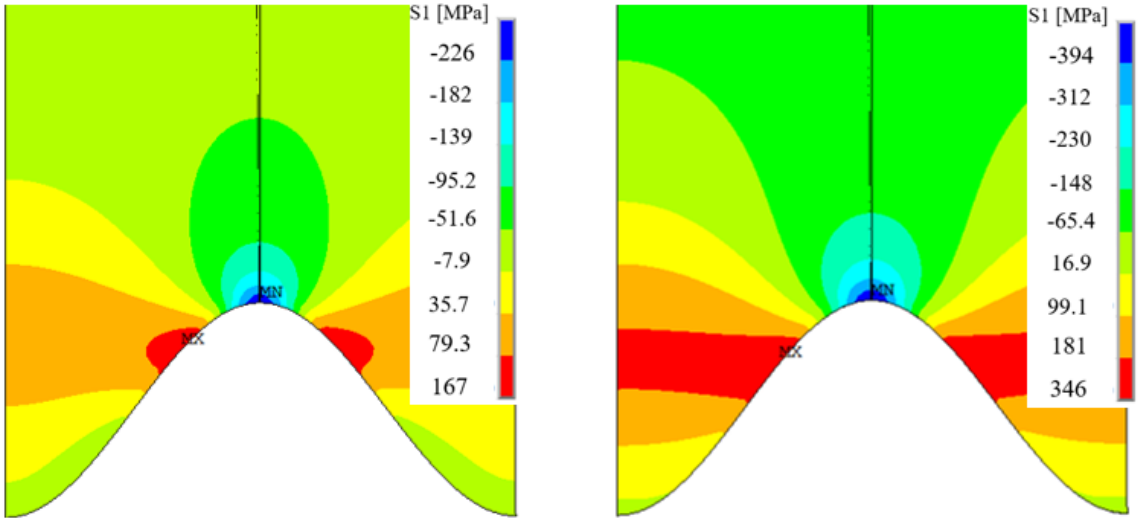

Figure 5.6. The residual stress distribution of the TBC system at the end of the a) second and b) third thermal cycle; the stress distribution of the TC layer at the end of the a) second and b) third thermal cycle.

addition, with BC plasticity included, the stress induced during the heating stage relaxed, whereas when the BC was not plastic, the swelling induced large growth stress is kept in the system.

From the contour plots in Figs.5.6 a) and b), one can see that the stress distribution in the BC layer was always similar, with the largest tensile stress in the peak location of the BC layer. This was mainly due to the thermal expansion mismatch between BC and TGO layers. The combined effects of material characteristics between TC and BC became less pronounced as the cycle time increased, because thickening of the TGO layer reduced the contractive effect from TC to BC. With BC plasticity included, stress within the BC layer increased slightly from cycle 2 to cycle 3. Even though tensile stress remained relatively high compared to the TC layer, the plasticity did reduce the magnitude of the BC residual tensile stress slightly from 837 MPa to 788 MPa at the end of the cooling period in the peak location, the qualitative repartition of the stress remained unchanged. This reduction in the BC tensile stress was also observed by Bäker et al. [2005] with similar rate of change. On the other hand, the compressive stress in the TGO layer became smaller as the TGO got thicker. The maximum tensile stress in the peak location of BC generated from BC plastic behaviour reflected the experimental result that the failure crack path is partially at BC, partially at TGO [Bednarz, P., 2007].

From Figs. 5.6 c) and d), one can also see that in the off-peak location, the tensile zone was more stretched out comparing to the result from previous thermal cycle. This phenomenon could result in a crack that would initiate in the off-peak location due to the large tensile stress coalesce with the adjacent off-peak location cracks.

5.2.2 **TC creep and aging behaviour**

The following section examines the effect of TC creep on stress relaxation and the effect of the aging effect on the stress distribution in the TC layer. Results were compared between cases where TC was elastic, with creep, with sintering, or both.

CASE	BC	TGO	YSZ(TC)
°*N 4*	Elasto-viscous	Elasto-viscous	Elastic
°*N 6*	Elasto-viscous	Elasto-viscous	Elasto-viscous
°*N 7*	Elasto-viscous	Elasto-viscous	Elasto-plastic
°*N 8*	Elasto-viscous	Elasto-viscous	Elasto-visco-plastic

It is acknowledged that as the thermal cycling time prolongs, the aging effect of ceramic TC becomes apparent [Caliez, Stainbrech, 2001]. The increase is most pronounced in the first 200 h, and tends to slow down for longer annealing periods. The stiffening shown in the Young's modulus from annealing is represented as sintering. The increase in elastic modulus results in the enhancement of thermal residual stresses.

For the present study, we introduced the Young's modulus increment by setting the function presented in Section 3.7.6. At the beginning of the Young's modulus increase, the change in Young's modulus was rapid and, with the exposure to hot temperature, the rate of the increase slowed down and eventually plateaued [Guang et al., 2017], while it got closer to a fully dense TC material with a Young's modulus of 210 MPa. As a result of sintering, the porosity of the YSZ TC layer got smaller, and the Young's modulus became greater, as illustrated in Fig.3.9.

5.2.2.1 Results

Figure 5.7 illustrates the residual stresses in the TC layer in three locations for the case where BC and TGO behaves elasto-viscously and the TC's creep behaviour is accounted for. The maximum stress was the largest in the initiation cycle. Starting from the end of the second cycle, the maximum tensile stress presented in the off-peak location. The value of the maximum tensile stress actually increased based on the results in Fig.5.10 i) and j). Why Fig. 5.6 shows the opposite is

because the location of the maximum stress in the off-peak location shifted downwards closer to the valley location, whereas the selected element of interest for the off-peak location was upward. Overall, the compressive stress became smaller (211 MPa *vs* 188 MPa), and the tensile maximum stress grew from 158 MPa to 195 MPa. Meanwhile, the TC peak location possessed the largest compressive stress at the end of cooling in cycle 3.

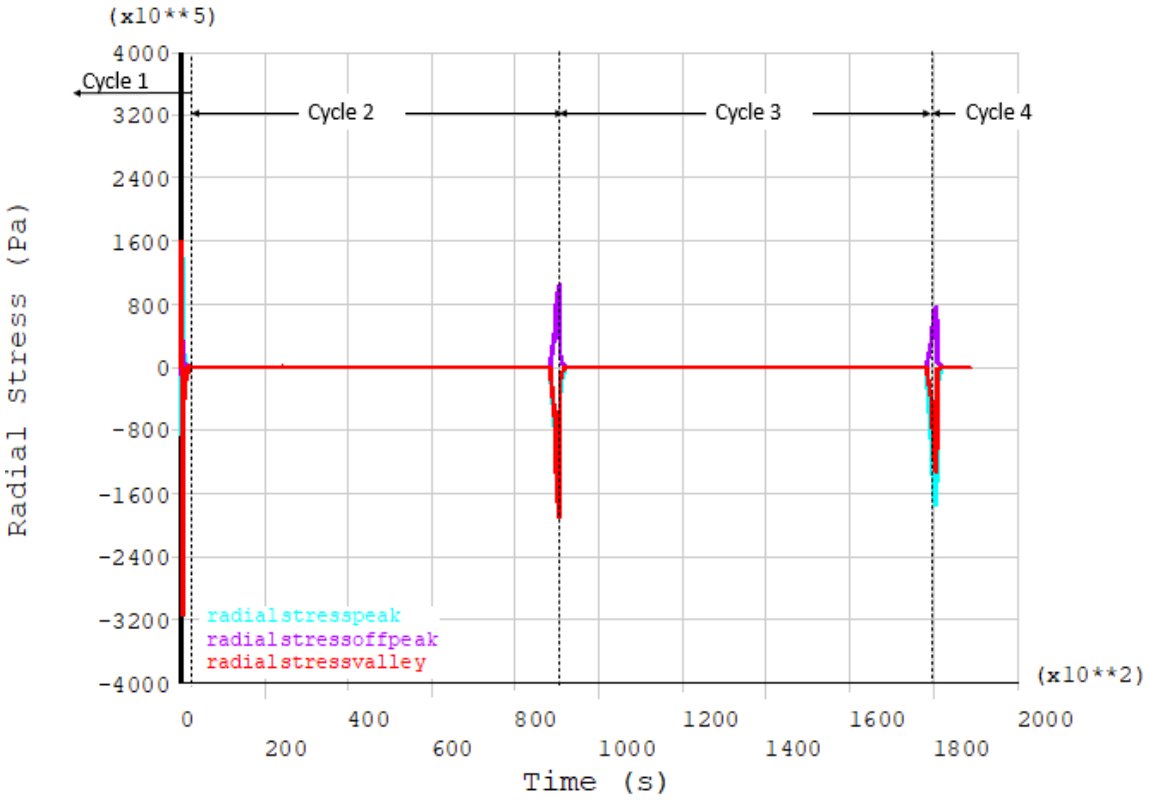

Figure 5.7. Radial residual stress plot for elasto-viscous BC, TGO and TC.

From Fig. 5.8, one can see for the case where BC behave elasto-viscously and TC underwent sintering, the stress rose during the time evolution of the thermal cycle. The peak location underwent tensile stress growing from 160 MPa at the end of the first thermal cycle to 1.5 GPa at the end of the third thermal cycle. By contrast, the valley location possessed a large compressive stress that grew over time. The stress state in the off-peak location was always around zero. During the heating stage of each thermal cycle, the residual stress of the system continued to increase.

As can be seen from Fig.5.9 where the TC layer was assumed to have both creep and sinter behaviour, the stress remained near zero when the system was heating. The off-peak location presented a tensile stress of 217 MPa at the end of the second cycle's cooling stage and a tensile stress of 303 MPa at the end of third cycle's. On the contrary, the valley location had a slight decrease between the end of the cooling periods of the second and the third thermal cycle (262 MPa vs 231 MPa).

Figure 5.10 a) shows that the tensile stress in the BC layer peak location gradually reduced from 1060 MPa in the 2nd thermal cycle to 630 MPa in the 3rd thermal cycle, when the system had creep present in the TC layer. The stress states in Fig. 5.10 of a) and b) were quite similar to those in e) and f), where the system underwent sintering and creep in the TC layer. The slight difference is that in plots e) and f) the maximum tensile stress at the TGO/BC interface decreased marginally, and the TGO compressive stress zone was gradually reduced away from the off-peak location, and the magnitude reduced much less compared in plots a) and b). Similarly, in the TC layer stress plot of the three cases, both the case when all TBC constituents behave elasto-viscously and the case where BC and TGO behaves elasto-viscously, TC behaves elasto-viscous-plastically show the off-peak locations had the largest tensile stresses in the TC layer (Fig.5.10 g), h) and k), l)). In the case where TC only presented its creep behaviour, there was a slight decrease in the compressive stress in the valley location, and a small increase in the tensile zone in the peak location. In the same fashion, a decrease was observed in the elasto-viscous-plastic TC's compressive zone and a greater increase in the off-peak tensile stress as shown in Fig.5.9. In the case with TC's densification, the stress distribution was different from that of the other cases: the peak location was under tensile stress and the TGO layer was also largely tensile.

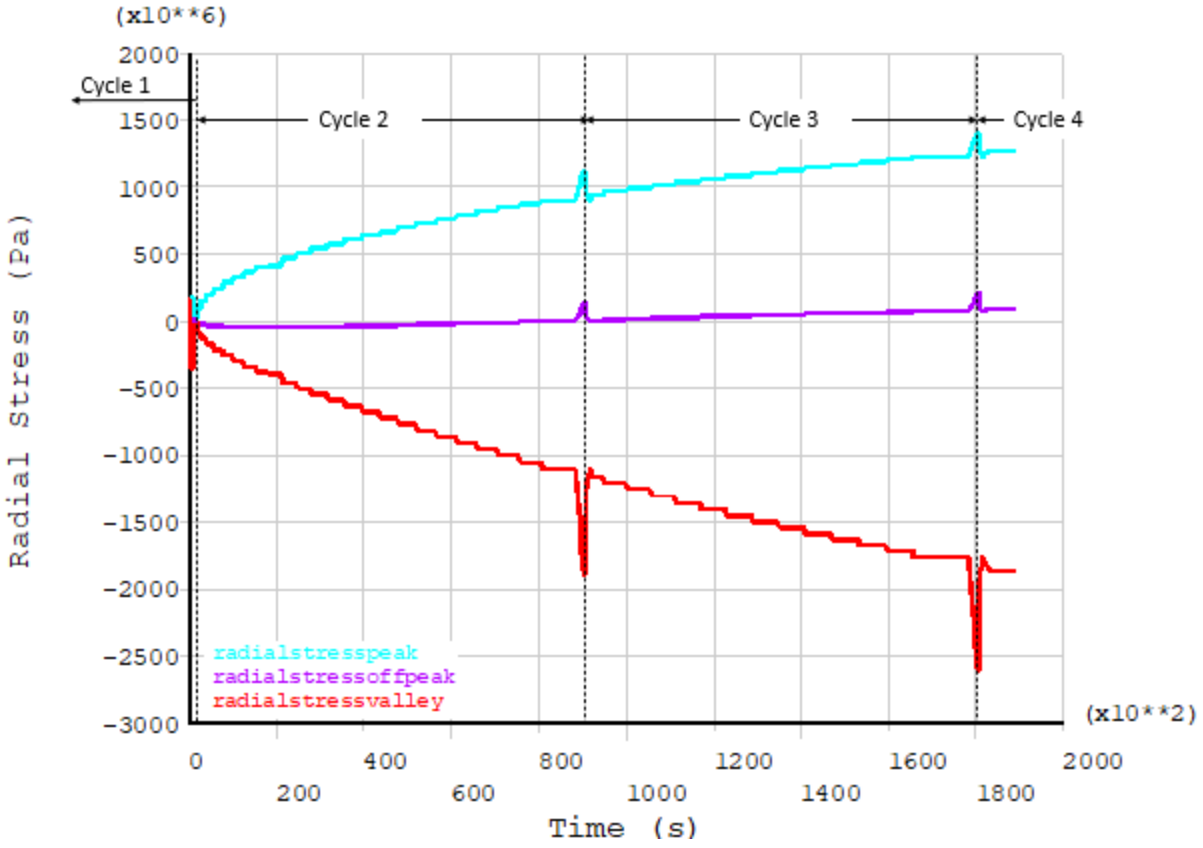

Figure 5.8. Radial residual stress plot for the case considered TC sinter, BC and TGO behaves elastic-viscously.

5.2.2.2 Discussion

When the creep was not present in the TC layer, the largest tensile stress appeared in the peak location (Fig. 5.10). When creep was added to the sintered TC, the tensile stress zone shifted to the off-peak location. The tensile zone became wider in the case where both creep and sinter present in TC layer, and the radial stresses in both peak and valley locations became largely compressive. This could lead to a prediction of the crack initiation location, which is the tensile zone in the off-peak location.

The residual stresses for case with only TC sinter showed that with the increasing Young's modulus, the TGO growth stress could not be relaxed properly by the TC and BC creep, and the

rapidly increase in the modulus also caused TC stress increase. The growth stress was so large that at the end of the 3.85 μm thickness TGO formation, the tensile stress reached 1.5 GPa which was much larger than the yield stress of TC.

Additionally, from the considerable build up of the maximum radial residual stress after cooling to ambient temperature was seen in the TC creep case, we can also conclude that as the material densified, the maximum stress increased compared to the material without aging taken into consideration. The increase in elastic modulus caused by the densification of the TC material should eventually become smaller and smaller as the material reaches a densified stage.

Linking the result of the case when all TBC behaves elasto-viscously to when BC, TGO behaves elasto-viscously and TC behaves elastically from Fig.5.7, at the beginning of the analysis in cycle 2, the stress relaxation from the creep of TC was more significant compared to the following cycles 3 and 4. This could be explained by the porosity of the model: at the beginning of the thermal cycle, the as-received TBC had higher porosity, which resulted in more significant stress relaxation from creep.

Comparing case solely with TC creep to the case solely with TC sinter, TC aging behaviour changed the location of the maximum stress at the end of cooling; when there was only sintering, the peak location had the maximum tensile stress, whereas when only creep was present in TC, the peak location was always under compression except for the initiation cycle. This was due to the growth of the TGO layer. As the thickening was assumed normal to the interface, the peak with almost zero curvature would be constantly subjected to compression from the swelling strain induced by the TGO growth. In the initiation cycle, both cases presented a 160 MPa stress. However, the stress at the end of third thermal cycle was 15 times larger with sintering (2.6 GPa versus 170 MPa). The sign and trend of the TC residual stress in the peak and off-peak locations was opposite. The maximum tensile stress went down with the increasing TGO thickness in the case where creep was present, whereas the compressive stress went up in both cases. Therefore, the TC sinter behaviour was most likely needed in the analysis of the residual stress. It is worth noting that the TC creep model presented much smaller tensile stresses when compared to any other models. This suggests that creep protects the TBC from spalling by relaxing the stresses at the high temperature.

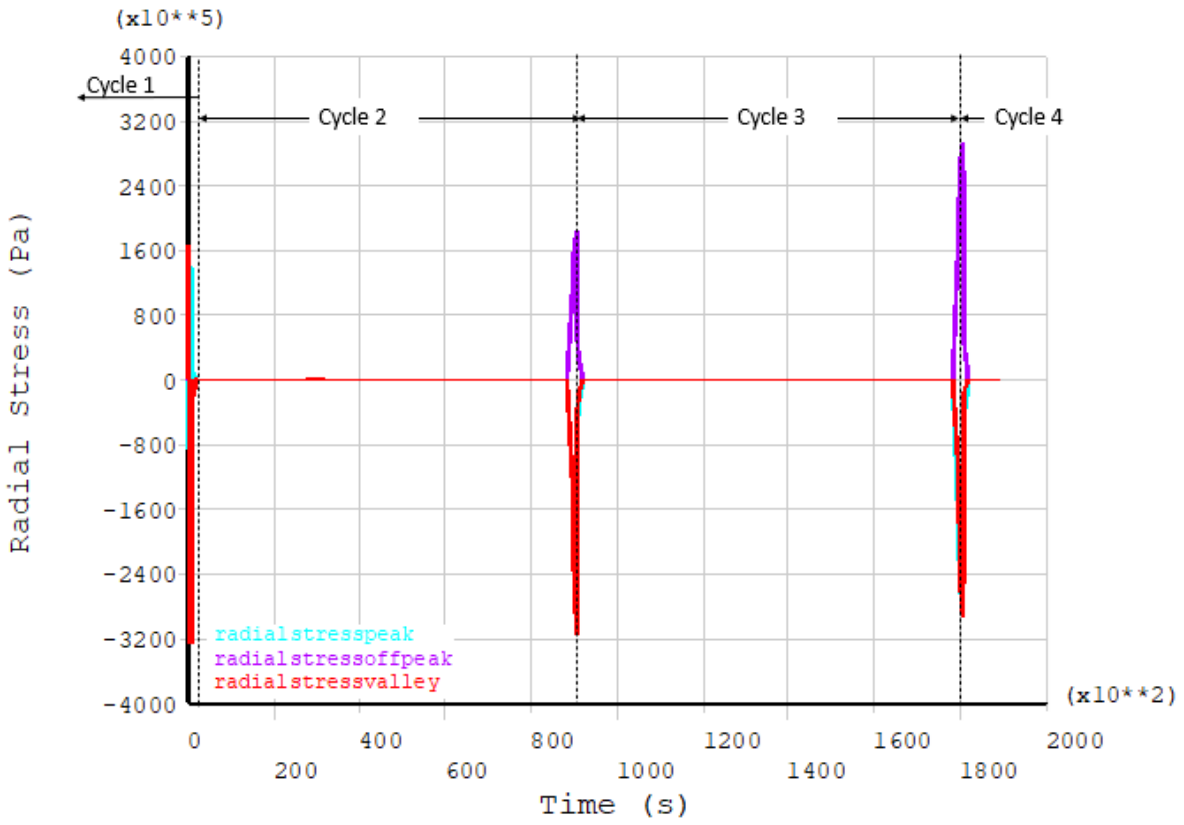

Figure 5.9. Radial residual stress plot for the case when both creep and sinter were considered in the model, and the BC, TGO layer behaves elasto-viscously.

Combining these findings, we can conclude that sintering enlarged the residual stresses in TC, whereas creep greatly relaxed the stress from the TGO growth, and the densification caused stress spikes in the TC layer. Not only did creep affect the TC stress distribution, sintering in TC modified the TGO layer's stress state significantly as shown in Fig. 5.10 c) and d) Therefore, we conclude that while conducting the stress analysis for the TBC system, it is vital to consider the importance of TC sintering.

a) TBC system residual stress contour plot at 90,600s under TC creep condition (°*N* 6)

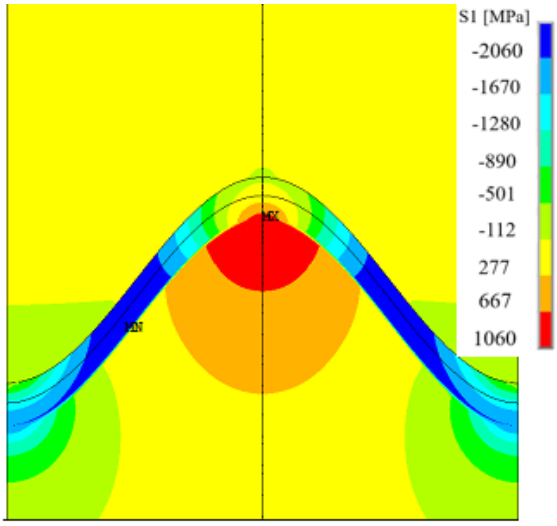

b) TBC system residual stress contour plot at 108,600s under TC creep condition (°*N* 6)

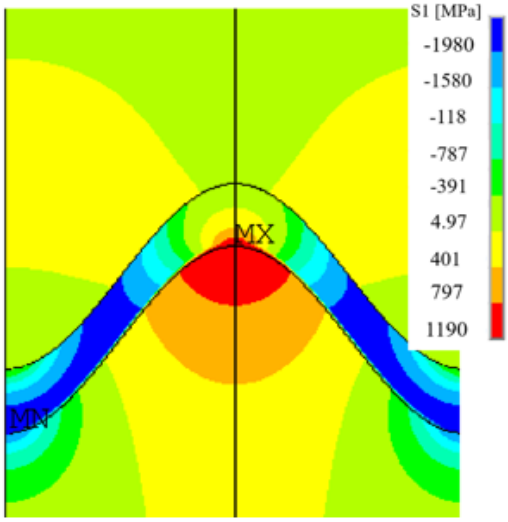

c) TBC system residual stress contour plot at 90,600s under TC sinter condition (°*N* 7)

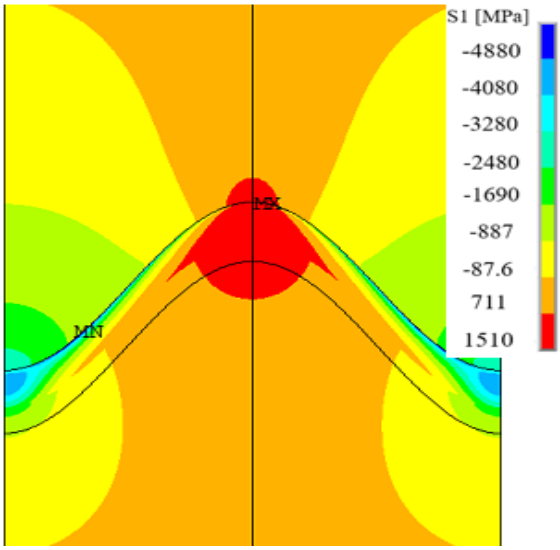

d) TBC system residual stress contour plot at 180,600s under TC sinter condition (°*N* 7)

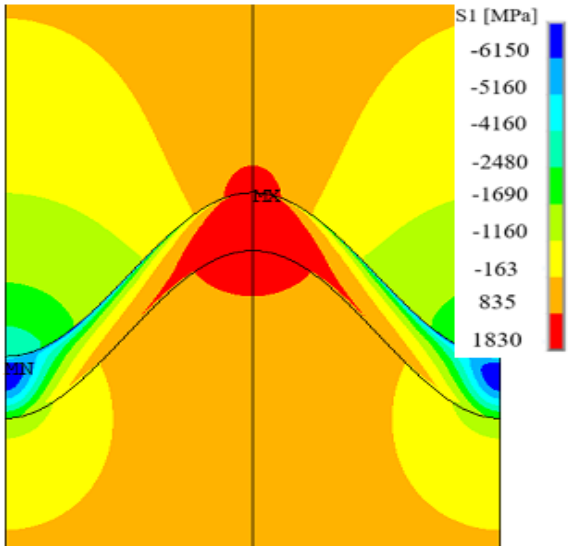

e) TBC system residual stress contour plot at 90,600s under TC creep & sinter condition (°*N* 8)

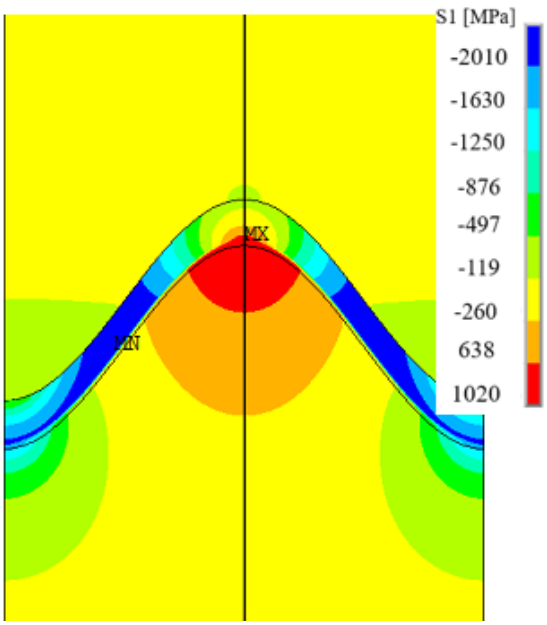

f) TBC system residual stress contour plot at 180,600s under TC creep & sinter condition (°*N* 8)

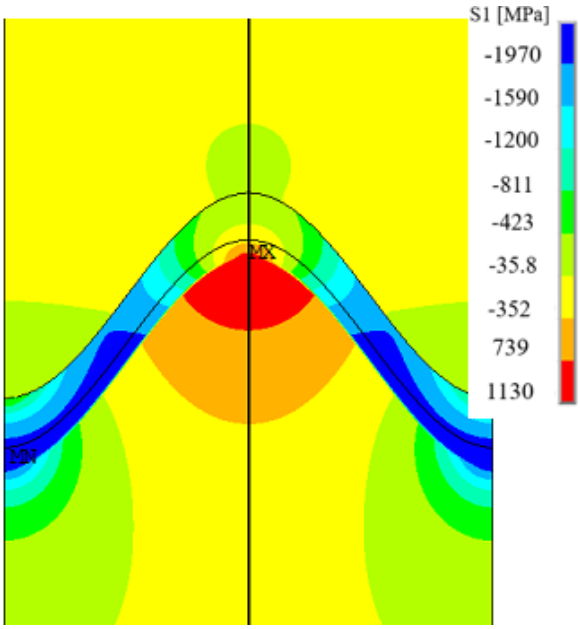

g) TC layer residual stress contour plot at 90,600s under TC creep condition (°N6)

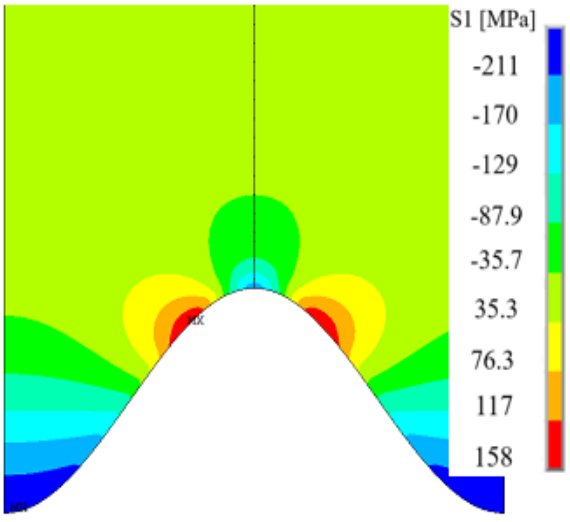

h) TC layer residual stress contour plot at 180,600s under TC creep condition (°N6)

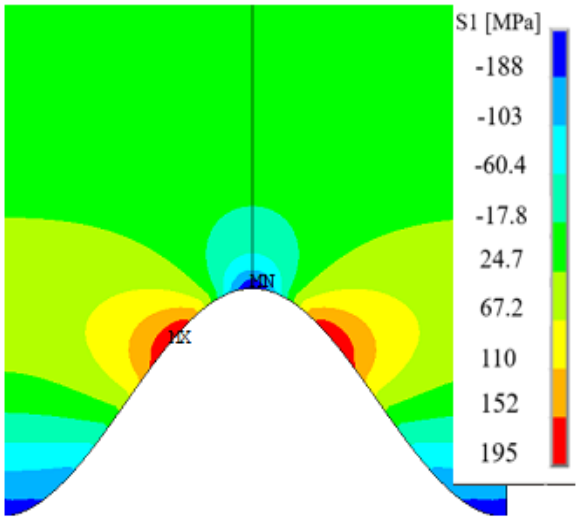

i) TC layer residual stress contour plot at 90,600s under TC sinter condition (°N 7)

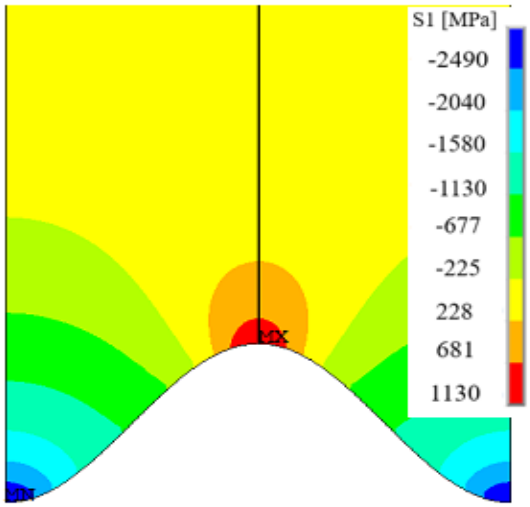

j) TC layer residual stress contour plot at 180,600s under TC sinter condition (°N 7)

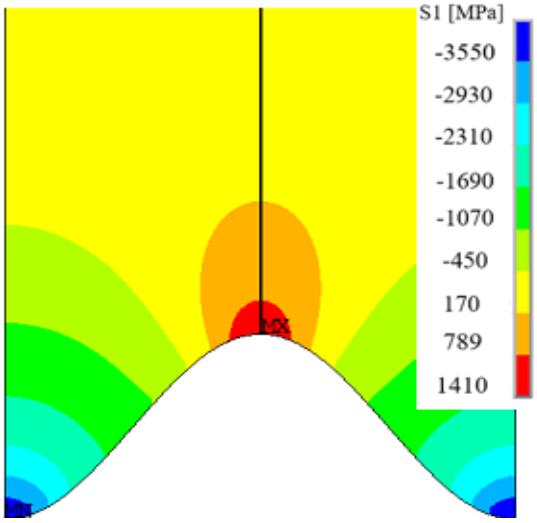

k) TC layer residual stress contour plot at 90,600s under TC creep & sinter condition (°*N* 8)

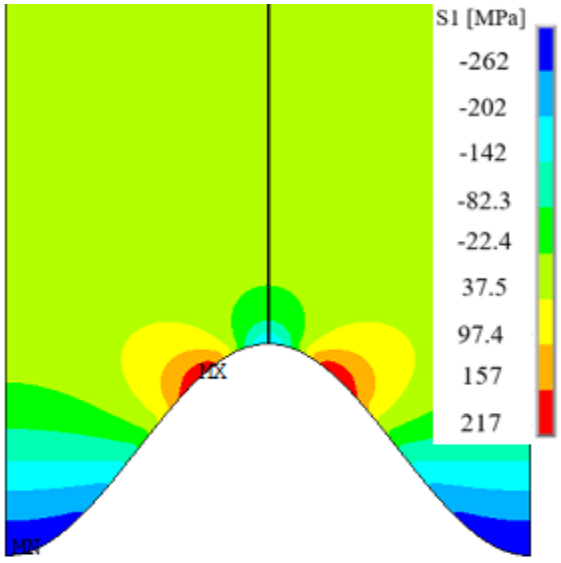

l) TC layer residual stress contour plot at 180,600s under TC creep & sinter condition (°*N* 8)

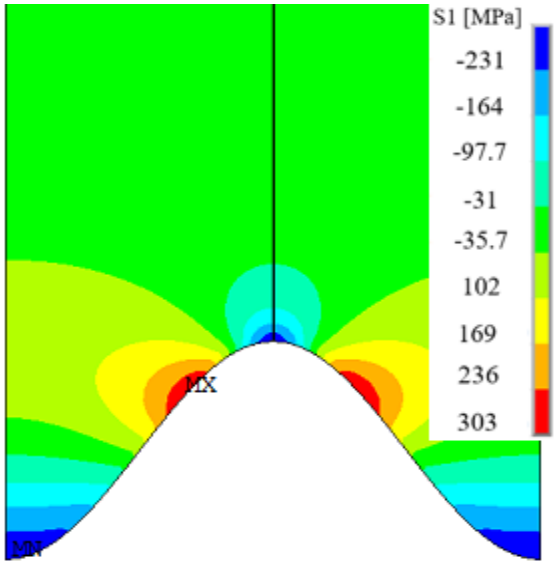

Figure 5.10. Contour plots of TC creep condition and TC creep and sinter condition, with the residual stress plot of a)-g) TBC system and h)-l) the TC layer.

5.2.2.3 TGO-growth-induced residual stress

TGO radial stress exerts significant influence on the crack growth initiation parallel to the oxide interface. The stress induced from the TGO growth can be alleviated by creep in the BC and TGO layers, as seen in Figs. 5.5, 5.6, 5.10 a), b). The redistribution of the stress was present when creep was taken into consideration. Compared to the case with no plasticity, when the BC inelastic behaviour was included in the model, the effect on residual stress was substantial.

When looking at the TGO residual stresses, one can note from Figure 5.10 that almost the entire TGO layer was under compressive stress, and that there was only some small tensile stress seen at the off peak and valley locations closer to the TC layer. In addition, the growth stress was more significant compared to the thermal stress in the system: it ranged from $1{,}290$ GPa to $2{,}010$ GPa. The stress values were largely affected by the swelling rate chosen for the TGO growth, as stated in the previous chapter. Thus, when comparing the stress distribution and magnitude, one should also consider the swelling rate differences between models. Ideally, it should be considered on a case- by- case basis when experimental work is combined for more convincing results when it comes to the stress analysis for system failure and lifetime analysis.

5.3 GENERAL DISCUSSION

The main causes of TBC damage are oxidation of BC as well as thermally- and mechanically induced stresses in the coating system. Coating failure may be further affected by a stiffness increase in the TBC due to sintering, as significant differences in the residual stress distribution in the TC material were observed, showing the importance of considering the Young's modulus nonlinearity during long dwelling periods.

In addition, creep induced stress relaxation in the BC and TC layers. Creep during the high temperature phase reduced the stresses at the end of dwelling time, resulting in a stress

redistribution at the TC-BC interface depending on materials properties as well as interface geometry. All these degradation mechanisms may influence the actual damage process in a complex way. Consequently, changes in the thermal loading scenario during service are expected to affect the failure mode and the lifetime of coated components.

5.4 LIMITATIONS OF THE TECHNIQUES USED AND/OR CONCLUSIONS DRAWN

The limited information we had of the real dynamic interface roughness of the model prevented us from programming an interface profile that changed with time. Nevertheless, the real dynamic interface roughness amplitude is an important factor as the stress distribution depended strongly on the roughness, as seen in Section 5. In addition, the whole microstructure of the model was strongly time dependent, as were the material's mechanical and thermal behaviours, but was not available. For future work, it would be important to combine experimental work along with simulations for accurate and reliable results. In particular, for implementing dynamic geometries, nodal locations could be updated at each timestep during the solution with the reference geometry information from the corresponding SEM image. As for a successful predictive model, if the result from the test conducted for residual stress (i.e. indentation test) could already match the full material behaviour model presented in Chapter 5 at over 90% accuracy, then one can conclude with confidence that, with the dynamic profile added to the simulation, the model could further predict material failure.

When considering the material creep behaviour, it is important to consider that the porosity difference would reflect as difference in variation in tangent modulus relating to sintering time. In the current model, the TC material was considered as a solid when it comes to its material behaviour in the modeling, but it was not the reality, because, from the material microstructure point of view, the TC layer close to the TGO has a very low porosity at less than 5%. This means that sintering may not be significant around the interface area, whereas TC close to the top surface could be affected by sintering greatly due to a larger porosity

In the present work, the oxide was assumed to consist solely of $\alpha\text{-}Al_2O_3$. However, other compositions should be evaluated as well. For example, from the microstructure point of view, oxidation causes Al depletion; therefore, the microstructural changes inside the BC layer affected by long exposure times during cycling should be addressed.

In addition, as the creep behaviour was assigned to the layer uniformly and homogeneously throughout the entire analysis, the effect of creep on porosity as the TC layer densified during the thermal loading was not reflected. This was not completely convincing, since densification does affect the effectiveness of the stress relaxation: the smaller the TC layer's porosity, the less the TC creep affects the residual stress.

The plasticity of the model could also be overestimated because plasticity is only implemented without considering the viscosity of the material which is actually visco-plastic.

Lastly, all layer's materials were considered isotropic; however, they present defects due to preferential orientation during the coating process. Therefore, this assumption was not entirely realistic. Overall, stress values in TBC constituents were likely overestimated for the reasons listed above, and because information on the microstructural behaviour was not included into the numerical model (i.e., the grain size changed during oxidation which result in a change in creep behaviour, or for longer analyses, where the crack initiates and the coalition of intrinsic mesocracks may affect the entire stress state). In the model described in the current study, with all the possible bias, the results may represent approximately 90% of reality. For example, the maximum compressive stress within the TGO layer at the end of second thermal cycle is 1.97 GPa compared to the result obtained from ruby fluorescence test (-1.83 GPa) by Wright et al. [1999] and under similar thermal environment in the case where the TGO, BC behaved elasto-viscously and TC behaved elasto-viscous plastically. And same scenario applied to TC's result (-231 MPa in the current model vs. roughly -220 MPa) via various experimental and modeling sources [Busso, Evans, He et al.].

5.5 CONCLUDING REMARKS

Based on the above considerations for the analysis, some conclusions can be drawn.

i. The roughness of the TBC interface was an important determinant of the magnitude of the radial residual stress. Larger amplitudes caused higher stress.

ii. The residual stress distribution in the TC layer was affected by the time evolution during the thermal cycle. With TGO formation, the stress was increased and redistributed.

iii. TGO experienced large compressions upon cooling. From the literature [Evan et. Al, 2001], we know that when a thin film undergoes large compressive stress, it will try to alleviate the stress by lengthening itself through displacement in the radial direction. The displacement can happen through buckling or by visco-plastic deformation of the bond coat. The tensile stress induced by such displacements may promote crack nucleation and growth in the system. In addition, imperfections in the TGO roughness also promote tension in the radial direction, which may result in crack coalescence leading to failure.

iv. The creep and plastic deformations in the TBC constituents resulted in stress relaxation during dwelling, and significantly influenced the stress during the cooling stage. When creep and plastic behaviours were included, the residual stresses were much smaller, which may improve the lifetime of the TBC system.

v. When aging acted alone in the TC layer, it induced an opposite stress state compared to that with no creep and no sintering, or no sintering but creep in the TC layer. In addition, aging in the TC layer magnified the residual stresses in the TC layer by two. Therefore, it is important to incorporate sintering in modelling the TC layer.

vi. As TGO formed gradually as a function of time, the stresses induced by BC plasticity caused a reversal in the sign of maximum residual stress. The off-peak location stress increased when the nonlinear behaviour of BC was present.

vii. The large tensile stresses seen at the off-peak location in TC and the peak location in BC could result in crack propagation at the TC-BC interface.

viii. Based on the results obtained from Chapters 4 and 5, we can also observe that the cyclic speed had significant impact on the stress magnitudes.

ix. Through the parametric studies, one can conclude that when the materials undergo long service cycles, material parameters changes and the effects caused by material behaviour became more complex. Specifically, the TC densification caused large compressive stress, which would be detrimental to the TBC system.

6 CONCLUSION

Finite element simulations of radial stresses in APS-TBC due to thermal loading has been presented. These simulations showed that material behaviour and stresses complex correlations. Conditions such as microcracks will totally reverse the stress state [Baker, M. and Seiler, P., 2017], For the current FE model, such noise has been neglected due to incomplete information from experiments and the length of the simulation is on the cusp of where the crack initiation would happen (roughly 1/3 of the amplitude is the point where the initiation of crack usually appear). For the current FE model, such noise has been neglected due to incomplete information from experiments

6.1 BRIEF SUMMARY AND MAJOR CONTRIBUTIONS

In the present work, a generic model was created and used for predicting the stress field in any TBC model with specific characteristics. A parametric study of TBC constituents' mechanical characteristics was developed and validated against data and results from the literature. The results obtained were promising as they were in good agreement with the reference works [Rösler et al, 2001].

In addition, kinetic processes (e.g., oxidation, creep, and sintering) were included to gain insights into the effects of material behaviour on the entire TBC stress field during cyclic loading. This is important for further analyses toward TBC system lifetime prediction. From the modeling results, one can make suggestion on the future coating design, such as larger porosity at the TC layer to prevent large sintering effect, as the densification of the TC material caused significant increase in Young's modulus, which adversely affected the stress magnitude which would result in earlier material failure above the TC valley region.

The TGO growth simulation method used in the present work was an improvement compared to previous work done by Rösler et al. [2001], as stress and creep could be examined layer-by-layer. The thickness of each layer, the total oxidized thickness, and the mesh were all controlled by the programmer.

To go around the limitation in the available number of elements or nodes in the FE model, an alternative approach of studying the coating components with respect to the substrate layer was used successfully, which involved relative coefficient of thermal expansion.

A method of generating realistic profiles for the TBC interface was also implemented. It is important to simulate a real-life geometry rather than a simplified sinusoidal profile to get a better sense of how it would affect the life span of the TBC system, so as to possibly make recommendations to modify the deposition method and material composition.

Overall, the FE approach is a valuable tool that can be used for verifying the results from other explicit simulations, and to make adjustments to the TBC composition, as the creation of the FE model established a good principal foundation for the future simulation. Lastly, it could be used as an alternative to testing for coupons that undergo long thermal cycles, as simulation could give predictions of material stress behaviour under similar conditions in much shorter time.

6.2 RECOMMENDATIONS FOR FUTURE WORK

To improve TBC stress prediction results, some advancements can be recommended, such as addressing the limitations identified above. In addition, from a modeling perspective, the aging effect of TC could be implemented more effectively. Also, as the whole system's stress distribution analysis is based on the global coordination system, but stresses at the TC/TGO interface should be considered at a local level. For instance, one refinement could be making the strain rate of oxidation correlate with the local coordinate system.

It is also important to notice that in the present study, the materials were considered to behave isotropically, but anisotropic material properties might also be investigated.

Due to the limited supporting data from the experimental work, stress analyses have been largely based on the sinusoidal profile, even though more realistic profiles can be introduced in the modeling, as shown. Specific profiles should be matched with specific TBC deposition methods for more relevance and accuracy regarding TBC lifetime predictions, instead of relying on generic data from the literature. In the future analyses, the work should include experiments to be able to include the dynamic morphology transformation during the thermal cycles to achieve ever more realistic results.

The damage mechanism should also be studied in detail. For instance, under fatigue loading, the intrinsic crack-like microdefects evolve within the YSZ layer, and the presence of cracks may release some stresses. Therefore, in future studies of the TBC system, crack modeling should be looked at specifically. In addition, since cracks usually form at low temperature, and behave in a complex fashion, more material data will be necessary to achieve a predictive understanding of the TBC system lifetime. For instance, one could consider that several phases co-exist in the newly grown oxide, with complex associated effects on stress and diffusion during oxidation.

Toward optimization of the coating system, another future step would involve variations is the material property parameters and the inclusions of defects from deposition. A good example for the latter would consist in increasing Young’s modulus of the TBC constituents by some percentage to simulate different compositions (i.e., adding sulfur dopant to TC layer), to investigate the related changes in stress distribution.

BIBLIOGRAPHY

Aktaa, J., Sfar, K. and Munz, D. Assessment of TBC systems failure mechanisms using a fracture mechanic approach. Acta Materialia, 2005; 53, pp.4399-4413.

Bäker, M., Rösler, J. and Heinze G., A Parametric Study of the Stress State of Thermal Barrier Coatings part II: Cooling Stresses. Acta Mater, 2005; 53, pp469–76.

Bäker, M. and Seiler, P., A Guide to Finite Element Simulations of Thermal Barrier Coatings, Thermal Spray Tech, 2017;26, pp.1146–1160.

Beck, T., Herzong, R., Trunova, O. et al., Damages Mechanisms and Lifetime Behaviour of Plasma-sprayed Thermal Barrier Coating Systems for Gas Turbines- Part II: Modelling, Surface & Coating Technology, 2008; 202, pp.5901-5908.

Bednarz, P., Finite Element Simulation of Stress Evolution in Thermal Barrier Coating Systems, Schriften des Forschungszentrums Jülich Reihe Energietechnik/ Energy Technology, 2007; Vol. 60.

Bialas, M., Finite Element Analysis of Stress Distribution in Thermal Barrier Coatings, Surface and Coatings Technology, 2008; 22(24), pp.6002-6010.

Busso, E.P. Oxidation-Induced Stresses in Ceramic-Metal Interfaces. J. Phys. IV. France 9, 1999.

Busso, E.P., Lin J., Sakurai, S., Nakayama, M., A Mechanistic Study of Oxidation Induced Degradation in a Plasma-Sprayed Thermal Barrier Coating System. Part I: Model Formulation, ActaMater,2001; 49, pp.1515-1528.

Busso, E.P., Lin, J., Sakurai, S., Nakayama, M., A Mechanistic Study of Oxidation Induced Degradation in a Plasma-Sprayed Thermal Barrier Coating System. Part II: Life Prediction Model, Acta Mater, 2001; 49/9, pp.1529-1536.

Busso, E.P., Qian, Z.Q., A Mechanistic Study of Microcracking in Transversely Isotropic Ceramic-Metal Systems, Acta Mater 2006; 52, pp.325-338.

Busso, E.P., Wright, L., Evans, H.E., McCartney, L.N., Saunders, S.R.J., Osgerby, S., Nunn, J., A Physics-Based Life Prediction Methodology for Thermal Barrier Coating Systems. Acta Mater 2007; 55, pp.1491-1503.

Busso, E.P., Qian Z.Q., Taylor M.P. et al., The Influence of Bondcoat and Topcoat Mechanical Properties on Stress Development in Thermal Barrier Coating Systems. Acta Materialia 2009; 57, pp.2349-2361.

Caliez, M., Feyel, F., Kruch, S. et al., Oxidation Induced Stress Fields in an EB-PVD Thermal Barrier Coating, Surface and Coatings Technology, 2002; 157, pp.103-110.

Caliez, M., Chaboche. J.L., Feyel F.et al., Numerical simulation of EBPVD thermal barrier coatings spallation, Acta Materialia 2003; 51(4), pp.1133-1141.

Chang, G.C. and Phucharoen, W., Behaviour of Thermal Barrier Coatings for Advanced Gas Turbine Blades, Surface and Coatings Technology, 1987; 30, pp.13-28.

Cheng, J., Jordan E.H., Barber B. et al., Thermal/Residual Stress in an Electron Beam Physical Vapor Deposited Thermal Barrier Coating System, Acta Mater 1998;46(16), pp. 5839-5850.

Echsler, H., Renusch, D., Schutze, M., Bond Coat Oxidation, and its Significance for Life Expectancy of Thermal Barrier Coating Systems, Material Science and Technology, 2004; Vol. 20, pp. 307-318.

Evan, A.G., Mumm, D., Hutchinson, J. et al., Mechanisms Controlling the Durability of the Thermal Barrier Coatings, Progress in Material Science, 2001; Vol. 46, pp. 505-553.

Evan, A.G., He, M.Y. and Hutchinson, J., Mechanics-based Scaling Laws for the Durability of the Thermal Barrier Coatings, Progress in Material Science, 2001; Vol. 46, pp. 249-271.

Evan, H.E., Oxide Failure of TBC systems: An Assessment of Mechanisms, Surface & Coating Technology, 2021; 206, pp. 1512-1521.

Frachon, J., Multiscale Approach to Predict the Lifetime of EB-PVD Thermal Barrier Coatings. Materials. Ecole Nationale Superieure des Mines de Paris, 2009; English.

Freborg, AM., Bäker, M., and Brindley, WJ., Modeling Oxidation Induced Stress in Thermal Barrier Coatings, Material Science & Engineering 1998; 245(2), pp.182-190.

Guang, R., Guan, J., Cheng, X. et al., A Comprehensive Mechanism for the Sintering of Plasma-sprayed Nanostructured Thermal Barrier Coatings, Ceramic International, 2017, 43(13), pp. 9600-9615.

He, M.Y., Evans A.G. and Hutchinson J.W., The Ratcheting of Compressed Thermally Grown Thin Films on Ductile Substrates, Acta Mater, 2000, 48, pp. 2593–601.

He, M.Y., Hutchinson, J.W. and Evans, A.G., Simulation of Stresses and Delamination in a Plasma-sprayed Thermal Barrier System upon Thermal Cycling, Material Science & Engineering 2003; Vol.345(1-2), pp.172-178.

Lapin, J., Effect of Aging on the Microstructure and Mechanical Behaviour of a Directionally Solidified Ni_3Al based Alloy, Intermetallics, 1997(5); 615-624.

Padture, N., Gell,M. and Jordan, E., Thermal Barrier Coatings for Gas-turbine Engine Applications, Science, 2002;296(5566),pp. 280-284.

Pilling, N. and Bedworth,R., The Oxidation of Metals at High Temperatures. J. Inst. Met., 1923; 29, pp. 529-582.

Rejda, E., Socie, D. and Beardsley, B. et al., Fatigue Behaviour of a Plasma-sprayed $8\%Y_2O_3 - ZrO_2$ Thermal Barrier Coating, Fatigue Fract. Engng Mater. Struct., 1997, Vol. 20, No.7, pp. 1043-1050.

Rösler, J., Bäker, M. and Volgmann, M., Stress State and Failure Mechanisms of Thermal Barrier Coatings: Role of Creep in Thermally Grown oxide, Acta Materialia 2001; 49:3659-3670.

Rösler, J., Bäker, M. and Aufzug, K., A Parametric Study of the Stress State of Thermal Barrier Coatings Part I: Creep Relaxation, Acta Materialia 2004;52:4809-4817.

Schulz, U., Saruhan, B., Fritscher et al, Review on Advanced EB-PVD Ceramic Topcoats for TBC Applications, Int. J. Appl. Ceram. Technol., 2004; 1(4), 302-315.

Schulz, U. and Schmöcker, M. Microstructure of ZrO_2 thermal barrier coating applied by EB-PVD. Material Science Engineering: A, 2000; 276: 1-8.

Sfar, K., Aktaa, J. and Munz,D., Numerical investigation of residual stress fields and crack behavior in TBC systems. Material Science Engineering: A, 2002; 333:351-360.

Steinbrech, R. W. and Basu, D., Ceramic Based Thermal Barrier Coating (TBC) for Gas Turbine Application: Elastic Behaviour of Plasma Sprayed TBC, Transactions of the Indian Ceramic Society, 2003;62(4):192-199.

Taylor, M., Gray, S., and Evans, H., Contract Report, 2006; SIEMENS.

Mei Wen, Eric H. Jordan, Maurice G., Effect of Temperature on Rumpling and Thermally Grown Oxide Stress in an EB-PVD Thermal Barrier Coating, Surface & Coatings Technology, 2006; 201, pp. 3289-3298.

Miller. R.A., Behavior of Thermal Barrier Coating for Advanced Gas Turbine Blades, Surface & Coatings Technology, 1987; 30:13-28.

Wang L., Zhao Y.X., Zhong X.H et al., Influence of "Island-like" Oxides in The Bond-Coat on the Stress and Failure Patterns of the Thermal- Barrier Coatings Fabricated by Atmospheric Plasma Spraying During Long- Term High Temperature Oxidation, Journal of Thermal Spray Technology, 2014; Vol. 23, No.3, pp.431.

Wright, P.K. and Evan, A.G., Mechanisms Governing the Performance of Thermal Barrier Coating, Current Opinion in Solid State & Material Science, 1999(4); 255-265.

Zhang, C., Fei, J., Guo et al., Thermal Cycling and Hot Corrosion Behavior of a Novel LaPO4/YSZ Double-ceramic-layer Thermal Barrier Coating, Materials Science Forum, 2007; Vol.546-549, pp.1713-1716.

Zhi, Y. and Hong, N., Comprehensive Effects of TGO Growth on the Stress Characteristic and Delamination Mechanism in Lamellar Structured Thermal Barrier Coatings, Ceramic International,2020; 46(2), pp 2220-2237.

Zhu, J., Chen, W. and Xie, H. et al., Simulation of Residual Stresses And their Effects on Thermal Barrier Coating Systems Using Finite Element Method, Science China, 2005; Vol. 58, No.3:034602.

APPENDIX

I. MESH SENSITIVITY ANALYSIS

A mesh sensitivity analysis is required because the solution of a FE model always depends on the size of elements used. While it is tempting to use the finest mesh possible, the physical memory available for solving the FE problem is also a concern, resulting in a trade-off. Several mesh simulations were done for the illustration of the ensuing differences in residual stress results. The simulations shown were for a purely elastic model that underwent four short thermal cycles that were identical to Chapter 4's scenario.

The first attempt for the FE mesh size in the refined area of the constituents was described by $nebc = 50$ and $netc = 60$, which represent 50 elements along the wavelength direction (ω) on the BC layer, and 60 elements along the wavelength direction on the TC layer. In the second mesh refinement, we doubled the element numbers along ω direction on the BC and TC layer, to 100 and 120, respectively. Lastly, the number of elements along ω on the two layers was increased from the previous case by another 20%. Note that these user customizable parameter inputs were entered at the beginning of the geometry ANSYS snippets to define the element size.

Not only was it important to examine the number of elements along the wavelength direction, but it was also good to check if the selected mesh refinement areas on TC and BC layers was appropriate. Consequently, residual stress results outside of the refined area were also compared. To achieve this goal, we selected three elements at the interface just outside of the refined TC elements.

Through examination of the results in Fig.A.1 b), one can see that by comparing the results from 50 elements along the BC, and 60 elements along the TC to 100 elements along the BC, and 120 elements along the TC, the results in the valley region varied by 10.87% under the same thermal loading history. In the off-peak location, the residual stress was 3.63 times higher. However, when we added 20% more elements along the refined area, the stresses showed close to zero variation

at all locations. Therefore, the selection was made of 120 elements along the width at TC and 100 elements for BC refined area in the width direction.

By checking outside of the refined area, one can see from Fig.A.1 c) that there was almost no compressive stress variation seen in the off-peak and peak location, and only a slight increase seen as opposed to the area close to the TGO interface. Hence, we assumed that the refined area was acceptable. It should be pointed out that the mesh refinement for the TGO area followed the same pattern, and will not be detailed.

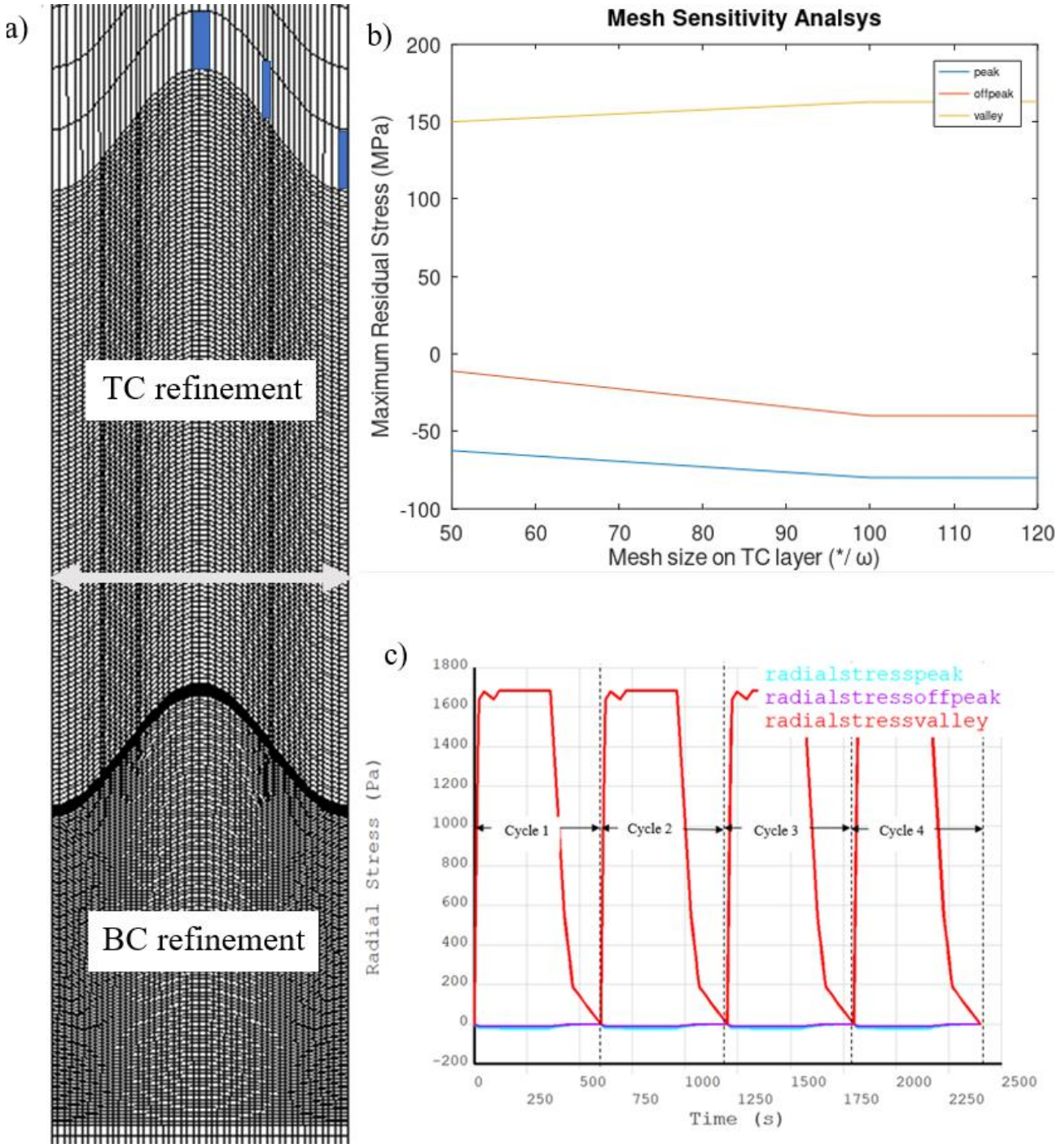

Figure A.1 a) illustration of the mesh refined area, where blue indicates three elements selected outside of the refined area at peak, off peak and valley location on TC layer, and ω characterise the wavelength; b) result for mesh sensitivity analysis, where the three line represents the maximum value of the residual stress at different element width; c) the residual stress plot obtained outside of the refined TC area, at three locations marked in a).

II. ANSYS CODE SNIPPET

In the following section, the ANSYS code for the analysis described in the thesis is listed. It contains the geometry set up, and then the structural and thermal material properties for each constituent. The program starts the thermal analysis using the temperature profile as thermal loading first. The LSSAVE command saves the results at each thermal load step, for use during the following structural analysis. Each of the time step of the structural analysis is perfectly aligned with the thermal load steps. The TBC residual stress is then analysed in the postprocessor.

The geometry codes should be called first while running the analysis. It includes the element type and key options of the selected elements, geometry of the model, including the embedded interface roughness. In the end, the thermal material properties are included, following with the structural material properties that is written into the program memory which would be called upon the material change at the start of the structural analysis.

After introducing all the necessary data for the study, the thermal analysis starts. In the thermal analysis, there are multiple load steps for one thermal cycle. The purpose of linearly interpolating the temperature changes into multiple small steps was to make sure the thermal profile looked as close as possible to the real heating-cooling environment while keeping the process manageable. The results of the thermal loading are saved at each load step.

With the saved thermal analysis results, the next step consists in running the main file of the corresponding structural analysis. Each of the material behaviour combination runs the same thermal and structural files. The only thing that needed to be changed between FE analyses was the material properties included in the structural material property file. The thermal properties assigned to the TBC constituents did not change throughout all runs because the analyses were assumed isothermal.

A.1 GEOMETRY EXAMPLE FOR THE TBC SYSTEM

```
/PREP7
/GRAPHIC,FULL
ET,1,PLANE55
! 2-D thermal conduction; 4 nodes, 1 dof (temperature) at each node
KEYOPT,1,3,1
/com, As the simulation is always isothermal, NO thermal properties were needed for calculations
/com, Define units as MKS unit
/UNITS,MKS
/com,================================================================
/com,Geometric Properties: Define parameters
/com,================================================================
stop = 1
pi = 4*atan(1)
H3 = 2.5e-4   ! Top coat (TC) thickness in m
H2 = 1e-6   ! Initial TGO thickness in m
H1 = 1.3e-4   ! Bond coat (BC) thickness in m
WL = 2.4e-5   ! Wave length
```

```
nWL = 0.5  ! number of wavelenths (could be 0.5, 1, 1.5, 2, 2.5, etc.)

w = nWL*WL  ! Width in m

HR = 1/5*H3 ! Refined mesh zone of TC

A = 10e-6   ! Amplitude of sine wave in m

!*ASK,A,what is the value of amplitude in m,10e-6

netc = 40 !# elements through TC

netgo = 12 !# elements through TGO

nebc = 100 !# elements through BC

newidth = 48 !# elements across width

netcmr = 120!# elements through refined TC

/com,============================================================

/com,Geometry

/com,============================================================

K,1,0,0,0

K,2,0,H1,0

K,3,0,H1+H2,0

K,4,0,H1+H2+HR,0

K,5,0,H1+H2+H3,0
```

K,6,w,H1+H2+H3,0

K,7,w,H1+H2+HR+A,0 !

K,8,w,H1+H2+A,0

K,9,w,H1+A,0 !

K,10,w,0,0

HBC_R=25e-6

!For BC mesh refinement

K,101,0,H1-HBC_R,0

K,102,w,H1-HBC_R,0

LSTR,1,101 ! L1

LSTR,2,3 ! L2

LSTR,3,4 ! L3

LSTR,4,5 ! L4

LSTR,5,6 ! L5

LSTR,6,7 ! L6

LSTR,7,8 ! L7

LSTR,8,9 ! L8

LSTR,102,10! L9

```
LSTR,10,1! L10

/com,============================================================

/com, Geometry -- BC -- profile between keypoints 2 and 9

/com,============================================================

npoints = 10 ! Plus KP 2 and 9, there will be npoints + 2 keypoints, therefore npoints + 1 intervals

*do,i,1,npoints,1

x = 0 + i*w/(npoints+1)

y = H1+A*0.5-0.5*A*cos(nWL*2*pi*x/w)

K,,x,y

*enddo



FLST,3,npoints + 2,2

FITEM,3,2

*DO,i,1,npoints,1

FITEM,3,10+i

*ENDDO

FITEM,3,9

BSPLIN,,P51X ! L11
```

```
LSTR,101,102 ! L12

LSTR,101,2 ! L13

LSTR,9,102 ! L14

AL,11,14,12,13 ! A1


LSEL,S,,,13,14,1

LESIZE,ALL,,,100

LSEL,S,,,11,12

LESIZE,ALL,,,newidth

TYPE,1,   ! element type 1

MAT,1

AMESH,1

ALLSEL

/com,============================================================

/com, Geometry -- TGO -- profile between keypoints 3 and 8

/com,============================================================

*do,i,1,npoints,1

x = 0 + i*w/(npoints+1)

y = H1+H2-0.5*A*cos(nWL*2*pi*x/w)+A*0.5
```

```
K,,x,y

*enddo


FLST,3,npoints + 2,2

FITEM,3,3

*DO,i,1,npoints,1

FITEM,3,10+npoints+i

*ENDDO

FITEM,3,8

BSPLIN,,P51X ! L12

AL,2,15,8,11 ! A2

LSEL,S,,,2,8,6

LESIZE,ALL,,,netgo

LSEL,S,,,11,15

LESIZE,ALL,,,newidth

TYPE,1,   ! element type 1

MAT,1

AMESH,2

ALLSEL
```

```
/com,============================================================

/com, Geometry -- TC -- profile between keypoints 4 and 7

/com,============================================================

*do,i,1,npoints,1

x = 0 + i*w/(npoints+1)

y = H1+H2+HR-0.5*A*cos(nWL*2*pi*x/w)+0.5*A

K,,x,y

*enddo



FLST,3,npoints+2,2

FITEM,3,4

*DO,i,1,npoints,1

FITEM,3,10+2*npoints+i

*ENDDO

FITEM,3,7

BSPLIN,,P51X ! L16



AL,3,16,7,15 ! A3

AL,4,5,6,16  ! A4
```

```
LSEL,S,,,3,7,4

LESIZE,ALL,,,netcmr

LSEL,S,,,15,16

LESIZE,ALL,,,newidth

TYPE,1,

MAT,3

AMESH,3

ALLSEL

LSEL,S,,,4,6,2

LESIZE,ALL,,,netcmr

LSEL,S,,,5,16,11

LESIZE,ALL,,,newidth

TYPE,1,

MAT,3

AMAP,4,4,5,6,7

ALLSEL

AL,1,12,9,10  ! A5

LSEL,S,,,1,9,8

LESIZE,ALL,,,115
```

```
LSEL,S,,,10,12,2

LESIZE,ALL,,,newidth

TYPE,1,   ! element type 1

MAT,1

AMESH,5

ALLSEL

*if,stop,eq,0,then

*endif
```

A.2 REALISTIC PROFILE FOR THE TBC INTERFACE

```
! Profile between keypoints 3 and 6

*do,i,1,npoints,1

x = 0 + i*w/(npoints+1)

y = 0

k = 1

ak = -0.25

bk = -0.03

y = y + ak*cos(k*2*pi*x/w)+bk*sin(k*2*pi*x/w)

k = 2
```

ak = -0.016

bk = -0.25

y = y + ak*cos(k*2*pi*x/w)+bk*sin(k*2*pi*x/w)

k = 3

ak = 0.04

bk = -0.17

y = y + ak*cos(k*2*pi*x/w)+bk*sin(k*2*pi*x/w)

k = 4

ak = 0.2

bk = -0.12

y = y + ak*cos(k*2*pi*x/w)+bk*sin(k*2*pi*x/w)

k = 5

ak = 0.01

bk = -0.09

y = y + ak*cos(k*2*pi*x/w)+bk*sin(k*2*pi*x/w)

k = 6

ak = -0.03

bk = 0.05

y = y + ak*cos(k*2*pi*x/w)+bk*sin(k*2*pi*x/w)

```
K,,x,H3+H0+y/1000000

*enddo


FLST,3,npoints + 2,2

FITEM,3,3

*DO,i,1,npoints,1

FITEM,3,8+npoints+i

*ENDDO

FITEM,3,6

BSPLIN,,P51X


AL,1,9,7,8

AL,2,10,6,9

AL,3,4,5,10
```

A.3 MATERIAL PROPERTIES FOR THE MODEL

```
/PREP7

ETCHG,TTS      ! Change element type from thermal PLANE55 to structural PLANE182

MPDELE,ALL,ALL ! Deletes linear thermal material properties

TBDELE,ALL,ALL ! Deletes previously defined material data tables

KEYOPT,1,3,1! Keyoption(3) = 1 means Axisymmetric

!-------------------------------------------------------------------------

! Define SUBSTRATE thermal expansion coefficient (10^-6/C)

!-------------------------------------------------------------------------

ALPX293=1.48e-5

ALPX473=1.52e-5

ALPX673=1.56e-5

ALPX873=1.62e-5

ALPX1073=1.69e-5

ALPX1273=1.75e-5

ALPX1373=1.80e-5

A1=ALPX293-1.36e-5

A2=ALPX473-1.42e-5
```

A7=ALPX673-1.46e-5

A3=ALPX873-1.52e-5

A4=ALPX1073-1.61e-5

A5=ALPX1273-1.72e-5

A6=ALPX1373-1.76e-5

reftemp=20

deptemp=400

tref, reftemp

/com,==========

/com, Material properties [ref.15 CHENG et al.]

/com,==========

MPTEMP,1,20 ! Defines a temperature table that can be used by all materials

MPTEMP,2,200

MPTEMP,3,600

MPTEMP,4,800

MPTEMP,5,1000

MPTEMP,6,1150

```
!------------------------------------------------------------------------

! Define BC Young's modulus which depends on Temperature (GPa)

!------------------------------------------------------------------------

MPDATA,EX,1,,200E9

MPDATA,EX,1,,190E9

MPDATA,EX,1,,160E9

MPDATA,EX,1,,145E9

MPDATA,EX,1,,120E9

MPDATA,EX,1,,110E9

MPDATA,PRXY,1,,0.30

MPDATA,PRXY,1,,0.30

MPDATA,PRXY,1,,0.31

MPDATA,PRXY,1,,0.32

MPDATA,PRXY,1,,0.33

MPDATA,PRXY,1,,0.33

!------------------------------------------------------------------------

! Define BC thermal expansion coefficient (10^-6/C)

!------------------------------------------------------------------------

UIMP,1,REFT,,,20
```

```
MPDATA,ALPX,1,,-A1

MPDATA,ALPX,1,,-A2

!MPDATA,ALPX,1,,-A7

MPDATA,ALPX,1,,-A3

MPDATA,ALPX,1,,-A4

MPDATA,ALPX,1,,-A5

MPDATA,ALPX,1,,-A6

!------------------------------------------------------------------------

! Define BC NORTON SECONDARY Creep: epsilon rate = C1*sigma^C2 //stress in Pa

!------------------------------------------------------------------------

TB,CREE,1,2,,10

TBTEMP,1000

TBDATA,,1.39E11,3,0,,,

TBTEMP,1150

TBDATA,,2.35E12,3,0,,,

!------------------------------------------------------------------------

! Define parameters for TGO

!------------------------------------------------------------------------

MPDATA,EX,2,1,400e9,390e9,370e9,355e9,325e9,320e9
```

MPDATA,PRXY,2,1,0.23,0.23,0.24,0.25,0.25,0.25

peaktemp=1150

UIMP,2,REFT,,,20

MPDATA,ALPX,2,1,8.0e-6-ALPX293,8.2e-6-ALPX473,8.7e-6-ALPX873,9.0e-6-ALPX1073,9.3e-6-ALPX1273,9.6e-6-ALPX1373

!---

! Define TGO NORTON SECONDARY Creep: epsilon rate = C1*sigma^C2

!---

TB,CREE,2,2,3,10

TBTEMP,1000

TBDATA,,7.3E-10,1,0,,,

TBTEMP,1150

TBDATA,,4.2E-8,1,0,,,

!---

! Define parameters for TC

!---

MPTEMP,,,,,,,,

MPTEMP,1,20

```
MPTEMP,2,200

MPTEMP,3,600

MPTEMP,4,800

MPTEMP,5,1000

MPTEMP,6,1100

MPDATA,EX,3,,48E9

MPDATA,EX,3,,47E9

MPDATA,EX,3,,40E9

MPDATA,EX,3,,34E9

MPDATA,EX,3,,26E9

MPDATA,EX,3,,22E9

MPDATA,PRXY,3,,0.10

MPDATA,PRXY,3,,0.10

MPDATA,PRXY,3,,0.11

MPDATA,PRXY,3,,0.11

MPDATA,PRXY,3,,0.12

MPDATA,PRXY,3,,0.12


UIMP,3,REFT,,,20
```

MPDATA,ALPX,3,,9.0e-6-ALPX293

MPDATA,ALPX,3,,9.2e-6-ALPX473

MPDATA,ALPX,3,,10.1e-6-ALPX873

MPDATA,ALPX,3,,10.8e-6-ALPX1073

MPDATA,ALPX,3,,11.7e-6-ALPX1273

MPDATA,ALPX,3,,12.2e-6-ALPX1373

!---

! Define BC non linear behaviour //stress in Pa

!---

TB,Biso,1,2,2,1

TBTEMP,20

TBDATA,,426e6,1.5e9,,,,

TBTEMP,1000

TBDATA,,202e6,1.5e9,,,,

!---

! Define TGO non linear behaviour //stress in Pa

!---

TB,Biso,2,2,2,1

TBTEMP,20

```
TBDATA,,8000e6,1.5e9,,,,

TBTEMP,1000

TBDATA,,300e6,1.5e9,,,,

!-----------------------------------------------------------------------------

! Define Swelling strain induced by phase transformation, epsilon = C3*(exp(-C4*x)-1)

!-----------------------------------------------------------------------------

!TB,SWELL,2,1,,EXPT

!TBTEMP,1150

!TBDATA,1,,,-0.0424,0.04167

!-----------------------------------------------------------------------------

! Define TC creep

!-----------------------------------------------------------------------------

TB,CREE,3,1,3,10

TBTEMP,0

TBDATA,,9.3e-15,0.48,0,,,
```

A.4 THERMAL LOADING HISTORY PROFILE

```
stop = 1

Theatup=1200

Tcooldown=2400

Tcyc2=Tcooldown+2*Theatup+600

Tcyc3=2*Tcooldown+3*Theatup+600

/SOLU

antype,static                          ! Perform a static analysis

nsub=5

/com,=================================================================

/com Thermal Cycle 1

/com,=================================================================

/com ****************************************

/com Load Step 1    temperature 20'C

/com ****************************************

temperature = 20

DL,10,,TEMP,temperature

KBC,1              ! Stepped (thermal) load (to avoid properties at 0 degrees)
```

```
TUNIF,temperature  ! Assigns a uniform temperature to all nodes
TIME,1e-8          ! Sets time in seconds at the end of loadstep
OUTRES,ALL,LAST
nsubst,nsub,nsub,nsub
allsel,all
SOLVE
SAVE,ThermalLS1,db
/com*************************************************************************
/com Load Step 2 increase temperature to 1150'C --part 1, to 900'C in 23.07s
/com*************************************************************************
temperature = 900
ti_1=23.07
DL,10,,TEMP,temperature
KBC,0              ! Ramped (thermal) load
TUNIF,temperature  ! Assigns a uniform temperature to all nodes
TIME,ti_1          ! Sets time in seconds at the end of loadstep
outres,all,-20                  ! Store results at 10 equal substeps
nsubst,nsub,nsub,nsub
allsel,all
```

```
SOLVE
SAVE,ThermalLS2,db
/com*************************************************************************
/com Load Step 3 increase temperature to 1150'C --part 2, to 1000'C in 23.07s
/com*************************************************************************
temperature = 1000
ti_2=23.07*2
DL,10,,TEMP,temperature
KBC,0            ! Ramped (thermal) load
TUNIF,temperature  ! Assigns a uniform temperature to all nodes
TIME,ti_2              ! Sets time in seconds at the end of loadstep
outres,all,last                    ! Store results at 10 equal substeps
nsubst,nsub,nsub,nsub
allsel,all
SOLVE
SAVE,ThermalLS3,db
/com*************************************************************************
/com Load Step 4 increase temperature to 1150'C --part 3, to 1100'C in 23.07*2s
/com*************************************************************************
```

```
temperature = 1100

ti_3=23.07*4

DL,10,,TEMP,temperature

KBC,0            ! Ramped (thermal) load

TUNIF,temperature  ! Assigns a uniform temperature to all nodes

TIME,ti_3            ! Sets time in seconds at the end of loadstep

outres,all,last                    ! Store results at 10 equal substeps

nsubst,nsub,nsub,nsub

allsel,all

SOLVE

SAVE,ThermalLS4,db

/com*************************************************************************

/com Load Step 5 increase temperature to 1150'C --part 4, to 1150'C in 23.07s

/com*************************************************************************

temperature = 1150

DL,10,,TEMP,temperature

KBC,0            ! Ramped (thermal) load

TUNIF,temperature  ! Assigns a uniform temperature to all nodes

TIME,120            ! Sets time in seconds at the end of loadstep
```

```
outres,all,last                    ! Store results at 10 equal substeps
nsubst,nsub,nsub,nsub
allsel,all
SOLVE
SAVE,ThermalLS5,db
/com ****************************************
/com Load Step 6 dwell at 1150'C
/com ****************************************
temperature = 1150
DL,10,,TEMP,temperature
KBC,0          ! Ramped (thermal) load
TUNIF,temperature  ! Assigns a uniform temperature to all nodes
TIME,360  ! Sets time in seconds at the end of loadstep
outres,all,last
nsubst,nsub,nsub,nsub
allsel,all
SOLVE
SAVE,ThermalLS6,db
```

```
/com*************************************************************************
/com Load Step 7 reduce temperature to 20'C --part 1,to 250'C in 23.07*2.9s
/com*************************************************************************
temperature = 250
td_1=23.07*18.5
DL,10,,TEMP,temperature
KBC,0              ! Ramped (thermal) load
TUNIF,temperature  ! Assigns a uniform temperature to all nodes
TIME,td_1   ! Sets time in seconds at the end of loadstep
outres,all,last
nsubst,nsub,nsub,nsub
allsel,all
SOLVE
SAVE,ThermalLS7,db
/com*************************************************************************
/com Load Step 8 reduce temperature to 20'C --part 2,to 100'C in 23.07*1.75s
/com*************************************************************************
temperature = 100
td_2=23.07*20.25
```

```
DL,10,,TEMP,temperature

KBC,0            ! Ramped (thermal) load

TUNIF,temperature  ! Assigns a uniform temperature to all nodes

TIME,td_2   ! Sets time in seconds at the end of loadstep

outres,all,last

nsubst,nsub,nsub,nsub

allsel,all

SOLVE

SAVE,ThermalLS8,db

/com*************************************************************************

/com Load Step 9 reduce temperature to 20'C --part 3, to 20'C in 23.07*5.75s

/com*************************************************************************

temperature = 20

td_3=600

DL,10,,TEMP,temperature

KBC,0            ! Ramped (thermal) load

TUNIF,temperature  ! Assigns a uniform temperature to all nodes

TIME,td_3        ! Sets time in seconds at the end of loadstep

outres,all,last
```

```
nsubst,nsub,nsub,nsub

allsel,all

SOLVE

SAVE,ThermalLS9,db

/com,================================================================

/com Thermal Cycle 2

/com,================================================================

/com*****************************************************************

/com Load Step 10 increase temperature to 1150'C --part 1, to 900'C

/com*****************************************************************

temperature = 900

ts_1=240+600

DL,10,,TEMP,temperature

KBC,0            ! Ramped (thermal) load

TUNIF,temperature  ! Assigns a uniform temperature to all nodes

TIME,ts_1            ! Sets time in seconds at the end of loadstep

outres,all,-20                    ! Store results at 10 equal substeps

nsubst,nsub,nsub,nsub

allsel,all
```

```
SOLVE
SAVE,ThermalL10,db
/com*************************************************************************
/com Load Step 11 increase temperature to 1150'C --part 2, to 1000'C
/com*************************************************************************
temperature = 1000
ts_2=480+600
DL,10,,TEMP,temperature
KBC,0            ! Ramped (thermal) load
TUNIF,temperature  ! Assigns a uniform temperature to all nodes
TIME,ts_2            ! Sets time in seconds at the end of loadstep
outres,all,last                    ! Store results at 10 equal substeps
nsubst,nsub,nsub,nsub
allsel,all
SOLVE
SAVE,ThermalLS11,db
/com*************************************************************************
/com Load Step 12 increase temperature to 1150'C --part 3, to 1100'C
/com*************************************************************************
```

```
temperature = 1100

ts_3=1058+600

DL,10,,TEMP,temperature

KBC,0            ! Ramped (thermal) load

TUNIF,temperature  ! Assigns a uniform temperature to all nodes

TIME,ts_3            ! Sets time in seconds at the end of loadstep

outres,all,last                    ! Store results at 10 equal substeps

nsubst,nsub,nsub,nsub

allsel,all

SOLVE

SAVE,ThermalLS12,db

/com*************************************************************************

/com Load Step 13 increase temperature to 1150'C

/com*************************************************************************

temperature = 1150

ts_4=1200+600

DL,10,,TEMP,temperature

KBC,0            ! Ramped (thermal) load

TUNIF,temperature  ! Assigns a uniform temperature to all nodes
```

```
TIME,ts_4              ! Sets time in seconds at the end of loadstep
outres,all,last                    ! Store results at 10 equal substeps
nsubst,nsub,nsub,nsub
allsel,all
SOLVE
SAVE,ThermalLS13,db
/com ****************************************
/com Load Step 14 dwell at 1100'C
/com ****************************************
temperature = 1150
c1dwell=87600+600
DL,10,,TEMP,temperature
KBC,0              ! Ramped (thermal) load
TUNIF,temperature  ! Assigns a uniform temperature to all nodes
TIME,c1dwell ! Sets time in seconds at the end of loadstep
outres,all,last
nsubst,nsub,nsub,nsub
allsel,all
SOLVE
```

```
SAVE,ThermalLS14,db
/com*********************************************************************
/com Load Step 15 reduce temperature to 20'C --part 1, to 550'C
/com*********************************************************************
temperature = 550
ts_c1=89000+600
DL,10,,TEMP,temperature
KBC,0              ! Ramped (thermal) load
TUNIF,temperature  ! Assigns a uniform temperature to all nodes
TIME,ts_c1   ! Sets time in seconds at the end of loadstep
outres,all,last
nsubst,nsub,nsub,nsub
allsel,all
SOLVE
SAVE,ThermalLS15,db
/com*********************************************************************
/com Load Step 16 reduce temperature to 20'C --part 2, to 150'C
/com*********************************************************************
temperature = 150
```

```
ts_c2=89512.5+600

DL,10,,TEMP,temperature

KBC,0            ! Ramped (thermal) load

TUNIF,temperature  ! Assigns a uniform temperature to all nodes

TIME,ts_c2   ! Sets time in seconds at the end of loadstep

outres,all,last

nsubst,nsub,nsub,nsub

allsel,all

SOLVE

SAVE,ThermalLS16,db

/com*************************************************************************

/com Load Step 17 reduce temperature to 20'C --part 3, to 20'C in 23.07*5.75s

/com*************************************************************************

temperature = 20

ts_c3=90000+600

DL,10,,TEMP,temperature

KBC,0            ! Ramped (thermal) load

TUNIF,temperature  ! Assigns a uniform temperature to all nodes

TIME,ts_c3        ! Sets time in seconds at the end of loadstep
```

```
outres,all,last
nsubst,nsub,nsub,nsub
allsel,all
SOLVE
SAVE,ThermalLS17,db
/com,================================================================
/com Thermal Cycle 3
/com,================================================================
/com*****************************************************************************
/com Load Step 18 increase temperature to 1150'C --part 1, to 900'C
/com*****************************************************************************
/SOLU
temperature = 900
ts_18=240+90000+600
DL,10,,TEMP,temperature
KBC,0            ! Ramped (thermal) load
TUNIF,temperature  ! Assigns a uniform temperature to all nodes
TIME,ts_18           ! Sets time in seconds at the end of loadstep
outres,all,-20                    ! Store results at 10 equal substeps
```

```
nsubst,nsub,nsub,nsub

allsel,all

SOLVE

SAVE,ThermalLS18,db

/com*************************************************************************

/com Load Step 19 increase temperature to 1150'C --part 2, to 1000'C

/com*************************************************************************

temperature = 1000

ts_19=600+480+90000

DL,10,,TEMP,temperature

KBC,0              ! Ramped (thermal) load

TUNIF,temperature  ! Assigns a uniform temperature to all nodes

TIME,ts_19             ! Sets time in seconds at the end of loadstep

outres,all,last                        ! Store results at 10 equal substeps

nsubst,nsub,nsub,nsub

allsel,all

SOLVE

SAVE,ThermalLS19,db
```

```
/com*****************************************************************************
/com Load Step 20 increase temperature to 1150'C --part 3, to 1100'C
/com*****************************************************************************
temperature = 1100
ts_20=600+1058+90000
DL,10,,TEMP,temperature
KBC,0              ! Ramped (thermal) load
TUNIF,temperature  ! Assigns a uniform temperature to all nodes
TIME,ts_20             ! Sets time in seconds at the end of loadstep
outres,all,last                        ! Store results at 10 equal substeps
nsubst,nsub,nsub,nsub
allsel,all
SOLVE
SAVE,ThermalLS20,db
/com*****************************************************************************
/com Load Step 21 increase temperature to 1150'C
/com*****************************************************************************
temperature = 1150
ts_21=1200+90000+600
```

```
DL,10,,TEMP,temperature

KBC,0            ! Ramped (thermal) load

TUNIF,temperature  ! Assigns a uniform temperature to all nodes

TIME,ts_21           ! Sets time in seconds at the end of loadstep

outres,all,last                    ! Store results at 10 equal substeps

nsubst,nsub,nsub,nsub

allsel,all

SOLVE

SAVE,ThermalLS21,db

/com ****************************************

/com Load Step 22 dwell at 1100'C

/com ****************************************

temperature = 1150

c2dwell=87600+90000+600

DL,10,,TEMP,temperature

KBC,0            ! Ramped (thermal) load

TUNIF,temperature  ! Assigns a uniform temperature to all nodes

TIME,c2dwell ! Sets time in seconds at the end of loadstep

outres,all,last
```

```
nsubst,nsub,nsub,nsub

allsel,all

SOLVE

SAVE,ThermalLS22,db

/com*************************************************************************

/com Load Step 23 reduce temperature to 20'C --part 1, to 550'C

/com*************************************************************************

temperature = 550

ts_c23=89000+90000+600

DL,10,,TEMP,temperature

KBC,0              ! Ramped (thermal) load

TUNIF,temperature  ! Assigns a uniform temperature to all nodes

TIME,ts_c23  ! Sets time in seconds at the end of loadstep

outres,all,last

nsubst,nsub,nsub,nsub

allsel,all

SOLVE

SAVE,ThermalLS23,db
```

```
/com*****************************************************************************
/com Load Step 24 reduce temperature to 20'C --part 2, to 150'C
/com*****************************************************************************
temperature = 150
ts_c24=600+89512.5+90000
DL,10,,TEMP,temperature
KBC,0              ! Ramped (thermal) load
TUNIF,temperature  ! Assigns a uniform temperature to all nodes
TIME,ts_c24   ! Sets time in seconds at the end of loadstep
outres,all,last
nsubst,nsub,nsub,nsub
allsel,all
SOLVE
SAVE,ThermalLS24,db
/com*****************************************************************************
/com Load Step 25 reduce temperature to 20'C --part 3, to 20'C in 23.07*5.75s
/com*****************************************************************************
temperature = 20
ts_c25=180000+600
```

```
DL,10,,TEMP,temperature

KBC,0            ! Ramped (thermal) load

TUNIF,temperature  ! Assigns a uniform temperature to all nodes

TIME,ts_c25        ! Sets time in seconds at the end of loadstep

outres,all,last

nsubst,nsub,nsub,nsub

allsel,all

SOLVE

SAVE,ThermalLS25,db

/com,=============================================================

/com Thermal Cycle 4

/com,=============================================================

/com*************************************************************************

/com Load Step 26 increase temperature to 1150'C --part 1, to 900'C

/com*************************************************************************

/SOLU

temperature = 900

ts_26=600+240+180000
```

```
DL,10,,TEMP,temperature

KBC,0            ! Ramped (thermal) load

TUNIF,temperature  ! Assigns a uniform temperature to all nodes

TIME,ts_26           ! Sets time in seconds at the end of loadstep

outres,all,-20                    ! Store results at 10 equal substeps

nsubst,nsub,nsub,nsub

allsel,all

SOLVE

SAVE,ThermalLS26,db

/com*************************************************************************

/com Load Step 27 increase temperature to 1150'C --part 2, to 1000'C

/com*************************************************************************

temperature = 1000

ts_27=480+180000+600

DL,10,,TEMP,temperature

KBC,0            ! Ramped (thermal) load

TUNIF,temperature  ! Assigns a uniform temperature to all nodes

TIME,ts_27           ! Sets time in seconds at the end of loadstep

outres,all,last                    ! Store results at 10 equal substeps
```

```
nsubst,nsub,nsub,nsub

allsel,all

SOLVE

SAVE,ThermalLS27,db

/com*************************************************************************

/com Load Step 28 increase temperature to 1150'C --part 3, to 1100'C

/com*************************************************************************

temperature = 1100

ts_28=600+1058+180000

DL,10,,TEMP,temperature

KBC,0              ! Ramped (thermal) load

TUNIF,temperature  ! Assigns a uniform temperature to all nodes

TIME,ts_28             ! Sets time in seconds at the end of loadstep

outres,all,last                        ! Store results at 10 equal substeps

nsubst,nsub,nsub,nsub

allsel,all

SOLVE

SAVE,ThermalLS28,db
```

```
/com*****************************************************************************
/com Load Step 29 increase temperature to 1150'C
/com*****************************************************************************
temperature = 1150
ts_29=1200+180000+600
DL,10,,TEMP,temperature
KBC,0              ! Ramped (thermal) load
TUNIF,temperature  ! Assigns a uniform temperature to all nodes
TIME,ts_29         ! Sets time in seconds at the end of loadstep
outres,all,last                    ! Store results at 10 equal substeps
nsubst,nsub,nsub,nsub
allsel,all
SOLVE
SAVE,ThermalLS29,db
/com ****************************************
/com Load Step 30 dwell at 1100'C
/com ****************************************
temperature = 1150
c3dwell=87600+180000+600
```

```
DL,10,,TEMP,temperature

KBC,0            ! Ramped (thermal) load

TUNIF,temperature  ! Assigns a uniform temperature to all nodes

TIME,c3dwell  ! Sets time in seconds at the end of loadstep

outres,all,last

nsubst,nsub,nsub,nsub

allsel,all

SOLVE

SAVE,ThermalLS30,db

/com*************************************************************************

/com Load Step 31 reduce temperature to 20'C --part 1, to 550'C

/com*************************************************************************

temperature = 550

ts_c31=600+89000+180000

DL,10,,TEMP,temperature

KBC,0            ! Ramped (thermal) load

TUNIF,temperature  ! Assigns a uniform temperature to all nodes

TIME,ts_c31 ! Sets time in seconds at the end of loadstep

outres,all,last
```

```
nsubst,nsub,nsub,nsub

allsel,all

SOLVE

SAVE,ThermalLS31,db

/com*************************************************************************

/com Load Step 32 reduce temperature to 20'C --part 2, to 150'C

/com*************************************************************************

temperature = 150

ts_c32=89512.5+180000+600


DL,10,,TEMP,temperature

KBC,0              ! Ramped (thermal) load

TUNIF,temperature  ! Assigns a uniform temperature to all nodes

TIME,ts_c32  ! Sets time in seconds at the end of loadstep

outres,all,last

nsubst,nsub,nsub,nsub

allsel,all

SOLVE

SAVE,ThermalLS32,db
```

```
/com*************************************************************************
/com Load Step 33 reduce temperature to 20'C --part 3, to 20'C in 23.07*5.75s
/com*************************************************************************
temperature = 20
ts_c33=270000+600
DL,10,,TEMP,temperature
KBC,0              ! Ramped (thermal) load
TUNIF,temperature  ! Assigns a uniform temperature to all nodes
TIME,ts_c33        ! Sets time in seconds at the end of loadstep
outres,all,last
nsubst,nsub,nsub,nsub
allsel,all
SOLVE
SAVE,ThermalLS33,db


*if,stop,eq,0,then
*endif
```

A.5 EXAMPLE OF MAIN ANALYSIS

```
*SET,stop , 1
/com, The current main file is for running 4 cycles with ELASTIC CASE,N1
/FILNAME,ThermalAnalysis
/INPUT,'C:\Users\anner\OneDrive\Desktop\Jan.M1\GEOMETRY','txt'
/INPUT,'C:\Users\anner\OneDrive\Desktop\Yajie_ main\Thermal MP','txt'
/INPUT,'C:\Users\anner\OneDrive\Desktop\Yajie_ main\Thermal loading','txt'
Finish
/FILNAME,StructuralAnalysis
/INPUT,'C:\Users\anner\OneDrive\Desktop\Jan.M2\MP-N1-Elastic','txt'
/INPUT,'C:\Users\anner\OneDrive\Desktop\Yajie_ main\BC_lhs','txt'
/com,================================================================
/com Thermal Cycle 1
/com,================================================================
/com ****************************************
/com Load Step 1    temperature 20'C
/com ****************************************
/SOLU
```

```
ANTYPE,TRANS      ! Transient analysis
TRNOPT,FULL       ! Specifies transient analysis option
NLGEOM,ON
TIME,1e-8
LDREAD,TEMP,1,,,,'ThermalAnalysis','rth'
ALLSEL
SOLVE
SAVE
/com*****************************************************************************
/com Load Step 2 increase temperature to 1150'C --part 1, to 900'C in 23.07s
/com*****************************************************************************
*SET,nsub,15
TIME,ts_1
LDREAD,TEMP,2,,,,'ThermalAnalysis','rth'
autots,on
outres,all,-20
nsubst,nsub,nsub,nsub
ALLSEL
SOLVE
```

```
SAVE
/com*************************************************************************
/com Load Step 3 increase temperature to 1150'C --part 2, to 1000'C in 23.07s
/com*************************************************************************
*SET,nsub,5
TIME,ts_2
LDREAD,TEMP,3,,,,'ThermalAnalysis','rth'
autots,on
outres,all,last
nsubst,nsub,nsub,nsub
ALLSEL
SOLVE
SAVE
/com*************************************************************************
/com Load Step 4 increase temperature to 1150'C --part 3, to 1100'C in 23.07*2s
/com*************************************************************************
*SET,nsub,5
TIME,ts_3
LDREAD,TEMP,4,,,,'ThermalAnalysis','rth'
```

```
autots,on

outres,all,last

nsubst,nsub,nsub,nsub

ALLSEL

SOLVE

SAVE

/com*************************************************************************

/com Load Step 5 increase temperature to 1150'C --part 4, to 1150'C in 23.07s

/com*************************************************************************

*SET,nsub,5

TIME,120

LDREAD,TEMP,5,,,,'ThermalAnalysis','rth'

autots,on

outres,all,-20

nsubst,nsub,nsub,nsub

ALLSEL

SOLVE

SAVE
```

```
/com ***************************************************

/com Load Step 6 dwell at temperature to 1150'C

/com ***************************************************

TIMINT,OFF,STRUC

TIME,360

LDREAD,TEMP,6,,,,'ThermalAnalysis','rth'

nsubst,nsub,nsub,nsub

deltim,,1,nsub

KBC,0 !step changed load step, useful for rate dependent behaviour(creep)

outres,all,-10

rate,0 !including creep effect

ALLSEL

SOLVE

SAVE

/com*****************************************************************

/com  Load Step 7 reduce temperature to 20'C --part 1, to 250'C in 23.07*2.9s

/com*****************************************************************

TIME,ts_c1

TIMINT,ON
```

```
LDREAD,TEMP,7,,,,'ThermalAnalysis','rth'

autots,on

outres,all,last

nsubst,nsub,nsub,nsub

ALLSEL

rate,0

SOLVE

SAVE

/com*************************************************************************

/com Load Step 8 reduce temperature to 20'C --part 2, to 250'C in 23.07*1.75s

/com*************************************************************************

TIME,ts_c2

LDREAD,TEMP,8,,,,'ThermalAnalysis','rth'

autots,on

outres,all,-20

nsubst,nsub,nsub,nsub

ALLSEL

rate,0

SOLVE
```

```
SAVE
/com*********************************************************************
/com Load Step 9 reduce temperature to 20'C --part 3, to 250'C in 23.07*5.75s
/com*********************************************************************
TIME,ts_c3
LDREAD,TEMP,9,,,,'ThermalAnalysis','rth'
autots,on
outres,all,-20
nsubst,nsub,nsub,nsub
ALLSEL
rate,0
SOLVE
SAVE
/com,=================================================================
/com Thermal Cycle 2
/com,=================================================================
/com*********************************************************************
/com Load Step 10 increase temperature to 1150'C --part 1, to 900'C in 23.07s
/com*********************************************************************
```

```
*SET,nsub,15
TIME,ts2_1
LDREAD,TEMP,10,,,,'ThermalAnalysis','rth'
autots,on
outres,all,-20
nsubst,nsub,nsub,nsub
ALLSEL
rate,0
SOLVE
SAVE
/com*************************************************************************
/com Load Step 11 increase temperature to 1150'C --part 2, to 1000'C in 23.07s
/com*************************************************************************
*SET,nsub,5
TIME,ts2_2
LDREAD,TEMP,11,,,,'ThermalAnalysis','rth'
autots,on
outres,all,last
nsubst,nsub,nsub,nsub
```

```
ALLSEL

rate,0

SOLVE

SAVE

/com*************************************************************************

/com Load Step 12 increase temperature to 1150'C --part 3,to 1100'C in 23.07*2s

/com*************************************************************************

*SET,nsub,5

TIME,ts2_3

LDREAD,TEMP,12,,,,'ThermalAnalysis','rth'

autots,on

outres,all,last

nsubst,nsub,nsub,nsub

ALLSEL

rate,0

SOLVE

SAVE
```

```
/com*************************************************************************
/com Load Step 13 increase temperature to 1150'C --part 4,to 1150'C in 23.07s
/com*************************************************************************
*SET,nsub,5
TIME,ts2_4
LDREAD,TEMP,13,,,,'ThermalAnalysis','rth'
autots,on
outres,all,last
nsubst,nsub,nsub,nsub
ALLSEL
rate,0
SOLVE
SAVE
/com ******************************************************
/com Load Step 14 dwell at temperature to 1150'C
/com ******************************************************
timint,off,struc
LDREAD,TEMP,14,,,,'ThermalAnalysis','rth'
outres,all,-20
```

```
rate,0
TIME,360+600
nsubst,nsub,nsub,nsub
deltim,,1,nsub
ALLSEL
SOLVE
SAVE
/com*************************************************************************
/com Load Step 15 reduce temperature to 20'C --part 1, to 250'C in 23.07*2.9s
/com*************************************************************************
TIME,ts2_c1
TIMINT,ON
LDREAD,TEMP,15,,,,'ThermalAnalysis','rth'
autots,on
outres,all,last
nsubst,nsub,nsub,nsub
ALLSEL
rate,0
SOLVE
```

```
SAVE
/com*****************************************************************************
/com Load Step 16 reduce temperature to 20'C --part 2, to 250'C in 23.07*1.75s
/com*****************************************************************************
TIME,ts2_c2
LDREAD,TEMP,16,,,,'ThermalAnalysis','rth'
autots,on
outres,all,-20
nsubst,nsub,nsub,nsub
ALLSEL
rate,0
SOLVE
SAVE
/com*****************************************************************************
/com Load Step 17 reduce temperature to 20'C --part 3, to 250'C in 23.07*5.75s
/com*****************************************************************************
TIME,ts2_c3
LDREAD,TEMP,17,,,,'ThermalAnalysis','rth'
autots,on
```

```
outres,all,-20
nsubst,nsub,nsub,nsub
ALLSEL
rate,0
SOLVE
! SAV
save
*SET,nsub,15
TIME,ts3_1
LDREAD,TEMP,18,,,,'ThermalAnalysis','rth'
autots,on
outres,all,-20
nsubst,nsub,nsub,nsub
ALLSEL
rate,0
SOLVE
SAVE
```

```
/com*****************************************************************************
/com Load Step 19 increase temperature to 1150'C --part 2, to 1000'C in 23.07s
/com*****************************************************************************
*SET,nsub,5
TIME,ts3_2
LDREAD,TEMP,19,,,,'ThermalAnalysis','rth'
autots,on
outres,all,last
nsubst,nsub,nsub,nsub
ALLSEL
rate,0
SOLVE
SAVE
/com*****************************************************************************
/com Load Step 20 increase temperature to 1150'C --part 3, to 1100'C in 23.07*2s
/com*****************************************************************************
*SET,nsub,5
TIME,ts3_3
LDREAD,TEMP,20,,,,'ThermalAnalysis','rth'
```

```
autots,on
outres,all,last
nsubst,nsub,nsub,nsub
ALLSEL
rate,0
SOLVE
SAVE
/com*************************************************************************
/com Load Step 21 increase temperature to 1150'C --part 4, to 1150'C in 23.07s
/com*************************************************************************
*SET,nsub,5
TIME,ts3_4
LDREAD,TEMP,21,,,,'ThermalAnalysis','rth'
autots,on
outres,all,last
nsubst,nsub,nsub,nsub
ALLSEL
rate,0
SOLVE
```

```
SAVE
/com ******************************************************
/com Load Step 22 dwell at temperature to 1150'C
/com ******************************************************
TIMINT,OFF,STRUC
LDREAD,TEMP,22,,,,'ThermalAnalysis','rth'
outres,all,-20
rate,0 !Turning the creep effect on in the solution
TIME,360+600*2
nsubst,nsub,nsub,nsub
deltim,,1,nsub
ALLSEL
SOLVE
SAVE
/com*************************************************************************
/com Load Step 23 reduce temperature to 20'C --part 1, to 250'C in 23.07*2.9s
/com*************************************************************************
TIME,ts3_c1
TIMINT,ON
```

```
LDREAD,TEMP,23,,,,'ThermalAnalysis','rth'

autots,on

outres,all,last

nsubst,nsub,nsub,nsub

ALLSEL

rate,0

SOLVE

SAVE

/com*************************************************************************

/com Load Step 24 reduce temperature to 20'C --part 2, to 250'C in 23.07*1.75s

/com*************************************************************************

TIME,ts3_c2

LDREAD,TEMP,24,,,,'ThermalAnalysis','rth'

autots,on

outres,all,-20

nsubst,nsub,nsub,nsub

ALLSEL

rate,0

SOLVE
```

```
SAVE
/com*********************************************************************
/com Load Step 25 reduce temperature to 20'C --part 3, to 250'C in 23.07*5.75s
/com*********************************************************************
TIME,ts3_c3
LDREAD,TEMP,25,,,,'ThermalAnalysis','rth'
autots,on
outres,all,-20
nsubst,nsub,nsub,nsub
ALLSEL
rate,0
SOLVE
SAVE
/com,=============================================================
/com Thermal Cycle 4
/com,=============================================================
/com*********************************************************************
/com Load Step 26 increase temperature to 1150'C --part 1, to 900'C in 23.07s
/com*********************************************************************
```

```
*SET,nsub,15
TIME,ts4_1
LDREAD,TEMP,26,,,,'ThermalAnalysis','rth'
autots,on
outres,all,-20
nsubst,nsub,nsub,nsub
ALLSEL
rate,0
SOLVE
SAVE
/com*************************************************************************
/com Load Step 27 increase temperature to 1150'C --part 2, to 1000'C in 23.07s
/com*************************************************************************
*SET,nsub,5
TIME,ts4_2
LDREAD,TEMP,27,,,,'ThermalAnalysis','rth'
autots,on
outres,all,last
nsubst,nsub,nsub,nsub
```

```
ALLSEL

rate,0

SOLVE

SAVE

/com*************************************************************************

/com Load Step 28 increase temperature to 1150'C --part 3, to 1100'C in 23.07*2s

/com*************************************************************************

*SET,nsub,5

TIME,ts4_3

LDREAD,TEMP,28,,,,'ThermalAnalysis','rth'

autots,on

outres,all,last

nsubst,nsub,nsub,nsub

ALLSEL

rate,0

SOLVE

SAVE
```

```
/com*************************************************************************
/com Load Step 29 increase temperature to 1150'C --part 4, to 1150'C in 23.07s
/com*************************************************************************
*SET,nsub,5
TIME,ts4_4
LDREAD,TEMP,29,,,,'ThermalAnalysis','rth'
autots,on
outres,all,last
nsubst,nsub,nsub,nsub
ALLSEL
rate,0
SOLVE
SAVE
/com ******************************************************
/com Load Step 30 dwell at temperature to 1150'C
/com ******************************************************
TIMINT,OFF,STRUC
LDREAD,TEMP,30,,,,'ThermalAnalysis','rth'
TIME,360+600*3
```

```
nsubst,nsub,nsub,nsub

deltim,,1,nsub

outres,all,-20

rate,0

ALLSEL

SOLVE

SAVE

/com*************************************************************************

/com Load Step 31 reduce temperature to 20'C --part 1, to 250'C in 23.07*2.9s

/com*************************************************************************

TIME,ts4_c1

TIMINT,ON

LDREAD,TEMP,31,,,,'ThermalAnalysis','rth'

autots,on

outres,all,last

nsubst,nsub,nsub,nsub

ALLSEL

rate,0

SOLVE
```

```
SAVE
/com*****************************************************************************
/com Load Step 32 reduce temperature to 20'C --part 2, to 250'C in 23.07*1.75s
/com*****************************************************************************
TIME,ts4_c2
LDREAD,TEMP,32,,,,'ThermalAnalysis','rth'
autots,on
outres,all,-20
nsubst,nsub,nsub,nsub
ALLSEL
rate,0
SOLVE
SAVE
/com*****************************************************************************
/com Load Step 33 reduce temperature to 20'C --part 3, to 250'C in 23.07*5.75s
/com*****************************************************************************
TIME,ts4_c3
LDREAD,TEMP,33,,,,'ThermalAnalysis','rth'
autots,on
```

outres,all,-20

nsubst,nsub,nsub,nsub

ALLSEL

rate,0

SOLVE

SAVE

FINISH